1993

Characterization of Epoxy Resins for use in the Resin Transfer Molding Process

Christina Kaye Short
College of William & Mary - Arts & Sciences

CHARACTERIZATION OF EPOXY RESINS FOR USE IN THE RESIN TRANSFER MOLDING PROCESS

A Thesis

Presented to the Department of Chemistry

The College of William and Mary in Virginia

In Partial Fulfillment

Of the Requirements for the Degree of

Master of Arts

---

by

Christina Kaye Short

August 1993

APPROVAL SHEET

This thesis is submitted in partial fulfillment of the requirements for the degree of

MASTER OF ARTS

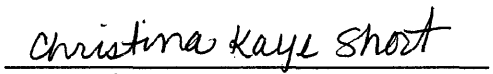

Christina Kaye Short

Approved, August 1993

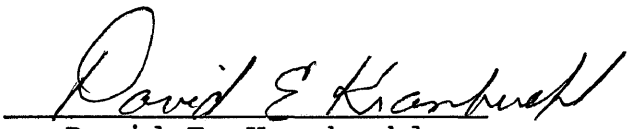

David E. Kranbuehl

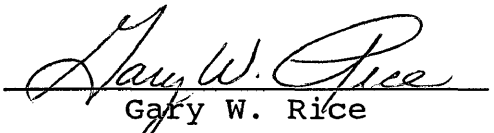

Gary W. Rice

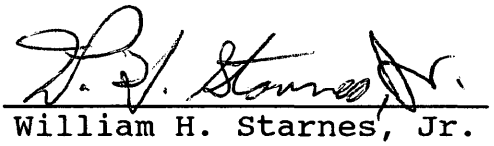

William H. Starnes, Jr.

TABLE OF CONTENTS

		Page
LIST OF FIGURES		v
ACKNOWLEDGEMENTS		ix
ABSTRACT		x
CHAPTER I.	CHEMISTRY OF EPOXY RESINS	2
	A. Introduction	2
	B. History	3
	C. Synthesis	4
	D. High Performance Resins	9
	E. Chemistry of Development Resins	11
	1. Epoxy Research Resin RSL 1895/ Epon Curing Agent® W	11
	2. PR500 Epoxy Resin	13
	3. E905L Triazine Epoxy Resin	14
	F. References	18
CHAPTER II.	DIFFERENTIAL SCANNING CALORIMETRY	20
	A. Theory	20
	B. Experimental	22
	C. Kinetic Analysis Methods for Epoxy-Amine Resins	22
	D. References	31
CHAPTER III.	FDEMS CURE MONITORING	32
	A. Theory	33
	B. Experimental	35
	C. Resin Transfer Molding Process	38
	D. References	42
CHAPTER IV.	CHARACTERIZATION OF SHELL 1895 RESIN	43
	A. Reaction Kinetics	43
	B. Correlation of Degree of Cure and Viscosity	48
	C. Correlation of α and η with a RTM Experiment	53
	D. References	99
CHAPTER V.	CHARACTERIZATION OF PR500 RESIN	100

TABLE OF CONTENTS (continued)

	A. Reaction Kinetics	100
	B. Correlation of Degree of Cure and Viscosity	102
	C. References	129
CHAPTER VI.	CHARACTERIZATION OF E905L RESIN	130
	A. Reaction Kinetics	130
	1. High Temperature Reaction	131
	2. Low Temperature Reaction	133
	B. References	145
CHAPTER VII.	CONCLUSIONS	146

LIST OF FIGURES

Figure		Page
1.1	Epoxide Structure	2
1.2	Bisphenol A and Epichlorohydrin	4
1.3	Preparation of Epoxy Resins, Method 1	5
1.4	Preparation of Epoxy Resins, Method 2	5
1.5	DGEBA	5
1.6	Chlorohydrin Intermediate	6
1.7	Homopolymerization using a Catalytic Curing Agent	7
1.8	Reaction of an Amine Curative with an Epoxide	7
1.9	Reaction of a Secondary Hydroxyl Group with an Epoxide	8
1.10	Trimolecular Transition State Resulting from the Accumulation of Hydroxyl Groups during the Amine-Epoxy Reaction	8
1.11	TGMDA and DDS	10
1.12	Epon HPT resin 1071	11
1.13	DETDA	12
1.14	Diglycidyl Ether of Fluorene Bisphenol	13
1.15	Triazine	15
1.16	Trisubstituted Triazine Ring, Prepolymer Resin	16
1.17	Crosslinked Triazine Resin	16
1.18	Diglycidyl Ether of Bisphenol	17
1.19	Amine Epoxy Toughening Agent	17
2.1	Schematic Diagram of the Cells in the Perkin-Elmer DSC.	20
2.2	Shell 1895 DSC Ramp from 50° to 300°C at 2°C/min	28
2.3	DSC Isothermal Cure of PR500 @ 160°C	29
2.4	DSC Temperature Ramp after a 160°C Isothermal Cure of PR500	30
3.1	Diagram Illustrating the Interdigitated Comb Electrodes of a DekDyne Sensor	36
3.2	Block Diagram of the FDEMS Apparatus	37
3.3	FDEMS Isothermal Cure of Shell 1895 @ 149°C	38
3.4	Block Diagram of the Intelligently Controlled Closed Loop RTM Apparatus	40
4.1	DSC Temperature Ramp of Shell 1895 from 50° to 300°C @ 2°C/min	57
4.2	α vs. Time Plot for Shell 1895 Isothermal Cures @ 121°, 135°, 149° and 177°C	58
4.3	α vs. Time Plot for Shell 1895 Isothermal Cure @ 149°C	59
4.4	Ln K vs. 1/T for Shell 1895	60

LIST OF FIGURES (continued)

4.5	α vs. Time Plot for Shell 1895 Isothermal Cure @ 121°C	61
4.6	α vs. Time Plot for Shell 1895 Isothermal Cure @ 135°C	62
4.7	α vs. Time Plot for Shell 1895 Isothermal Cure @ 149°C	63
4.8	α vs. Time Plot for Shell 1895 Isothermal Cure @177°C	64
4.9	α vs. Time Plot Comparing Old and New Batches of Shell 1895 for Isothermal Cure @ 121°C	65
4.10	α vs. Time Plot Comparing Old and New Batches of Shell 1895 for Isothermal Cure @ 135°C	66
4.11	α vs. Time Plot Comparing Old and New Batches of Shell 1895 for Isothermal Cure @ 149°C	67
4.12	α vs. Time Plot Comparing Old and New Batches of Shell 1895 for Isothermal Cure @ 177°C	68
4.13	α vs. Time Plot for New Batch of Shell 1895 for Isothermal Cure @ 90°C	69
4.14	α vs. Time Plot for New Batch of Shell 1895 for Isothermal Cure @ 121°C	70
4.15	α vs. Time Plot for New Batch of Shell 1895 for Isothermal Cure @ 135°C	71
4.16	α vs. Time Plot for New Batch of Shell 1895 for Isothermal Cure @ 149°C	72
4.17	α vs. Time Plot for New Batch of Shell 1895 for Isothermal Cure @ 177°C	73
4.18	FDEMS Isothermal Cure of Shell 1895 @ 90°C	74
4.19	FDEMS Isothermal Cure of Shell 1895 @ 121°C	75
4.20	FDEMS Isothermal Cure of Shell 1895 @ 135°C	76
4.21	FDEMS Isothermal Cure of Shell 1895 @ 149°C	77
4.22	FDEMS Isothermal Cure of Shell 1895 @ 177°C	78
4.23	η^* vs. Time for Isothermal Cure of Shell 1895 @ 90°C	79
4.24	η^* vs. Time for Isothermal Cure of Shell 1895 @ 121°C	80
4.25	η^* vs. Time for Isothermal Cure of Shell 1895 @ 135°C	81
4.26	η^* vs. Time for Isothermal Cure of Shell 1895 @ 149°C	82
4.27	η^* vs. Time for Isothermal Cure of Shell 1895 @ 177°C	83
4.28	log η vs. log $\epsilon''*\omega$ Plot for 90°, 121°, 135° and 149°C Isothermal Data	84
4.29	G′ and G″ vs. Time Plot for Isothermal Cure of Shell 1895 @ 149°C	85
4.30	α and log η vs. log $\epsilon''*\omega$ for 90°C Calibration	86
4.31	α and log η vs. log $\epsilon''*\omega$ for 121°C Calibration	87
4.32	α and log η vs. log $\epsilon''*\omega$ for 135°C Calibration	88
4.33	α and log η vs. log $\epsilon''*\omega$ for 149°C Calibration	89

LIST OF FIGURES (continued)

4.34	Slope $(d\epsilon''/dt)/\epsilon''$ and α vs. Time for 177°C Calibration using Successive Points	90
4.35	Slope $(d\epsilon''/dt)/\epsilon''$ and α vs. Time for 177°C Calibration using Five Point Method	91
4.36	FDEMS Output for RTM Experiment DH042293	92
4.37	FDEMS Output for RTM Experiment DH042393	93
4.38	Degree of Cure Correlation with RTM Experiment DH042293	94
4.39	Degree of Cure Correlation with RTM Experiment DH042393	95
4.40	Viscosity Correlation with RTM Experiment DH042293	96
4.41	Viscosity Correlation with RTM Experiment DH042393	97
4.42	FDEMS Signal vs. Time for DH042293	98
5.1	DSC Temperature Ramp of PR500	106
5.2	α vs. Time Plot for PR500 Isothermal Cure @ 160°C	107
5.3	α vs. Time Plot for PR500 Isothermal Cure @ 180°C	108
5.4	α vs. Time Plot for PR500 Isothermal Cure @ 200°C	109
5.5	η^* vs. Time for PR500 Isothermal Cure @ 160°C	110
5.6	η^* vs. Time for PR500 Isothermal Cure @ 170°C	111
5.7	η^* vs. Time for PR500 Isothermal Cure @ 180°C	112
5.8	FDEMS Isothermal Cure of PR500 @ 160°C	113
5.9	FDEMS Isothermal Cure of PR500 @ 170°C	114
5.10	FDEMS Isothermal Cure of PR500 @ 180°C	115
5.11	FDEMS Isothermal Cure of PR500 @ 190°C	116
5.12	FDEMS Isothermal Cure of PR500 @ 200°C	117
5.13	log η vs. log $\epsilon''*\omega$ Plot for 160°C Calibration	118
5.14	log η vs. log $\epsilon''*\omega$ Plot for 170°C Calibration	119
5.15	log η vs. log $\epsilon''*\omega$ Plot for 180°C Calibration	120
5.16	G′ and G″ vs. Time for PR500 Isothermal Cure @ 180°C	121
5.17	α and log η vs. log $\epsilon''*\omega$ for 160°C Calibration	122
5.18	α and log η vs. log $\epsilon''*\omega$ for 170°C Calibration	123
5.19	α and log η vs. log $\epsilon''*\omega$ for 180°C Calibration	124
5.20	Slope $(d\epsilon''/dt)/\epsilon''$ and α vs. Time for 190°C	125
5.21	Slope $(d\epsilon''/dt)/\epsilon''$ and α vs. Time for 200°C	126
5.22	Slope $(d\epsilon'/dt)/\epsilon'$ and α vs. Time for 190°C	127
5.23	Slope $(d\epsilon'/dt)/\epsilon'$ and α vs. Time for 200°C	128
6.1	DSC Ramp of E905L from 50° to 300°C @ 5°C/min	136
6.2	Ln$[d\alpha/dt/(1-\alpha)^n]$ vs. 1/T for High Temperature Ramp of E905L @ 5°C/min	137
6.3	Ln$[d\alpha/dt/(1-\alpha)^n]$ vs. 1/T for High Temperature Ramp of E905L @ 2°C/min	138

LIST OF FIGURES (continued)

6.4	α vs. Time Plot for E905L Isothermal Cure @ 110°C	139
6.5	α vs. Time Plot for E905L Isothermal Cure @ 120°C	140
6.6	α vs. Time Plot for E905L Isothermal Cure @ 130°C	141
6.7	α vs. Time Plot for E905L Isothermal Cure @ 180°C	142
6.8	α vs. Time Plot for E905L Isothermal Cure @ 190°C	143
6.9	α vs. Time Plot for E905L Isothermal Cure @ 215°C	144

ACKNOWLEDGEMENTS

The writer wishes to express her sincere appreciation to Dr. David Kranbuehl for his guidance and understanding throughout her undergraduate and graduate research. The author would also like to thank Dr. William Starnes and Dr. Gary Rice for their careful reading and criticism of the manuscript. The author would like to recognize Maria Argiriadi and the undergraduates, who assisted in setting up experiments and performing various calculations, and NASA Langley Research Center for their partial support of this project. A thank you is also owed to Michael Gibson and my family for supporting me throughout this past year.

ABSTRACT

This thesis investigates the morphological, kinetic, electrical and rheological properties of three epoxy resins during their cure in order to answer questions about the ideal processing conditions of these high performance resins.

Chapter I reviews the chemistry of epoxy resins and considers the three experimental resins discussed in this investigation, Research Resin RSL 1895 with Curing Agent® W, PR500 Epoxy Resin, and E905L Triazine Epoxy Resin.

Chapter II discusses the primary characterization method used in this analysis, Differential Scanning Calorimetry. This method provided information about the curing reaction of each of the resins.

Chapter III explores the second characterization method, Frequency Dependent Electromagnetic Sensing (FDEMS). This method provided a means to monitor the cure processing properties of the experimental resins. This chapter also discusses the Resin Transfer Molding process for which all these resins were developed.

Chapter IV describes the characterization of Research Resin RSL 1895/Curing Agent® W. This includes the development of a kinetic model, the correlation of macromolecular quantities α and η with the micromolecular quantity $\epsilon''*\omega$, and the correlation of these quantities with dielectric sensor output from RTM experiments.

Chapter V describes a similar characterization process for the PR500 epoxy resin system, but does not discuss the correlation of dielectric sensor output with RTM experiments.

Chapter VI describes the kinetic analysis of a complex curing reaction. In this analysis, kinetic models were developed for the high and low temperature reaction.

CHARACTERIZATION OF EPOXY RESINS FOR USE IN THE RESIN TRANSFER MOLDING PROCESS

Chapter I

Chemistry of Epoxy Resins

An epoxy resin is a group of oligomeric molecules containing one or more epoxy groups that can be converted to a thermoset form.[1,2] An epoxy, or epoxide, group is composed of an oxygen bonded to two adjacent carbons to form a three membered ring (Fig. 1.1).

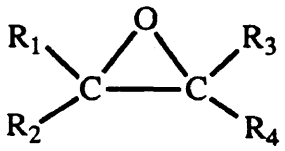

Figure 1.1

The strained and polar nature of the epoxy ring causes these resins to be highly reactive. Epoxy resins thus have the versatility of reacting with a variety of compounds.

Cured epoxy resins exhibit a wide range of properties that justify their use in high performance products. One of the most recognized properties is excellent adhesion to numerous substrates and reinforcements. This produces strong and durable composites. The low shrinkage of epoxy resins upon cure explains the phenomenal adherence of these resins[2]. The characteristic of low shrinkage minimizes

stresses that could possibly weaken the structure. Epoxy resins also display superior mechanical and electrical properties that are maintained even during severe operating conditions[2]. Thermal stability, good chemical and solvent resistance, and low moisture uptake are additional properties which have contributed to the success of epoxy resins in industry.

Another important advantage of epoxy resins is the ability to tailor them to meet manufacturer's specifications. Resins can exhibit varying properties by merely adjusting the backbone type (aliphatic, cycloaliphatic, or aromatic), curing agent, curing temperature, and/or degree of cross-linking. These factors control properties like the toughness, chemical flexibility and hardness, adhesive strength, and electrical resistance of resins[3]. Other materials can be included in a resin to assist in processing or to modify the end properties of the resin. These constituents can be fillers, solvents, diluents, plasticizers, or accelerators[2].

History

Epoxy resins were first synthesized by Pierre Castan of Switzerland and Sylvan Greenlee of the United States. In 1936 Castan synthesized an epoxy resin based on bisphenol-A and epichlorohydrin (Fig. 1.2).

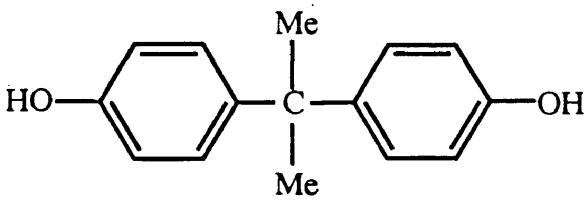

Bisphenol A

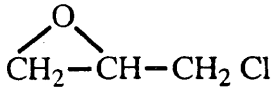

Epichlorohydrin

Figure 1.2

He found that when combined with phthalic anhydride the resin produced a thermoset, or crosslinked material[4]. At Devoe-Raynolds, Greenlee investigated similar compounds to produce high molecular weight resins later used in coatings[5]. These discoveries were the basis for the production of many epoxy resins.

Early applications for epoxy resins were in coatings and encapsulating of electrical and electronic components. Epoxy resins have since been applied to a variety of industries. In 1983 the United States sold 135 metric tons of epoxy resins. A majority of these resins (55%) were used for composites, adhesives, laminants, tooling, casting and molding[4]. In recent years, epoxy resins have become the predominant type of resin used for aerospace technology.

Synthesis

Epoxy resins can be prepared by either of two possible reactions. In one reaction, compounds with an active hydrogen are reacted with epichlorohydrin followed by

dehydrohalogenation (Fig. 1.3).

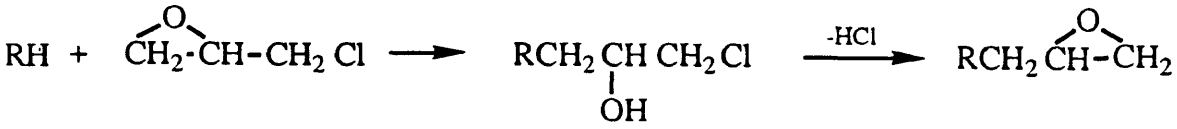

Figure 1.3

The second reaction involves the direct epoxidation of olefins by peracids (Fig. 1.4)[4].

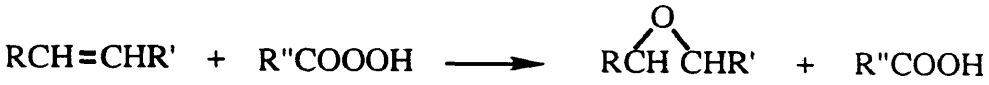

Figure 1.4

The most commonly used epoxy resins are based on the difunctional molecule, diglycidyl ether of bisphenol A (DGEBA) (Fig. 1.5)[2].

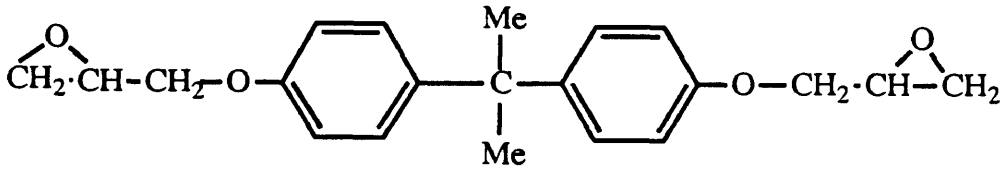

DGEBA

Figure 1.5

DGEBA is synthesized from the condensation of epichlorohydrin and bisphenol A in the presence of NaOH via a two-step reaction. First, the base catalyzes the nucleophilic cleavage of the epichlorohydrin epoxide to produce the chlorohydrin intermediate (Fig. 1.6).

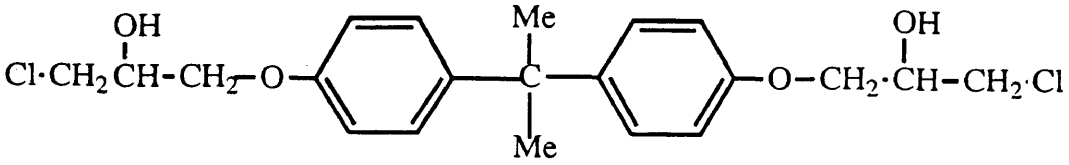

Chlorohydrin Intermediate

Figure 1.6

In the second step, the chlorohydrin intermediate is dehydrohalogenated to produce DGEBA. The hydrochloric acid formed in the reaction is neutralized with NaOH. In practice the two steps occur simultaneously. This allows DGEBA to be formed before all the bisphenol A molecules are consumed. The bisphenol hydroxyl groups are thus enabled to attack the epoxide resin DGEBA instead of the epichlorohydrin epoxy groups. In order to obtain high yields of the monomeric DGEBA, bisphenol A is added to an excess of epichlorohydrin accounting for the possibility of side reactions[4].

The neat resin is cured, or crosslinked, by a curing agent to form a high molecular weight, three-dimensional network[6]. The curing reaction entails the opening of an epoxide ring followed by the addition of the oligomers. This reaction typically occurs through an anionic or cationic mechanism.

Curing agents are substances that initiate the polymerization reaction and influence the development of the crosslinked network. There are two types of curing agents: catalytic and coreactive. If the curing agent is not

permanently affected by the reaction and causes the homopolymerization of the epoxide oligomers, it is catalytic. However, if the curing agent acts as a bridge for cross-linking several molecules, then it is coreactive.

Catalytic curing agents are usually Lewis acids or bases. They act as "catalysts" by promoting and/or accelerating the reaction between the epoxide oligomers. Figure 1.7 shows a simple homopolymerization reaction.

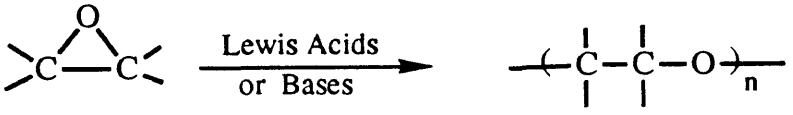

Figure 1.7

The use of difunctional and multifunctional epoxy resins in the homopolymerization reaction results in a three-dimensional, crosslinked network. Two commonly used catalysts are tertiary amines and monoethylamine boron trifluoride[3].

Coreactive curing agents are typically amines or acid anhydrides. They react by opening the epoxy ring ionically and adding onto the oligomer. Figure 1.8 is an example of the reaction using an amine curative.

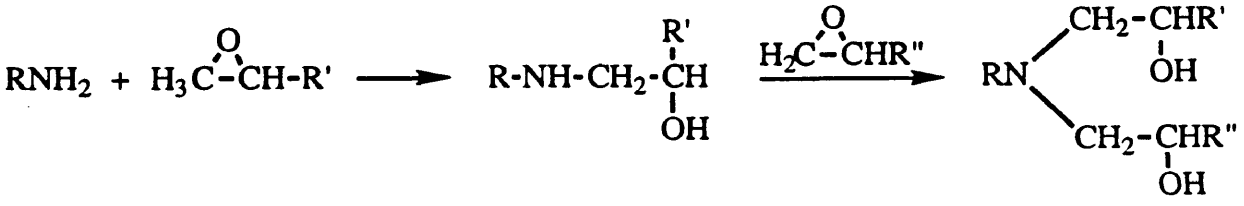

Figure 1.8

The secondary amine formed reacts with other epoxides but at a much slower rate[4]. To a lesser extent, the secondary hydroxyl group can add onto the epoxide oligomers. The etherification reaction is shown in Figure 1.9.

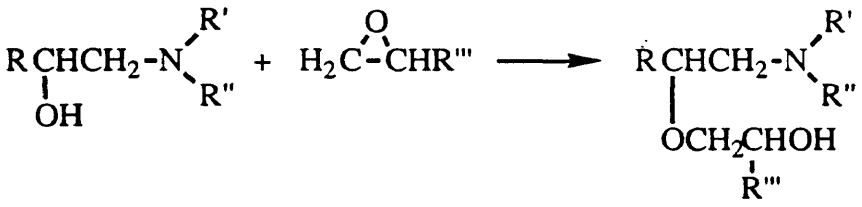

Figure 1.9

As hydroxyl groups accumulate in the reaction, the epoxy-amine curing takes on an autocatalytic character. The hydroxyl groups promote the reaction between the amine and epoxy groups through the formation of a trimolecular transition state (Fig. 1.10)[7].

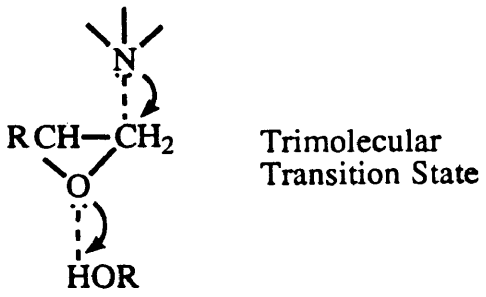

Figure 1.10

This allows the epoxide to become more susceptible to nucleophilic attack by the amine curing agents.

There are three types of amines typically considered

for curing agents: aliphatic, cycloaliphatic and aromatic. Aliphatic amines react rapidly with the epoxides causing the resin to be cured at room temperature. Cycloaliphatic amines being more hindered react sluggishly and typically require heat for curing. Aromatic amines such as 4,4'-diaminodiphenyl sulfone (DDS) and p,p'-methylene dianiline (MDA) need moderate temperatures to cure and typically must be melted from the solid state into the epoxy. While they cure at higher temperatures, aromatic amines have longer working lives and are used in many composites.

Acid anhydrides produce excellent high temperature properties in the cured resin. There is a low incidence for exotherms and lower toxicity than for amine resins. In order to avoid long cure times associated with acid anhydrides, tertiary amines can be added to reduce the processing time[2]. Phthalic anhydride and tetrahydrophthalic anhydride (HET) are two commonly used curing agents.

High Performance Resins

Bisphenol-A based resins, such as DGEBA, are generally insufficient for use as high performance epoxy resins. In aerospace applications, for example, the cured resin must withstand temperatures of 180° to 200°C. This is achieved by creating resins with glass transition temperatures (T_g) above their use temperature. Since T_g is related to the

crosslink density of the material, increasing the functionality of the monomers increases the density and in effect the T_g. This explains why multifunctional epoxy resins such as novolacs, multifunctional phenols or diamines are used to obtain high performance capabilities. In previous years, the tetrafunctional resins such as N,N, N'N'-tetraglycidyl-4,4'- diaminodiphenylmethane (TGMDA), cured with DDS, were employed in high temperature composites (Fig. 1.11).

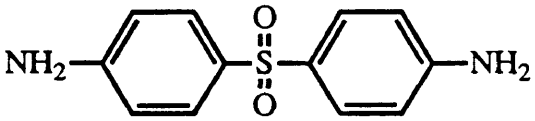

DDS

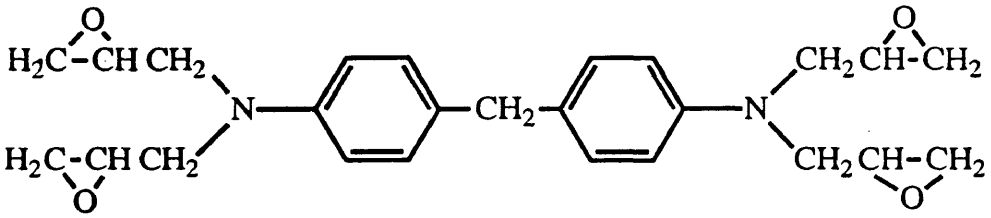

TGMDA

Figure 1.11

TGMDA is sold under the trade name Araldite MY 720 by Ciba-Geigy and was used in several high performance resins such as Hercules 3501-6.

The poor hot/wet performance and brittleness of the cured TGMDA/DDS resin system have since led to the development of new resins[2]. Recently, Shell Chemical Company produced a tetraglycidyl amine Epon HPT resin 1071 that exhibits superior hot/wet performance when cured with aromatic amines (Fig. 1.12).

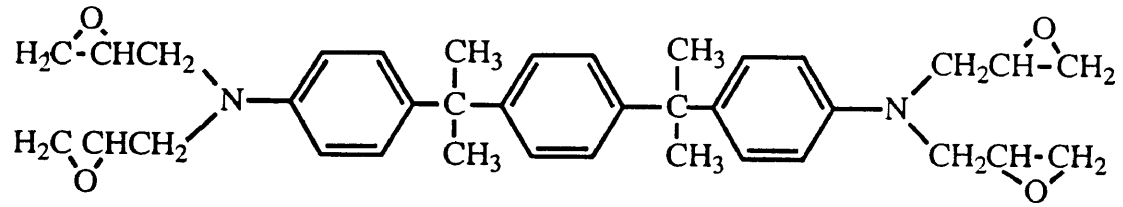

Epon HPT resin 1071

Figure 1.12

The tetrafunctionality of the resin increases the crosslink density of the product, while the incorporation of an additional aromatic ring in the backbone improves the rigidity of the structure. The most important difference, however, is the lower levels of moisture absorption that allows for the increased strength and fracture resistance of the final product[2,8].

Epoxy Research Resin RSL-1895/EPON CURING AGENT® W

Shell Chemical Company's epoxy research resin RSL 1895/Epon Curing Agent® W is a high performance resin system specifically designed for use in resin transfer molding (RTM) and filament winding processes. This resin system provides a superior combination of stiffness, temperature resistance and processability.

Epoxy Research Resin RSL-1895 contains epoxy resins A, B and C with a proprietary additive. These resins are described as a combination of difunctional and

multifunctional epoxy resins. The multifunctional epoxy resin is based on the glycidyl amine Epon HPT Resin 1071 (Fig. 1.12)[9]. Due to the proprietary nature of these resins, the exact structures are not available.

The second component Epon Curing Agent® W is described as a non-MDA, aromatic amine curing agent. It contains 100% diethyl toluene diamine (DETDA)[9]. Figure 1.13 is a possible structure for DETDA.

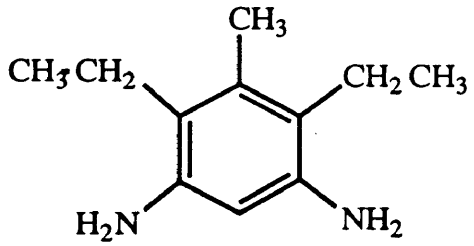

Figure 1.13

The epoxy resins and curing agent are mixed in the ratio of 100/33.5 by weight. The aromatic amine is a comonomer in the curing reaction with the difunctional and multifunctional epoxide oligomers. In the curing reaction the amino hydrogens on DETDA are replaced by the epoxy oligomers, similar to the reaction in Figure 1.8. The amine group nucleophilically attacks the epoxide oligomer resulting in the cleavage of the epoxy ring and addition of the oligomer to the amine curative. This reaction continues until all the epoxides are consumed. When difunctional and multifunctional epoxies and curing agents are used, the reaction results in the formation of a highly crosslinked, tough solid.

PR500 Epoxy Resin

PR500 resin system is a one-part epoxy resin developed by 3M for use in aerospace RTM composite parts. This high performance resin system has a number of advantages. First, as a one-part epoxy there is no mixing involved in the preparation of the resin for RTM processing. This eliminates the potential for mistakes by providing total assurance of the resin to curative ratio. The combination of a high viscosity resin and curatives remain unreacted at room temperature. As the resin is heated, the viscosity decreases dramatically allowing the resin and curative to interact. The most important advantage, however, is the formulation of PR500 resin. The incorporation of high viscosity and high performance components allows for a higher T_g and modulus to be built into the resin[10].

PR500 epoxy resin is based on the diglycidyl ether of fluorene bisphenol (Fig. 1.14)[10].

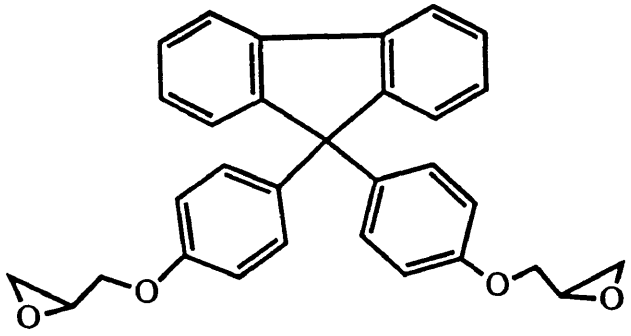

Figure 1.14

The fluorene group enhances the properties of the resin by introducing a rigid structure pendant on the polymer backbone. These resins, therefore, produce tough, lightly crosslinked networks with high T_g as a result of the backbone structure. Derivatives of diglycidyl ether of fluorene bisphenol impart several desirable properties to the resultant polymer including thermal stability, improved solubility, and increased temperature performance[11].

Fluorene bisphenol oligomers can be synthesized by dissolving fluorenone in an excess of a phenol or aromatic amine. A strong protic acid is used to catalyze the reaction[11]. The fluorene bisphenol can then be converted to a glycidyl ether by reactions with epichlorohydrin as previously discussed.

PR500 resin system contains the following ingredients: 35-50% non-MDA aromatic amine curative, 30-40% epoxy resin C.A.S# 1675-54-3, 10-20% aromatic diglycidyl ether, and 1-10% epoxy resin C.A.S.# 5026-74-4[12]. The structures of these components have not been disclosed for proprietary reasons.

E905L Triazine Epoxy Resin

British Petroleum Chemicals' E905L is a triazine-epoxy amine resin. E905L has ideal processing properties along with high performance mechanical properties as the result of

a two-stage reaction process. E905L resin system is prepared by mixing the two components in 50/50 ratio by weight. The resin was found to be highly exothermic upon heating. Additionally, it is recommended that the resin should never be heated in bulk over 180°F[13].

Part A of the resin is composed of a mixture of medium and low molecular weight triazine resins. The triazine resins are present in the ratio of 70/30 percent by weight, respectively[13]. A triazine resin is a group of oligomers containing a reactive cyanate group on an aromatic ring[14]. A structure for the triazine is illustrated in the figure below.

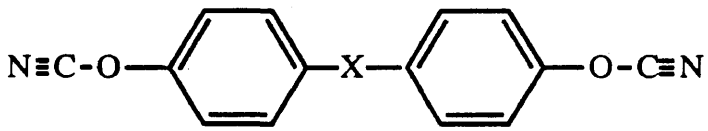

Figure 1.15

A crosslinked polymer is formed by heating the dicyanate oligomers or monomers. Initially, the R-OCN functionality undergoes a cyclotrimerization reaction to form a trisubstituted triazine ring, prepolymer resin (Fig. 1.16).

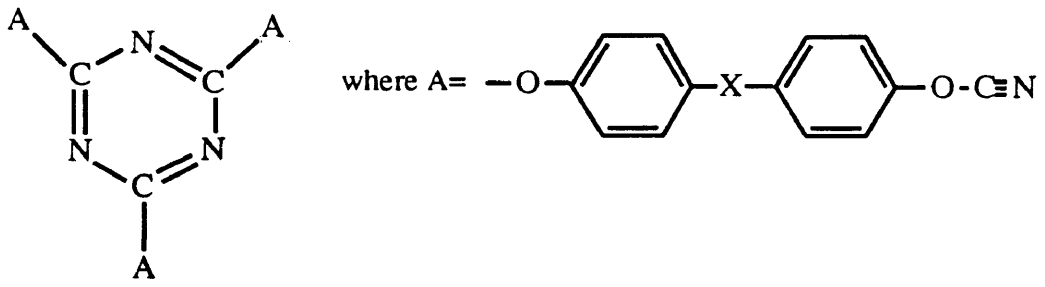

Figure 1.16

Continued heating stimulates reactions among the cyanate groups to form other triazine rings[14]. This eventually results in the formation of a crosslinked solid (Fig. 1.17).

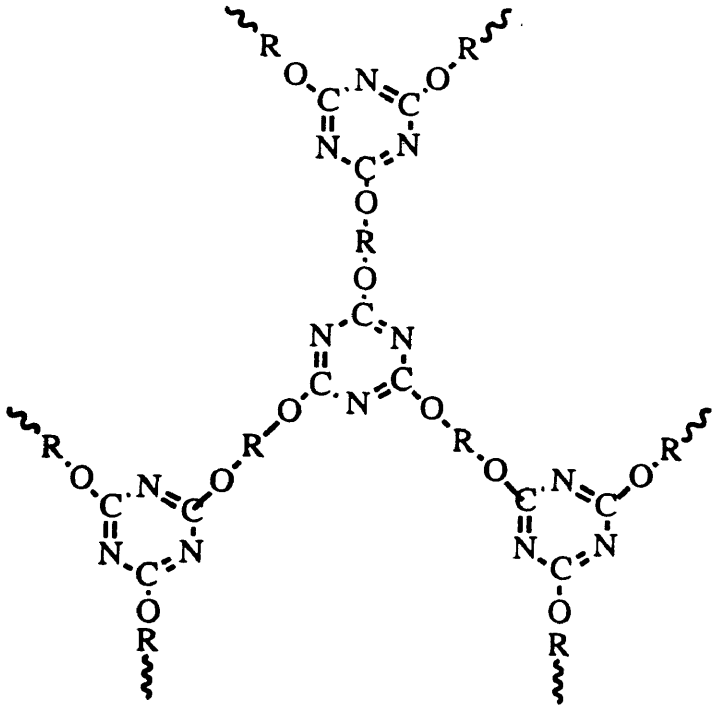

Figure 1.17

This process can be stopped in order to recover stable oligomers. Thus low and medium molecular weight triazine resins are found as limited networks of trisubstituted triazine ring systems.

Component B is a mixture of three constituents. The main ingredient, 75±10% by weight, is the diglycidyl ether of bisphenol A (Fig. 1.18).

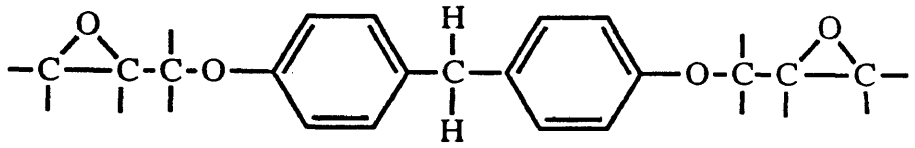

Figure 1.18

The second constituent is an amine epoxy toughening agent similar to the structure below.

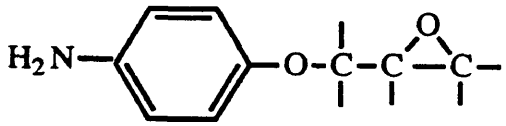

Figure 1.19

The final ingredient is an organometallic catalyst that is present at less than 1% by weight[13].

Chapter I References

1. Drzal, L. T., "The Interphase in Epoxy Composites," **Epoxy Resins and Composites II**, Springer-Verlag, Berlin, 1986.

2. Bauer, R. S., "Epoxy Resins," *International Encyclopedia of Composites*, Vol. 2, VCH Publishers Inc., New York, 1990.

3. Bauer, R. S., "Curing Agents," *International Encyclopedia of Composites*, Vol. 1, VCH Publishers Inc., New York, 1990.

4. Mark, Bikales, Overberger, Menges, "Epoxy Resins," **Encyclopedia of Polymer Science and Engineering**, Vol. 6, John Wiley and Sons, 1985.

5. Lee, H., Neville, K., **Handbook of Epoxy Resins**, McGraw-Hill Book Company, New York, 1967.

6. Kamon, T., Furukawa, H., "Curing Mechanisms and Mechanical Properties of Cured Epoxy Resins," **Epoxy Resins and Composites IV**, Springer-Verlag, Berlin, 1986.

7. Rozenberg, B. A., "Kinetics, Thermodynamics and Mechanism of Reactions of Epoxy Oligomers with Amines," **Epoxy Resins and Composites II**, Springer-Verlag, Berlin, 1986.

8. Shell Chemical Company "Preliminary Technical bulletin-Epon HPT® Resin 1071/Research Curing Agent RSC-12461/Research Curing Agent RSC-1327."

9. Shell Chemical Company "Preliminary Technical Bulletin-Epoxy Research Resin RSL-1895/Epon Curing Agent® W."

10. Hackett, S.C. "A Perspective on resins for Aerospace RTM," 3M Aerospace Department, 1991.

11. Bauer, R. S., "Epoxy Resins, Fluorene Systems," *International Encyclopedia of Composites*, Vol. 2, VCH Publishers Inc., New York, 1990.

12. 3M Aerospace Materials Department, "Material Safety Data Sheet."

13. HITCO Materials Division, U.S. Polymeric, "Materials Safety Data Sheet."

14. Bauer, R.S., "Cyanate Ester Resins," *International Encyclopedia of Composites*, Vol. 1, VCH Publishers Inc., New York, 1990.

Chapter II

Differential Scanning Calorimetry

Differential Scanning Calorimetry is a thermal analysis technique routinely used in the characterization of polymer resins. This useful technique provides information about the properties of a polymer such as glass transition temperature, thermal degradation, extent of polymerization and enthalpy of reaction.

A Differential Scanning Calorimeter, DSC, is an instrument that simultaneously measures the difference in heat transferred between two calorimetric cells while monitoring heat transfer as a function of time or temperature[1,2,3]. A resin sample and an inert reference are placed in individual cells, each containing a temperature sensor and a heating device.

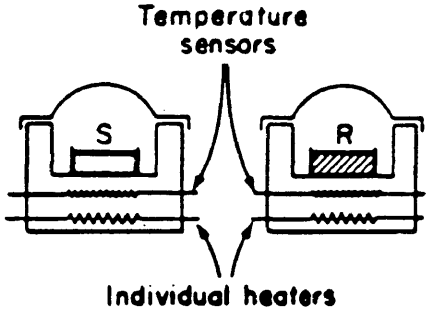

Figure 2.1

The two cells are maintained at a zero temperature difference by either adding heat to the sample cell for an endothermic reaction or to the reference for an exothermic reaction. The power differential required to sustain the programmed time-temperature process is recorded as the ordinate with time or temperature as the abscissa. Figure 2.2 is the curve recorded for a temperature ramp from 50° to 300°C at a rate of 2°C per minute.

The area under the curve is directly related to the enthalpic changes occurring in the sample. By integrating the area under the curve from 0 to the total run time, it is possible to accurately determine the heat of reaction, H_R.

[2-1] $$H_R = \int (dQ/dt)dt$$

The heat of reaction in Figure 2.2 was 314.574 Joules per gram.

The extent of polymerization, or degree of cure, is determined by

[2-2] $$\alpha = H/H_R$$

where H is the amount of heat generated by the reaction at a given time, t. The rate of reaction, $d\alpha/dt$, also can be resolved from the experimental data as follows:

[2-3] $$d\alpha/dt = (dQ/dt)/H_R$$

The combination of these three parameters, heat of reaction, α, and $d\alpha/dt$, can be used to describe the progression of the curing reaction over time or changing temperature.

Experimental

For this analysis, a Perkin Elmer DSC-7 instrument combined with a 7500 series professional computer was used to carry out DSC experiments. Aluminum pans were filled with 7 to 10 mg of the epoxy resin and then sealed with a crimper. A hole was punched in the top of the pan to allow for the release of any volatiles. The reference was a cured resin sample for isotherms or an empty aluminum pan for ramps.

Isotherms were completed for each of the epoxy resins at the selected temperatures. Figure 2.3 is the trace of a 160°C isotherm for 4 hrs. The isotherms were immediately followed by a ramp of the cured resin to obtain any residual heat not evolved during the isotherm (Fig. 2.4). The residual heat was combined with the heat of reaction gives the total heat of reaction, H_R. Isothermal and ramp data were converted to ASCII files and inserted into respective integration programs. The heat of reaction for each of the runs was obtained by dividing the area to be integrated into several rectangles. The integration programs were then used to transform the raw data, heat flow, time, and temperature, into the heat of reaction, α, and $d\alpha/dt$.

Kinetic Analysis Methods for Epoxy-Amine Resins

Modeling the processing of epoxy based composites has become a primary interest in the optimization of high quality parts and in the design of cure cycles. By understanding the mechanism and kinetics of the cure reaction, the network morphology of a resin can be determined such that the mechanical and physical properties of the cured composite can be enhanced[4,5]. While the epoxy-amine reaction has already been described, the goal now is to develop a kinetic model to reflect the mechanism of the curing reaction.

The progression of the epoxy-amine reaction is described quantitatively in terms of the fraction of converted epoxide groups, α. A kinetic model is typically expressed in terms of $d\alpha/dt$ as a function of α and temperature. Several equations have been proposed as models for the epoxy-amine reaction.

Horie et al. developed a model to describe the reaction kinetics between an epoxy and a primary amine[4].

[2-4] $$d\alpha/dt = (k_1 + k_2\alpha)(1-\alpha)(\beta-\alpha)$$

In this equation, separate rate constants, k_1 and k_2, were derived to explain the autocatalytic nature of the reaction. The rate constant k_1 represented the reaction catalyzed by groups initially present in the resin, while k_2 was the rate constant for the reaction catalyzed by the accumulated

hydroxyl groups formed later in the reaction. The parameter β was determined as the ratio of nitrogen-hydrogen bonds to epoxide rings initially present in the resin. While the possibility of other reactions was not considered in the model, application of this equation to experimental resins was limited[4].

The most widely used thermoset polymers in the fabrication of advanced composites consist of epoxy resins cured with aromatic amines. These polymers require high curing temperatures and an excess of epoxides to react, making them prone to etherification reactions. In this case, the Horie model is ineffective. Unfortunately, the attempts to include the etherification reactions have resulted in mathematics too complex to yield an exact equation[4].

Kamal et al. developed a modified version of the Horie model that makes it possible to obtain a good fit of experimental data[6,7].

[2-5] $$d\alpha/dt = (k_1 + k_2\alpha^m)(1-\alpha)^n$$

The parameters m and n are known as the reaction order and are generally temperature dependent. Although the Kamal model does not provide a clear description of the chemistry or curing reaction, it can accurately predict the kinetic behavior of the reaction when the Horie equation is ineffective[4].

Following the determination of an equation best suited

for the epoxy-amine reaction, kinetic parameters must be estimated to fit the experimental rate data to the kinetic model. Three methods employed to estimate kinetic parameters will be discussed as a basis for the technique used in this investigation. They are the Lam technique[8], the Ryan-Dutta technique[9] and non-linear least squares analysis.

In the Lam analysis technique, the Kamal model was simplified to readily obtain estimates of the kinetic parameters[8].

[2-6] $$d\alpha/dt = k\alpha^m (1-\alpha)^n$$

$$\text{where } m + n = 2$$

Patrick Lam proposed that the contribution made by k_1 was negligible and the values of m and n could be summed to 2[6]. By differentiating the Lam model with respect to α and setting it equal to zero, a equation for the maximum degree of cure was determined.

[2-7] $$\alpha_{max} = m/2$$

This equation was then substituted back into the Lam model that was subsequently divided by α^2 and rearranged to give the resulting equation:

[2-8] $$\ln [(d\alpha/dt)(1/\alpha^2)] = \ln k + (n * \ln[(1-\alpha)/\alpha])$$

Using experimental α data, the values of k, m and n are determined from a plot of $\ln[(d\alpha/dt)(1/\alpha^2)]$ versus $\ln[(1-\alpha)/\alpha]$. The slope and y-intercept provide values for n and ln k, respectively. The value of m can be determined from

n. The Lam model provided initial estimates of the parameters; however, there was no theoretical reasoning found to support restricting values of m and n[10].

Similarly, M. E. Ryan and A. Dutta investigated a technique to rapidly estimate kinetic parameters for the Kamal model. They maintained that the maximum rate of reaction was the limiting factor in predicting the behavior of an autocatalytic reaction[9]. In the Ryan-Dutta analysis, equations were derived to determine m, n and k,

$$[2\text{-}9] \quad m = \{\ln[d\alpha/dt/(1-\alpha_p)^n - k_1/2\text{-}mk_0\alpha_p(1-m)](m-2\alpha_p)\}/\ln \alpha_p$$

$$[2\text{-}10] \quad k_1 = [(2-m)k_0\alpha_p(1-m)]/(m-2\alpha_p)$$

$$[2\text{-}11] \quad n = 2-m$$

where α_p is the degree of cure at the maximum rate of reaction. Thus, the value of m can be used to determine k_1. Due to the intrinsic dependence on the peak of the autoacceleration cure, it most accurately estimated the time to the maximum rate of reaction but overestimated other parts of the curve[10].

In the non-linear least squares fitting method, experimental values of α and $d\alpha/dt$ were read into a statistics program. Combinations of k_1, k_2, m and n were evaluated using the Kamal model. The combination yielding the smallest loss value was iterated by small amounts until the loss converged. The best fit was obtained when k_1 was neglected, indicating that the term is not significant[10].

These fitting techniques were primarily used to provide

initial estimates of the parameters for a given model and resin. Choosing a technique that provides the best ball-park figure will ultimately influence the accuracy of the final values of these kinetic parameters[9].

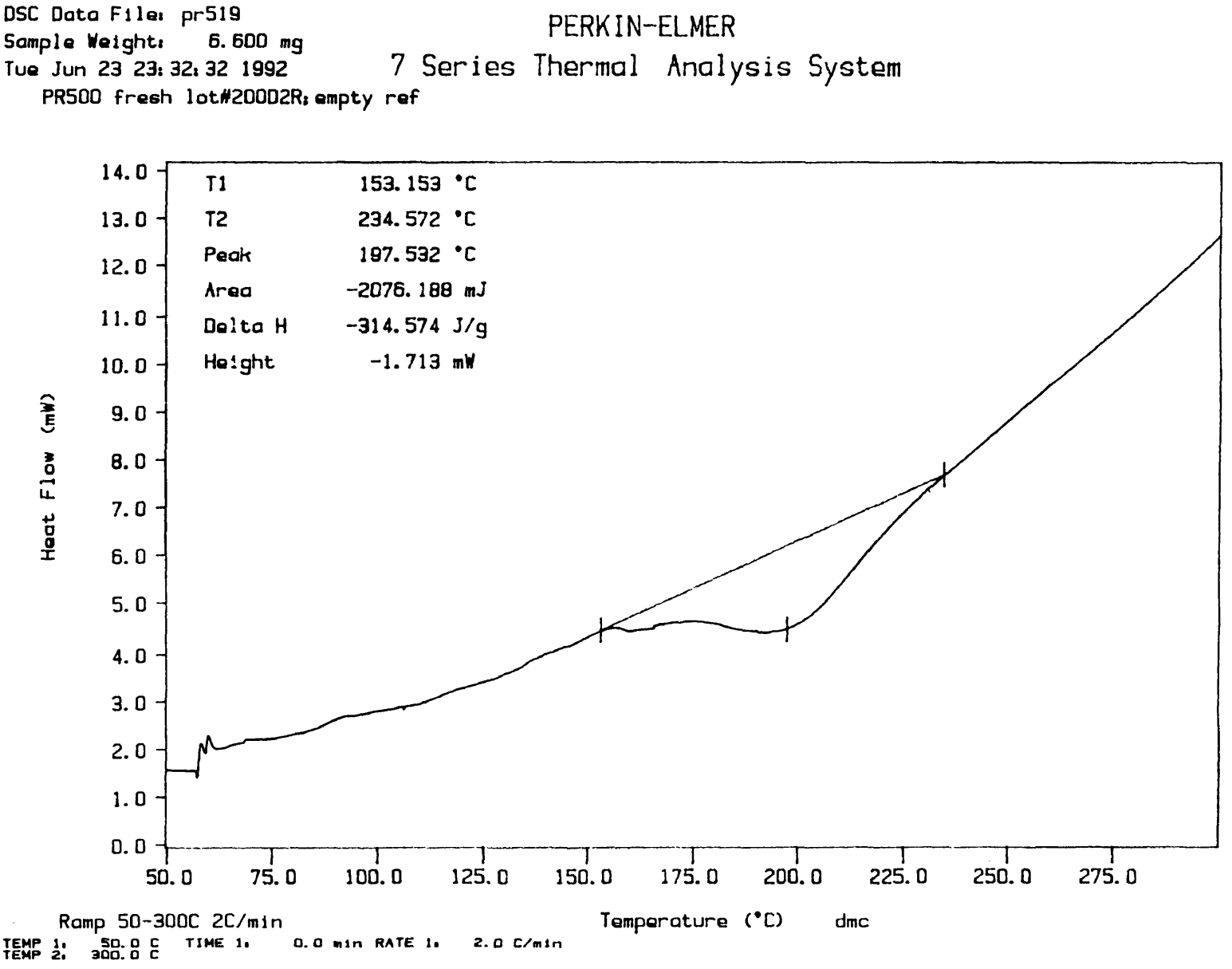
DSC Data File: pr519
Sample Weight: 6.600 mg
Tue Jun 23 23:32:32 1992
PR500 fresh lot#20002R; empty ref
PERKIN-ELMER
7 Series Thermal Analysis System
T1 153.153 °C
T2 234.572 °C
Peak 197.532 °C
Area -2076.188 mJ
Delta H -314.574 J/g
Height -1.713 mW
Heat Flow (mW)
14.0
13.0
12.0
11.0
10.0
9.0
8.0
7.0
6.0
5.0
4.0
3.0
2.0
1.0
0.0
50.0
75.0
100.0
125.0
150.0
175.0
200.0
225.0
250.0
275.0
Ramp 50-300C 2C/min
Temperature (°C) dmc
TEMP 1: 50.0 C TIME 1: 0.0 min RATE 1: 2.0 C/min
TEMP 2: 300.0 C

Figure 2.2

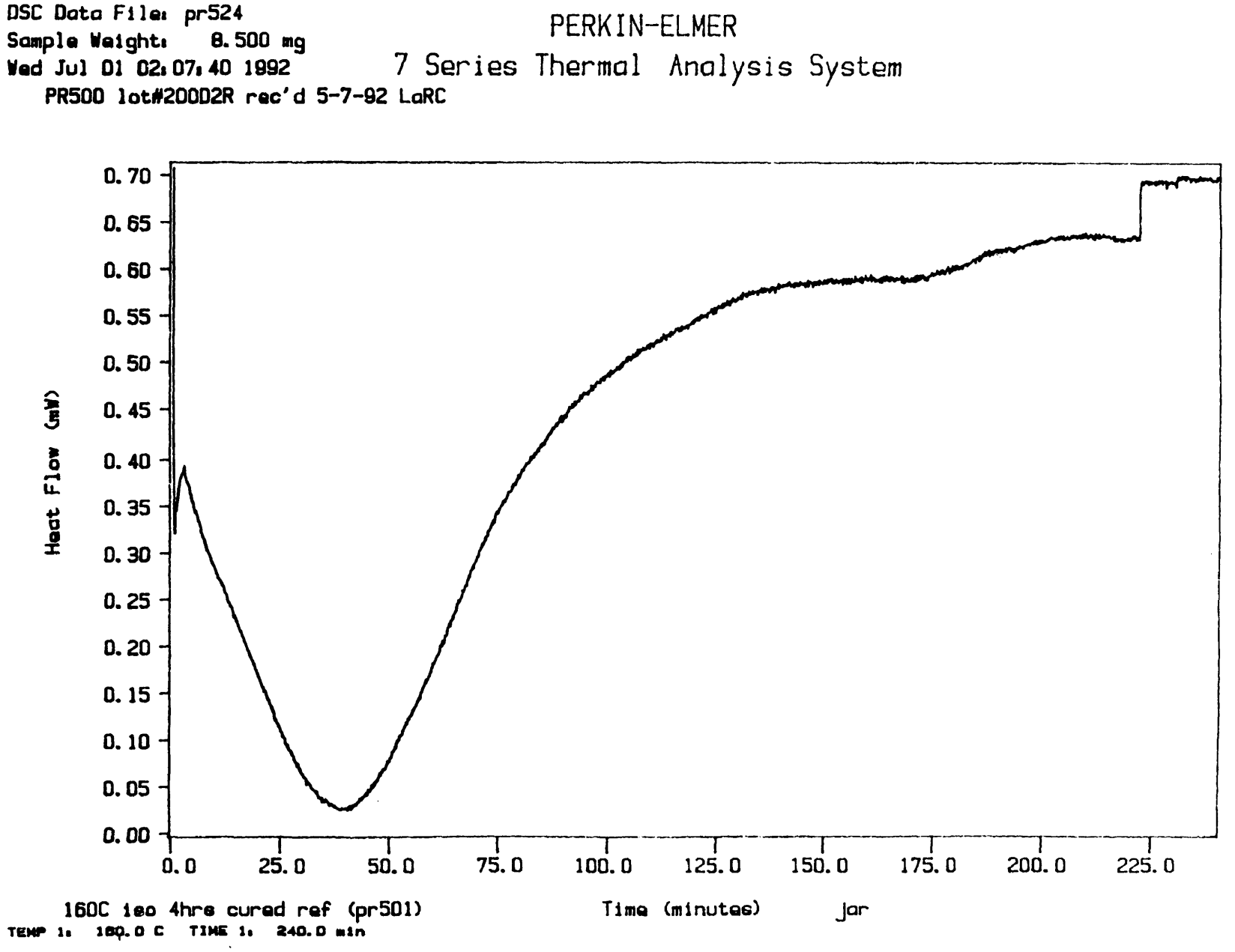
DSC Data File: pr524
Sample Weight: 8.500 mg
Wed Jul 01 02:07:40 1992
PR500 lot#200D2R rec'd 5-7-92 LaRC
PERKIN-ELMER
7 Series Thermal Analysis System
Heat Flow (mW)
0.70
0.65
0.60
0.55
0.50
0.45
0.40
0.35
0.30
0.25
0.20
0.15
0.10
0.05
0.00
0.0
25.0
50.0
75.0
100.0
125.0
150.0
175.0
200.0
225.0
160C iso 4hrs cured ref (pr501)
Time (minutes)
Jar
TEMP 1: 180.0 C TIME 1: 240.0 min

Figure 2.3

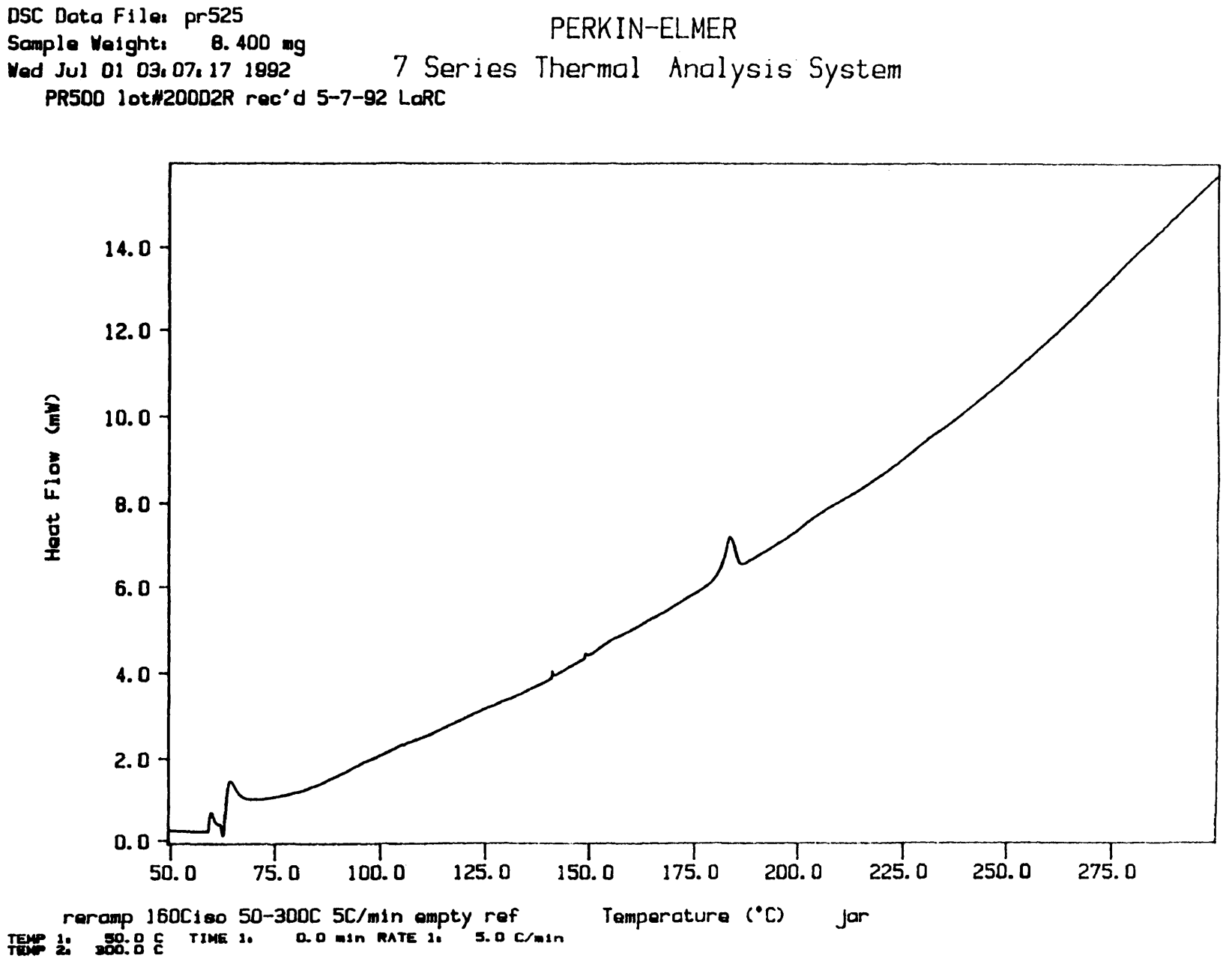
DSC Data File: pr525
Sample Weight: 8.400 mg
Wed Jul 01 03:07:17 1992
PR500 lot#200D2R rec'd 5-7-92 LaRC
PERKIN-ELMER
7 Series Thermal Analysis System
Heat Flow (mW)
14.0
12.0
10.0
8.0
6.0
4.0
2.0
0.0
50.0
75.0
100.0
125.0
150.0
175.0
200.0
225.0
250.0
275.0
reramp 160Ciso 50-300C 5C/min empty ref
Temperature (°C)
jar
TEMP 1: 50.0 C TIME 1: 0.0 min RATE 1: 5.0 C/min
TEMP 2: 300.0 C

Figure 2.4

References for Chapter II

1. Bares, J., Billmeyer, F. W. Jr., Collins, E. A., **Experiments in Polymer Science**, John Wiley & Sons Inc., New York, 1973.

2. Wunderlich, Bernard, **Thermal Analysis**, Academic Press Inc., Boston, 1990.

3. Campbell, D., White, J. R., **Polymer Characterization Physical Techniques**, Chapman and Hall, New York, 1989.

4. Cole, K. C., "A New Approach to Modeling the Cure Kinetics of Epoxy Amine Thermosetting Resins. 1. Mathematical Development," *Macromolecules*, Vol. 24, 1991.

5. Mijovic, J., Fishbain, A., Wijaya, J., "Mechanistic Modeling of Epoxy-Amine Kinetics. 1. Model Compound Study," *Macromolecules*, Vol. 25, 1992.

6. Kamal, M. R., Sourour, S., "Kinetics and Thermal Characterization of Thermoset Cure," *Polymer Engineering and Science*, Vol. 13, No. 1, 1973.

7. Kamal, M. R., "Thermoset Characterization for Moldability Analysis," *Polymer Engineering Science*, Vol. 14, No.3, 1974.

8. Lam, P. W., "The Characterization of Thermoset Cure Behavior by Differential Scanning Calorimetry: Part 1 Isothermal and Dynamic Study," *Polymer Composites*, Vol. 18, No. 5, 1987.

9. Ryan, M. E., Dutta, A., "Kinetics of Epoxy Cure: a Rapid Technique for Kinetic Parameter Estimation," *Polymer*, Vol. 20, 1979.

10. Tully, Patricia, Masters Thesis, "Dielectric and Kinetic Analysis of Thermosetting Polyester Resin," College of William and Mary, 1989.

Chapter III

FDEMS Cure Monitoring

Frequency Dependent Electromagnetic Sensing (FDEMS) is a convenient, nondestructive cure monitoring technique used to characterize the processing properties of thermoset resins. Impedance measurements taken over the hertz to megahertz range are used to examine the chemical and physical changes occurring throughout the polymerization reaction. FDEMS is one of a few techniques that can continuously monitor the cure process in-situ as the resin changes from an oligomeric liquid to a crosslinked, insoluble solid[1]. FDEMS is capable of monitoring several curing properties, including the reaction onset, point of maximum flow, degree of cure, Tg, reaction completion, solvent evolution, variations due to resin age or vendor batch, and moisture uptake[2].

In this investigation, FDEMS was used to evaluate and control resin properties prior to use. The relationship between the dielectric sensor output, ϵ' and ϵ'', and the cure processing properties were therefore characterized for each of the resin systems. An understanding of this relationship was essential in order to intelligently control

the cure process of a given resin system.

Theory

A sensor was used to measure the geometry dependent capacitance, C, and conductance, G, from the dielectric impedance of the experimental resin. The intensive geometry-independent complex permittivity, ϵ^*, was then determined by [3-1] $\epsilon^* = \epsilon' - i\epsilon''$ where ϵ' is the dielectric permittivity and ϵ'' is the dielectric loss factor associated with the time-dependent orientation polarization and conduction. The two components of ϵ^*, ϵ' and ϵ'', were calculated from

[3-2] $$\epsilon' = C_{material}/C_o$$

and

[3-3] $$\epsilon'' = G_{material}/C_o\omega$$

where C_o is the air-replaceable capacitance of the sensor, which is constant for all frequencies, and ω is $2\pi f$ with the frequency, f, in Hz.

The real and imaginary components of ϵ^* have both a dipolar and an ionic component.

[3-4] $$\epsilon' = \epsilon'_d + \epsilon'_i$$

[3-5] $$\epsilon'' = \epsilon''_d + \epsilon''_i$$

The dipolar component, ϵ_d, results from rotational diffusion of bound charge and molecular dipole moments. The Cole-Davidson function is used to show the frequency dependence

of the dipolar component

[3-6] $$\epsilon^*_d = (\epsilon_r - \epsilon_u)/(1-i2\pi f\tau)^\beta + \epsilon_u$$

where ϵ_r and ϵ_u are the limiting low and high frequency values of ϵ_d, τ is the dipolar relaxation time and β is the relaxation time distribution ($0<\beta<1$). The dipolar component dominates the dielectric measurements at high frequencies and in extremely viscous media[1].

The ionic component, ϵ_i, arises from the translational diffusion of charge. This results in localized layers of charge near the electrodes. Consequently, the ionic component dominates at low frequencies, low viscosities and sometimes at high temperatures. Johnson and Cole[3] derived equations for the ionic contribution to ϵ^*

[3-7] $$\epsilon'_i = \epsilon_u + (\epsilon_r - \epsilon_u)/(1+(2\pi f\tau)^2)$$

[3-8] $$\epsilon''_i = \sigma/2\pi f\epsilon_o + (\epsilon_r - \epsilon_u)2\pi f\tau/(1+(2\pi f\tau)^2)$$

where ϵ_o is permittivity in a vacuum (8.85×10^{-14} Farads/cm) and σ is the ionic conductivity. The first term in equation [3-8] is due to conductance of ions translating through the medium. The second term represents the charge polarization effects which are minimal at frequencies above 10 Hz. These effects are responsible for high values of σ typically associated with a highly fluid resin state.

By neglecting these charge polarization effects, the values of $\omega\epsilon''(\omega)$ in the overlapping frequencies (Hz to Khz range) can be used to track the ionic mobility through the parameter σ^2.

[3-9] $$\sigma = \epsilon_o \omega \epsilon''_i(\omega)$$

Similarly, the dipolar component of the loss factor can be determined by subtracting the ionic component from the complex permittivity.

[3-10] $$\epsilon''_d(\omega) = \epsilon''(\omega) - \sigma/\omega\epsilon''_i$$

The magnitude of the ionic mobility, σ, and the rotational mobility of the dipole, τ, determined from the frequency dependence of $\epsilon^* * \omega$ can be quantitatively related to the reaction advancement and viscosity during a cure. This is due to the dependence of σ and τ on the extent of reaction and physical state of the resin. The frequency dependence of $\epsilon^* * \omega$, therefore, provides a molecular probe for monitoring properties such as the degree of cure and viscosity[1]. Furthermore, the chemistry and rheology of the cure process can be related to the changing electrical properties of the resin system through a correlation of the time, temperature, and the frequency dependence of the impedance with DSC and rheological characterization measurements.

Experimental

Frequency dependent impedance measurements were made using either a Hewlett-Packard 4192A LF Impedance Analyzer or a Schlumberger 1620 Impedance Analyzer controlled by a microcomputer. Measurements at frequencies from 5 Hz to 5 x

10^6 Hz were taken continuously throughout the entire cure process at regular intervals. The impedance measurements were then converted to the complex permittivity.

A geometry independent microsensor, patented by Kranbuehl, was used to measure the impedance of the three epoxy resin systems. The sensor consists of a fine array of two interdigitated comb electrodes and is constructed from noble metals and high temperature ceramics (Fig. 3.1)

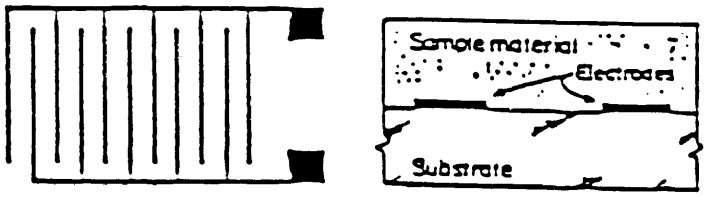

Figure 3.1

The DekDyne sensor is inert and designed to withstand temperatures exceeding 400°C, pressures up to 1000 psi and oxidative conditions typically experienced in the processing environment.

The combined ability of the microsensor, impedance analyzer and microcomputer allows for continuous uninterrupted measurements of both ϵ' and ϵ'' over ten decades in magnitude at all frequencies[4]. Figure 3.2 is a diagram of the FDEMS setup. Several microsensors can be used at one time and placed at various positions in the mold. Additionally, measurements can be made in the laboratory or in-situ in the mold during the processing of a

composite part.

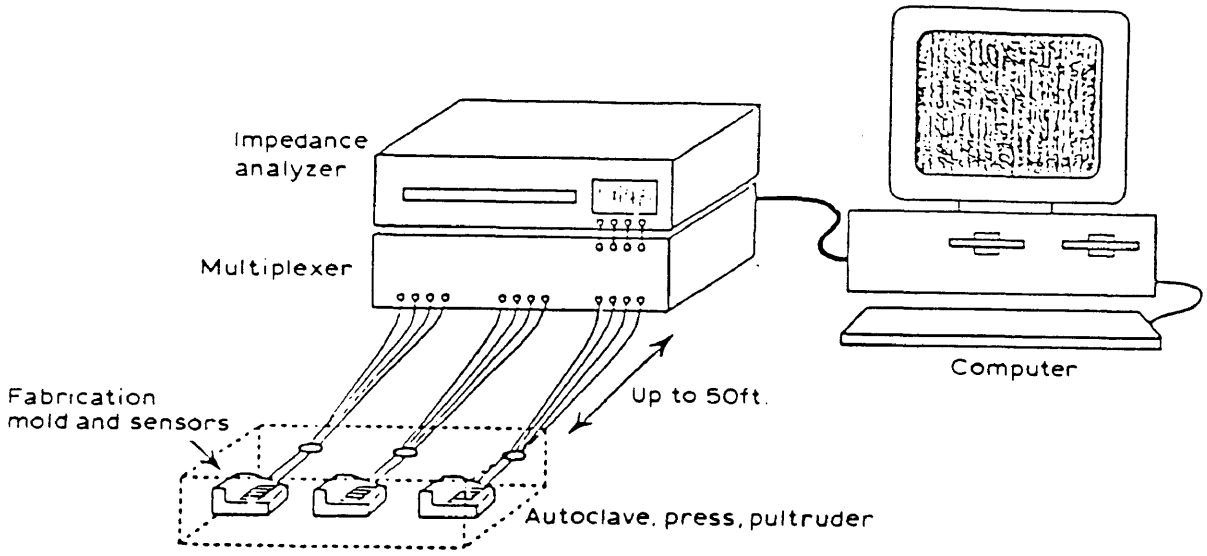

Figure 3.2

In the acquisition of FDEMS isothermal data, a sensor was placed in the bottom of an aluminum pan with two thermocouples. The aluminum pan was then positioned in an oven which was then preheated to the desired isothermal temperature. The leads from the sensor and the thermocouple were attached to the impedance analyzer and thermocouple board, respectively. Once the oven reached the desired temperature, the mixed epoxy resin was poured into the aluminum pan, covering the microsensor and thermocouples. Measurements were taken starting immediately after the oven reached the isothermal temperature.

Figure 3.3 shows a plot of the frequencies multiplied by the imaginary component of the complex permittivity $\epsilon''*\omega$,

along with the temperature of the material during 135°C cure, versus time.

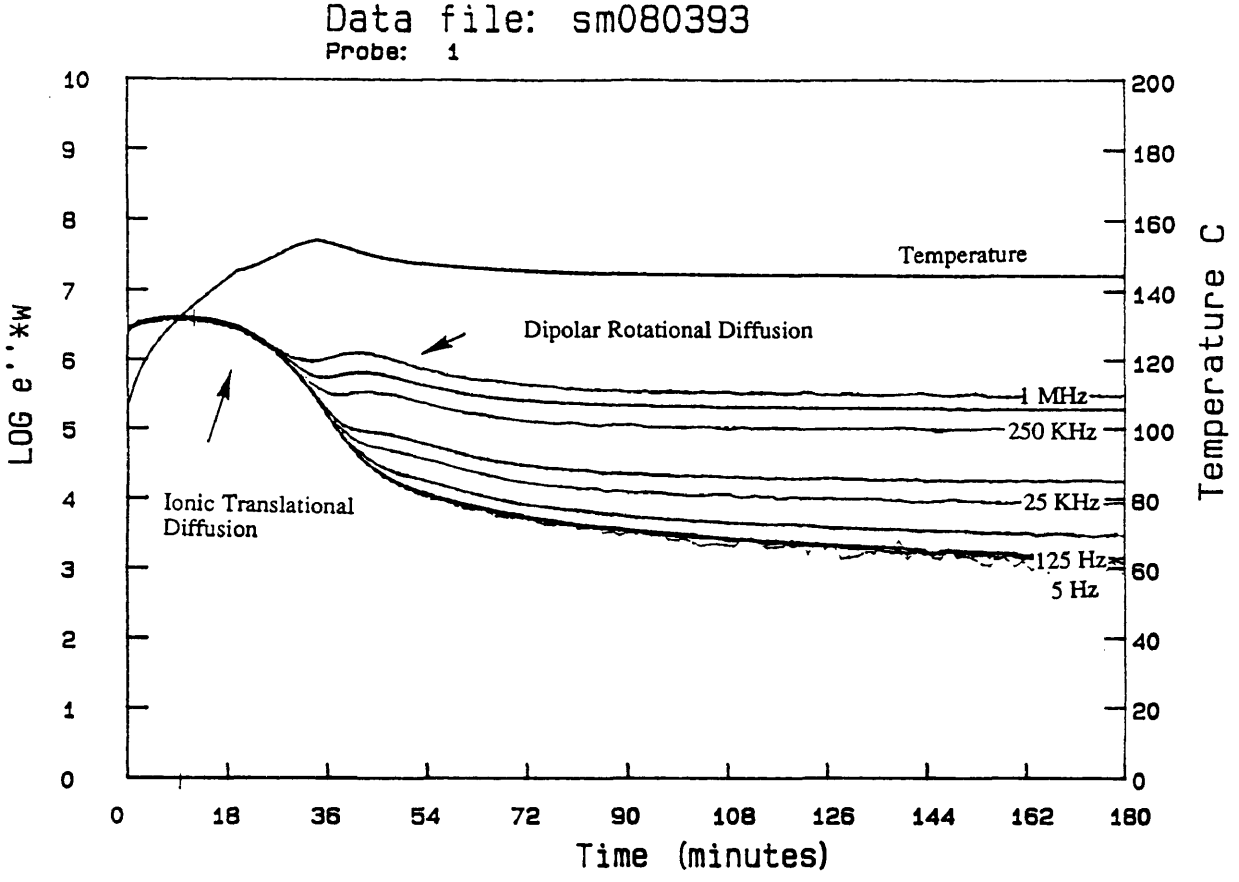

Figure 3.3

The peaks in the $\epsilon''*\omega$ curves for the individual frequencies indicate when dipolar rotational diffusion processes contribute to ϵ''. Overlap of the $\epsilon''*\omega$ curves for differing frequencies indicates that ionic translational diffusion is the dominant physical process affecting the loss term.

In the polymerization reaction, or cure, the reaction onset is marked by a sudden drop in the $\epsilon''*\omega$ at 36 minutes into the run reflecting the decreasing mobility of ions. The curves separate after reaching a maximum value of $\epsilon''*\omega$

for the individual frequencies. This suggests that the frequency dependent dielectric permittivity is no longer dominated by just the ionic mobility, and that the rotational diffusion of bound charge and molecular dipole moments is increasingly the dominant physical process. Reaction completion is detected by the change in ϵ'' with time approaching zero[2].

RTM

The Resin Transfer Molding (RTM) manufacturing process offers several advantages over labor intensive, multi-step processes. First, RTM process allows complex components to be easily manufactured using short, simple cure cycles. Since a closed system is used, the RTM process is able to control the volume of fiber in the composite and produce low void content parts[5]. Recently, this process has been favorably considered by aerospace companies for use with expensive high performance resins. This process would serve to reduce manufacturers costs while producing minimal waste. All the resins considered in this analysis were specifically designed for aerospace RTM.

In the RTM process, a reinforcement, such as a three-dimensional stitched fiber architecture, is placed in a mold without resin present. The mold is heated, and low viscosity resin is injected until the entire cavity is

filled. The mold is then heated to a higher temperature to advance the reaction to full cure. The mold can then be opened and the composite part removed.

The RTM experiments considered in this analysis were intelligently controlled through a closed loop process as shown in Fig. 3.4.

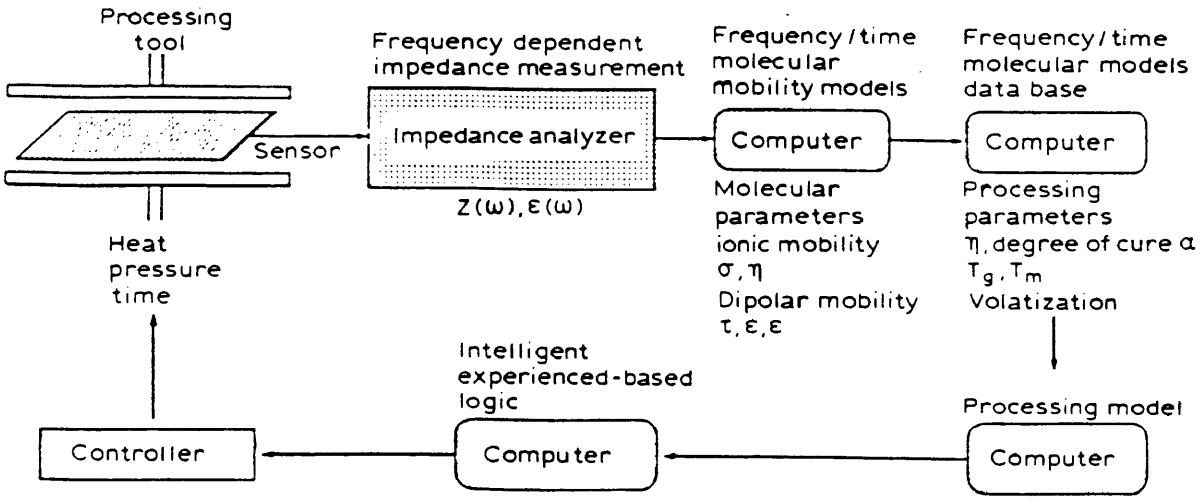

Figure 3.4

In this process, the FDEMS system was used to gather in-situ data from the composite part. The collected measurements were interpreted using a computer software program on a second computer. This on-line feedback was then used to control the heating/press device and ultimately the curing cycle of the resin.

The intelligently controlled closed loop process is, therefore, able to advance the resin to the next stage of the process based on the achievement of critical molecular states[2]. There are six critical steps or stages in this closed loop process. First, the resin must achieve a

minimum viscosity. This viscosity minimum must then be maintained until impregnation of the mold is complete. This is achieved by holding the mold at a temperature where there is only a minimal amount of reaction occurring. The mold is then heated to a higher temperature to advance the reaction, while avoiding excessive internal exothermic effects. The resin is ramped to final cure temperature where the degree of cure is monitored. Finally, the process cycle is turned off when the resin reaches full cure.

This approach to controlling the RTM cure process is a more efficient way to cure resins systems than the standard cure cycles previously employed. The standard cure cycles were generally manufacturers' recommendations of the times and temperatures required to cure the resin. These cycles, however, did not take into consideration variations in vendor batches or differences in the equipment and/or processing environment. This resulted in composite parts with varied properties. This inconsistency was due to the fact that the molecular state of the curing resin was ignored by this strict time, temperature scheme. The intelligent closed loop system is based entirely on the achievement of critical molecular states. Therefore, resins are not held at temperatures unnecessarily, wasting time and money. This process also provides immediate quality assurance, since the resulting composite parts must have attained the required molecular states[6].

References Chapter III

1. Bauer, R. S., "Cure Monitoring," *International Encyclopedia of Composites*, Vol. 1, VCH Publishers Inc., New York, 1990.

2. Kranbuehl, D. E., "In-situ On-line Measurement of Composite Cure with Frequency Dependent Electromagnetic Sensors," *Plastics, Rubber and Composites Processing and Applications*, Vol. 16, 1991.

3. Senturia, S., and Sheppard, N. F., "Dielectric Analysis of Thermoset Cure," **Epoxy Resins and Composites IV**, Springer-Verlag, Berlin, 1986.

4. Kranbuehl, D., Polis, D., Short, C., Wang, Y., "Use of FDEMS Sensing for In Situ, On-Line Monitoring of Degree of Cure During Polymerization of a 2-Stage, High Performance RTM Composite Resin," *Society of Plastic Engineers*, Vol. 2, 1993.

5. Hackett, S.C. "A Perspective on resins for Aerospace RTM," 3M Aerospace Department, 1991.

6. Kingsley, P. J., Masters Thesis, "Dielectric Monitoring and Control of an Automated Resin Transfer Molding Process," College of William and Mary, 1991.

Chapter IV

Characterization of Shell 1895 Development Resin

Epoxy Research Resin RSL 1895/Epon Curing Agent® W resin system was characterized with respect to the viscosity, the degree of cure, and the frequency independent dielectric behavior of the resin. Calibration plots relating α, η, and $\epsilon''*\omega$ through a temperature and time correlation were used to monitor the RTM processing of a composite part.

Reaction Kinetics

In the characterization of Epoxy Research Resin RSL 1895/Epon Curing Agent® W resin system, a kinetic analysis was undertaken to develop a mathematical model that could accurately predict the curing rate of the resin for temperatures from 90° to 177°C. A Differential Scanning Calorimeter (DSC) was the instrument used to determine the equation and the kinetic parameters for the epoxy-amine reaction.

Initially, a ramp, or temperature sweep, of uncured Shell 1895 development resin was performed to determine the

isothermal temperatures at various stages in the curing reaction (Fig. 4.1). Measurements were then obtained for DSC isothermal holds at 90°, 121°, 135°, 149° and 177°C. The first two temperatures, 90°C and 121°C, were chosen because Shell 1895 development resin is injected into the mold in the manufacturing of composite parts at these temperatures. In this temperature range, the viscosity remains low and steady over a period of time, allowing for effective impregnation. The higher temperature isotherms were evaluated for use as holds in the RTM process.

For each of the isotherms, experimental values of the degree of cure, α, and the rate of reaction, $d\alpha/dt$, were determined using the integration program described in Chapter II. Examination of the resulting alpha versus time plots establishes that increasing the temperature increases the rate of reaction. At higher temperatures the reaction terminates sooner and attains a higher degree of cure as seen in Fig. 4.2.

Kinetic models were then developed to predict the curing reaction for the individual DSC isotherms. The kinetic analysis commenced with determining the rate equation

[4-1] $$d\alpha/dt = k\, f(\alpha)$$

where the reaction rate, $d\alpha/dt$, is related to some reaction function $f(\alpha)$ and a rate constant k. The reaction function is typically either an nth order reaction,

[4-2] $$f(\alpha) = (1-\alpha)^n$$

or an autocatalytic reaction

[4-3] $$f(\alpha) = \alpha^m(1-\alpha)^n$$

where m and n are the reaction orders[1]. In this analysis, three rate equations were considered as likely models for Shell 1895 resin.

[4-4] $$d\alpha/dt = k\ (1-\alpha)^n$$

[4-5] $$d\alpha/dt = k\alpha^m\ (1-\alpha)^n$$

[4-6] $$d\alpha/dt = (k_1 + k_2\alpha^m)(1-\alpha)^n$$

Equation [4-6] is the Kamal rate equation previously described[2,3,4].

SYSTAT® software was used to evaluate each of the rate equations as a possible kinetic model. The values of the parameters k, k_1, k_2, m and n were generated by SYSTAT® for each of the equations based on the individual isothermal data. A least-square fit analysis was used to generate a nonlinear estimation of the parameters[5]. The deviation from the experimental $d\alpha/dt$ curve for each of the isothermal fits revealed the equation that consistently produced the least deviation. The second order polynomial equation [4-5] emerged as the best fit of the experimental $d\alpha/dt$ curves.

In addition to determining a rate equation for the polymerization reaction, the resulting parameters were optimized to produce a better fit of the experimental data. The parameters generated in SYSTAT® produced sufficient agreement for selecting a model, but the theoretical back-

calculated values of α only marginally agreed with experimental data. Consequently, a program was created to test each possible combination of the three parameters k, m and n using a specified range of values. The best fit values were resolved as the combination producing the smallest squared total deviation in theoretical alpha from experimental alpha values. Figure 4.3 demonstrates the fit of the theoretical curve to the experimental alphas for the 149°C isotherm.

After individual fits of $d\alpha/dt$ were generated, a comprehensive model for the resin system was developed. First, the Arrhenius equation was used to relate the rate constant k with the activation energy and temperature

[4-7] $$k = Ae^{-E/RT}$$

where A is the Arrhenius preexponential factor, E is the activation energy, R is the ideal gas constant equal to 1.987 cal/K mol, and T is the temperature in degrees Kelvin[1]. The Arrhenius equation can also be rearranged to the form:

[4-8] $$\ln(k) = \ln(A) - B/T$$

Figure 4.4 shows the natural log of the isothermal rate constants versus inverse temperature. The rate constant for the 149°C isotherm was omitted, since the value was much lower than expected (0.14 instead of 0.30). A line drawn through the points yields a slope of B, where B is equal to E/R, and a y-intercept of ln(A). The values for B and A

were found to be 9541 K^{-} and 2.24 x 10^{9} min^{-}, respectively. Second, an average value of m and n was calculated from the individual isothermal fits.

The final kinetic equation produced from this analysis was as follows

[4-9] $$d\alpha/dt = (2.24 \times 10^{9}\ e^{(-9541/T)})\ \alpha^{.71}\ (1-\alpha)^{2.3}$$

The accuracy of this kinetic model was verified using graphs of the experimental and theoretical degree of cure versus time for each of the isotherms (Fig. 4.5 - Fig. 4.8). Aside from the theoretical fit of the 149°C data, the kinetic model provided a good estimate of the experimental alpha values. The contrasting kinetic behavior of the 149°C isotherm is most likely a result of improper mixing of the resin or some other variation in the experiment.

Aging effects and variations in batches led to an entirely different model for the new batch of resin (Shell RSL 1895 resin Lot#21408-13 and Epon Curing Agent® W Lot#10MHC261). These variations are best illustrated by comparing the advancement of the experimental degree of cure of the old and new batches of resin (Fig. 4.9 - Fig. 4.12). The new batch of resin attained a higher degree of cure than the old resin, but at a slower rate. The 149°C isothermal data did not display this behavior. This can be attributed to the disparity between the 149°C kinetic behavior and that of the other isothermal data.

As a result of the variations between the old and new

batches of resin, a second model was developed by A. Loos to predict the degree of cure for the current batch of resin. This general kinetic equation is as follows

[4-10]
$$d\alpha/dt = (H_T/H_U)(d\beta/dt)$$

$$d\beta/dt = (k_1 + k_2\,\beta^m)(1-\beta)^n$$

$$H_T/H_U = 0.0033874\ T - 0.521654 \quad \text{if } T<450°K$$

$$H_T/H_U = 1 \quad \text{if } T\geq 450°K$$

$$m = 1.4597 - 247.12\ (1/T) \qquad k_1 = 76496\ e^{(-8640/T)}$$

$$n = 4.2432 - 1313.79\ (1/T) \qquad k_2 = 39140\ e^{(-7076/T)}$$

where the temperature (T) is in degrees Kelvin. Figures 4.13 through 4.17 show the alphas predicted by this equation along with the experimental alphas for 90°, 121°, 135°, 149° and 177°C. Notice that the theoretical values agree well for the initial stages of the reaction but are restricted to a maximum degree of cure by the factor H_T/H_U.

This kinetic model is used to predict both the time and the temperature dependence of the degree of cure and will calculate α in subsequent correlations.

Correlation of Degree of Cure and Viscosity

The degree of cure and viscosity were correlated with time, temperature, and the magnitude of the frequency dependent dielectric measurement ϵ'', the dielectric loss. These correlations, or calibration plots, were used to predict changes in the chemical and physical state of the

resin during the RTM process. Parameters such as the injection temperature and the duration of various isothermal holds, therefore, could be intelligently controlled based on the predicted behavior of the resin. Furthermore, these calibration plots made it possible to determine the degree of cure and viscosity of the resin system at the various stages in the RTM process.

FDEMS and rheometric measurements were taken at 90°, 121°, 135°, 149° and 177°C corresponding to the isothermal DSC experiments (Fig. 4.18 - Fig. 4.27). Since dielectric measurements were taken over a wide range of frequencies, a single frequency was selected to provide information about the changing chemical, physical and rheological state of the resin.

The viscosity and $\epsilon''*\omega$ were correlated using the 90°, 121°, 135° and 149°C isothermal data (Fig. 4.28). At 177°C, the resin crosslinked instantly and was therefore neglected in these correlations. Since the viscosity remained constant throughout the 90°C isotherm, the correlation only contains a single point at this temperature.

The calibration plot of log $\epsilon''*\omega$ versus log η was prepared using the following procedures. First, a frequency of 125 Hz was selected for the dielectric data. This frequency is found in the overlapping portion of the $\epsilon''*\omega$ data known as the ionic band. In using a frequency in the ionic band, the decreasing mobility of ions was measured as

a function of the buildup in viscosity.

Next, an initial time t(0) was determined for dielectric and rheological data. A correction factor was required for the FDEMS and rheometric isotherms to compensate for the time delay incurred in reaching the programmed temperature. For the dielectric measurements, the correction factor was the time required for the temperature to come within 4°C of the desired isothermal temperature. In two instances the temperature required 20 to 30 minutes to reach the isothermal temperature of the experiment. As a result, the highest point on the dielectric peak, marking the onset of the reaction, was selected for t(0). A time t(0) was designated for the rheometric data as the first congruous, or "smooth", point in the viscosity curve. Since the points at the beginning of the run are often scattered and inconsistent with the rest of the experiment, the correction factor allows the time needed for the resin and the rheometer oven to achieve thermal equilibrium. This time is also necessary for the viscosity to reach a minimum value. For a few of the isotherms, the viscosity measurements were scattered for a large portion of the run. In these cases, a smooth curve was drawn through the viscosity measurements, and points were extrapolated from the curve.

The values of η and $\epsilon''*\omega$ then were correlated with respect to time and temperature. In the correlation of the

149°C data, for example, the correction factor for the FDEMS isotherm was 14.038 minutes. At the adjusted time(0), $\epsilon''*\omega$ had a value of 4101.98. This value of $\epsilon''*\omega$ was then related to the viscosity at time(0). Since the correction factor for the rheometer run was 0.1 minute, the viscosity at time(0) was 0.4254. The other points were then related in a similar fashion.

The correlations for the individual isotherms were complete when the complex moduli G′ and G″ crossed over in the rheometric isothermal data (Fig. 4.29)[6]. Table 4.1 gives the time corresponding to the G′ and G″ crossover for the individual isotherms.

Temperature	Gel Point(min)
121°C	111.5
135°C	63.9
149°C	34.5

Table 4.1

This crossover, known as the gel point, indicates that the resin has formed a crosslinked network. At this point, the viscosity is no longer a useful measure of the resin flow.

Calibration plots were also devised for 90°, 121°, 135°, and 149°C relating $\epsilon''*\omega$ to the viscosity, η, and the degree of cure, α. The FDEMS and rheology data were modified to account for the correction factor and correlated, similar to the correlation of η with $\epsilon''*\omega$. The

only difference was the added correlation with α. The α's used were the theoretical values predicted by the Loos kinetic model. The values of $\epsilon''*\omega$ at the modified times were matched with the α values occurring at similar times. Figures 4.30 through 4.33 are the resulting graphs of α and log η versus log $\epsilon''*\omega$ for the individual isotherms. In each of the calibration plots, the degree of cure and viscosity increased with decreasing $\epsilon''*\omega$. This implies that the mobility of the ions, or molecules, is decreasing as the resin becomes more crosslinked, constraining the activity of the molecules.

A third type of correlation considered the high temperature reaction at 177°C. In this correlation, a frequency above the ionic band was selected to monitor the polar contributions in the final stages of cure. The sensitivity and stability of FDEMS made it possible to monitor the long-time buildup in final properties hours after the DSC had lost sensitivity. The normalized rate of change of ϵ'', $(d\epsilon''/dt)/\epsilon''$, at 5 kHz was correlated with theoretical alpha values back-calculated using the Loos kinetic equation. This resulted in a plot of $(d\epsilon''/dt)/\epsilon''$ and α versus time.

Two different approaches were selected to determine the values of $(d\epsilon''/dt)/\epsilon''$. In the first method, $d\epsilon''$ and dt were calculated as the difference between successive values of ϵ'' and time, respectively (Fig. 4.34). The second method

determined the change in ϵ'' and time by calculating the difference between a given point and a point five measurements later (Fig. 4.35). The latter method produced a "smooth" curve which proved to be more useful as a calibration plot for RTM experiments.

Correlation of α and η with a RTM Experiment

In the fabrication of a composite material, the degree of cure and viscosity can be monitored in the mold using FDEMS techniques and previously determined calibrations of α and η with $\epsilon''*\omega$. In this investigation, the RTM experiments DH042293 and DH042393 were examined. The two experiments were performed at NASA Langley Research Center using similar procedures. Figures 4.36 and 4.37 report the sensor measurements from these two experiments along with the part temperature during the curing process.

The $\epsilon''*\omega$ versus time plots can be divided into three stages to describe the RTM process. The first stage of the run initially shows the resin temperature at 90°C. This was the temperature used to infiltrate the mold and wet-out the sensors. The FDEMS data, however, were not collected until after these two steps were complete. In the second stage of the RTM process, the temperature of the mold is increased to 149°C. The higher temperature decreases the viscosity to allow the amine curing agents to react with the epoxy resin.

The dielectric peak marks the onset of the epoxy-amine reaction. The third and final stage of the RTM process involves a hold at 177°C to further advance the resin to full cure. The reaction completion is characterized by leveling of the $\epsilon''*\omega$ curves.

It is important to notice that the two experiments vary in lengths of time the resin was held at 90°, 149° and 177°C. This is because the resins achieved certain molecular states, required by the system to advance to the next stage of cure, at different times. These variations can be attributed to slight changes in the mold temperature, the equipment and/or the resin mixture from day to day.

Given the dielectric measurements of ϵ'' from the two RTM experiments, the degree of cure and viscosity could be determined at any point in the experiment. The RTM dielectric measurements of ϵ' and ϵ'' were obtained for 125 Hz and 5kHz, corresponding to the frequencies used for the calibration plots. The value $\epsilon''*\omega$ was calculated by multiplying ϵ'' times $2\pi f$, where f is the frequency. The 90°, 121°, 135°, 149° and 177°C calibrations, previously described, were then used to correlate the $\epsilon''*\omega$ values at these temperatures with values of α and η.

The correlation for the 149°C and 177°C holds will be described for illustrative purposes. First, the values of $\epsilon''*\omega$ were calculated from the dielectric measurements taken during the 149°C hold at 125 Hz. The values of α and η

corresponding to the log of these $\epsilon''*\omega$ values were then extrapolated from the 149°C calibration plot. For the dielectric measurements taken during the 177°C hold, the slope, $(d\epsilon''/dt)/\epsilon''$, was calculated using the five-point method. The calculated values of the slope were correlated with respective values of α using the 177°C calibration plot. The viscosity, however, was not determined for the 177°C hold, since the resin had become a crosslinked solid at this point.

This method was used to determine α and η for as many points as possible from the RTM dielectric measurements. For the 90°C hold, only a few points were obtained using this method, while most of the points had to be taken directly from the 90°C calibration. Since the resin remains virtually unreacted, the values determined for the 90°C hold are not as critical.

Figures 4.38 through 4.41 depict the degree of cure and viscosity with respect to time and temperature for the two RTM runs. Additionally, Figure 4.42 shows the $\epsilon''*\omega$ values used in the correlations for RTM experiment DH042293. Although the temperature is shown from the point when the resin was first heated to 90°C, the correlation does not begin until the sensors are wet-out. After advancing the resin to the 149°C hold, the viscosity and degree of cure increased rapidly in the initial stages of the hold. The viscosity correlations end as the temperature is increased

to 177°C. At this point, the resin has become a crosslinked solid such that the viscosity is no longer a good measure of the resin's flow properties. The degree of cure correlations continue until the resins are fully cured, i.e., α equals 1.

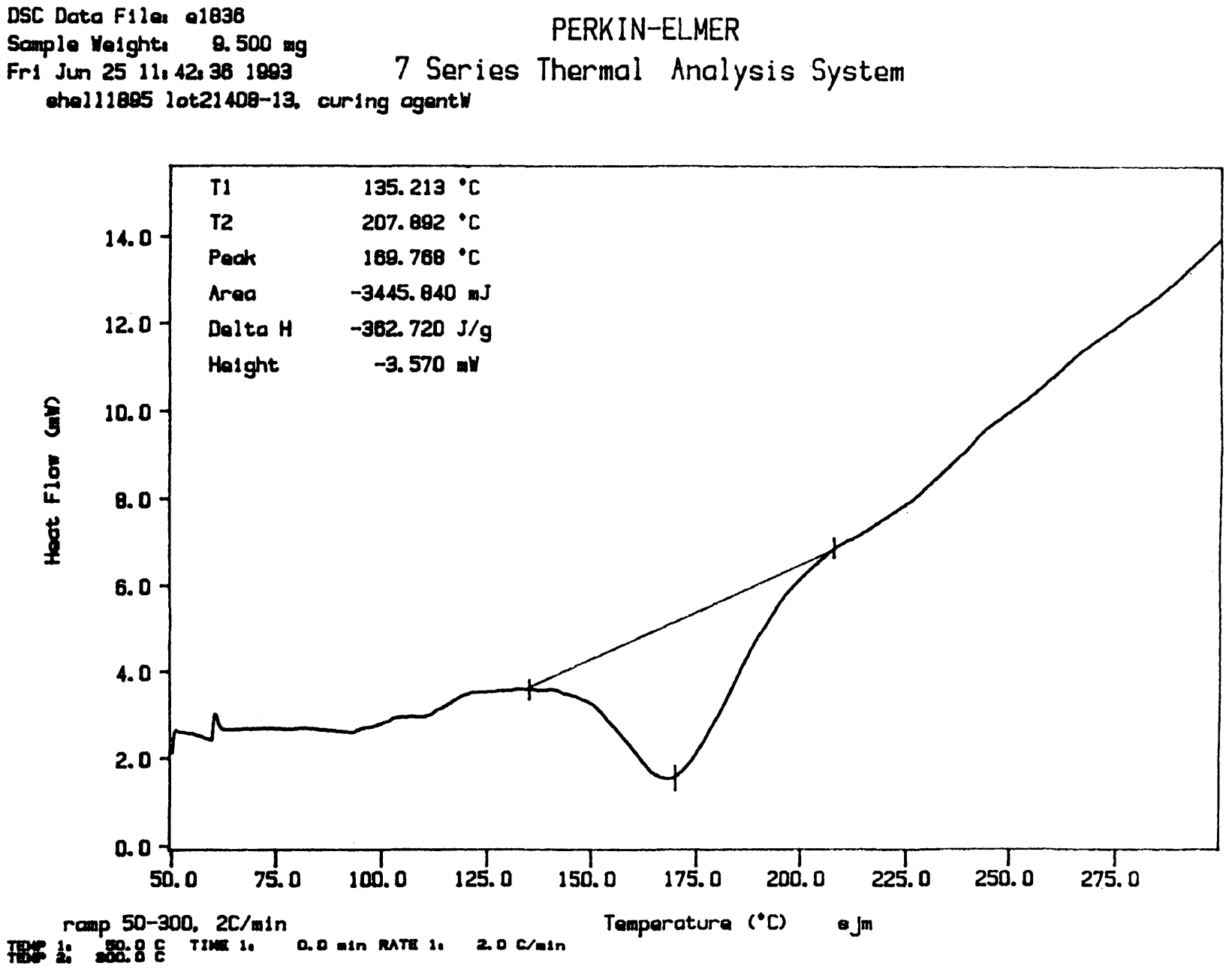
DSC Data File: e1836
Sample Weight: 9.500 mg
Fri Jun 25 11:42:38 1993
shell1895 lot21408-13, curing agentW
PERKIN-ELMER
7 Series Thermal Analysis System
T1 135.213 °C
T2 207.892 °C
Peak 189.768 °C
Area -3445.840 mJ
Delta H -362.720 J/g
Height -3.570 mW
Heat Flow (mW)
14.0
12.0
10.0
8.0
6.0
4.0
2.0
0.0
50.0
75.0
100.0
125.0
150.0
175.0
200.0
225.0
250.0
275.0
ramp 50-300, 2C/min
Temperature (°C)
TEMP 1: 50.0 C TIME 1: 0.0 min RATE 1: 2.0 C/min
TEMP 2: 300.0 C

Figure 4.1

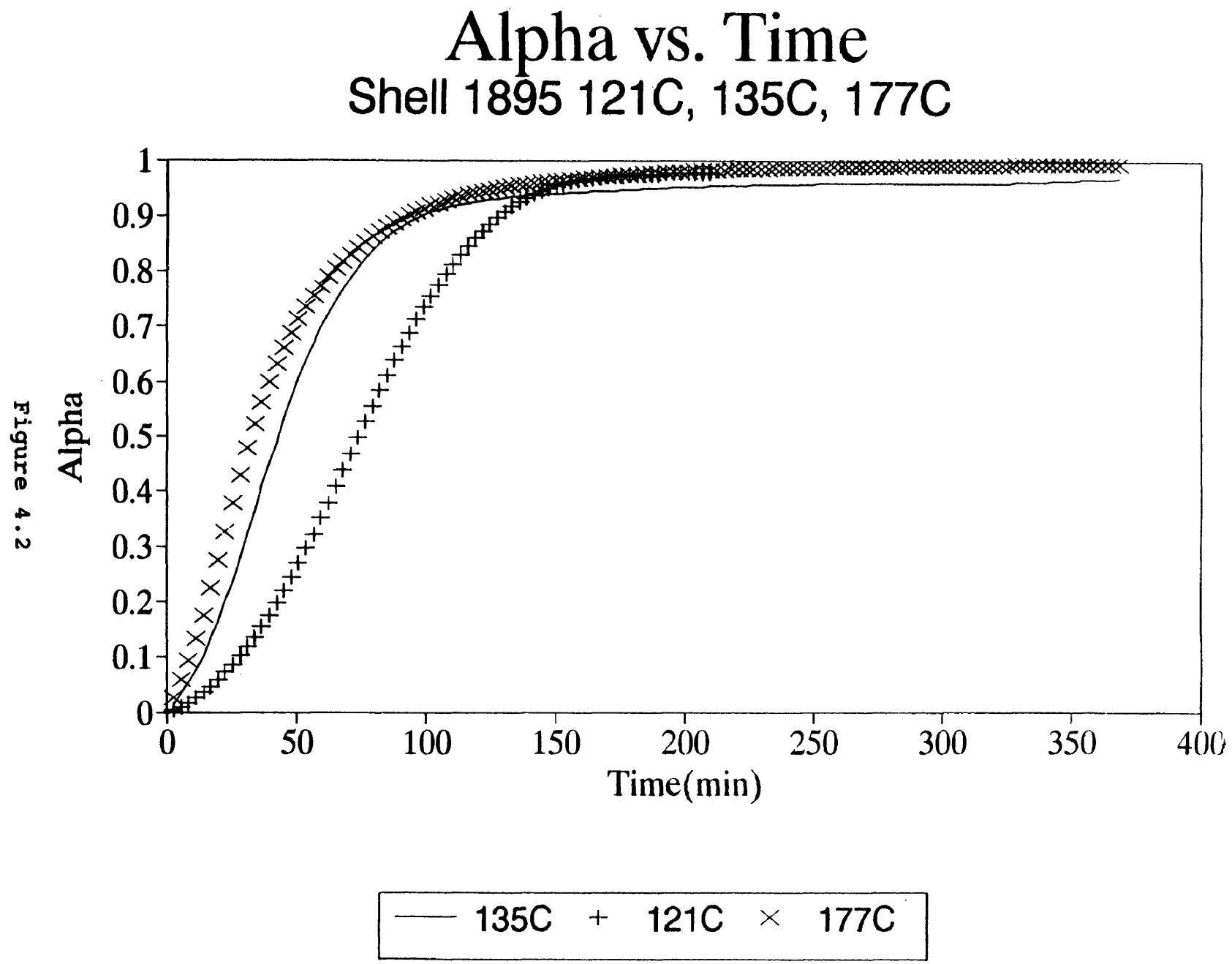
Alpha vs. Time
Shell 1895 121C, 135C, 177C
Alpha
1
0.9
0.8
0.7
0.6
0.5
0.4
0.3
0.2
0.1
0
0
50
100
150
200
250
300
350
400
Time(min)
135C
121C
177C

Figure 4.2

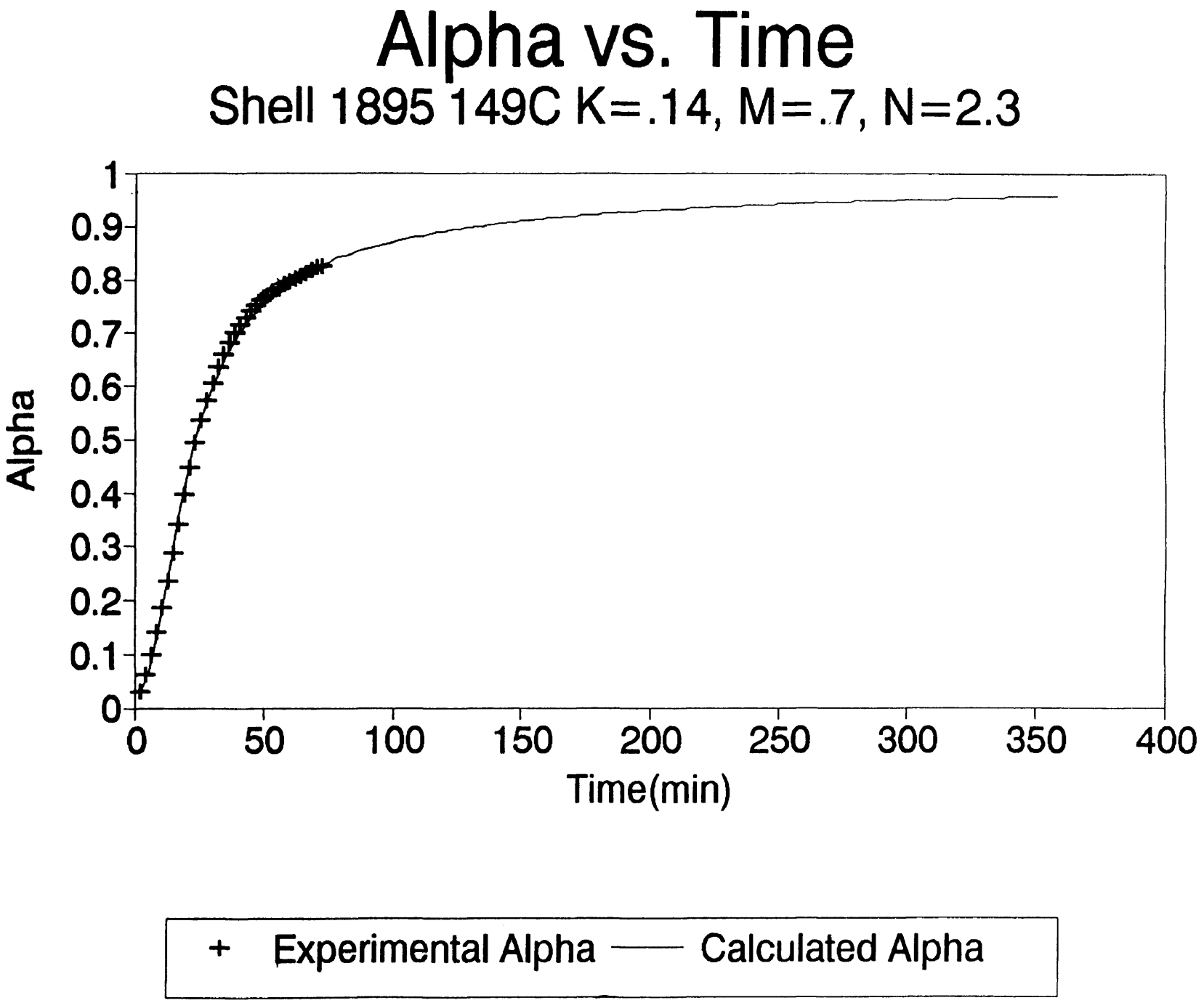
Alpha vs. Time
Shell 1895 149C K=.14, M=.7, N=2.3
Alpha
1
0.9
0.8
0.7
0.6
0.5
0.4
0.3
0.2
0.1
0
0
50
100
150
200
250
300
350
400
Time(min)
+ Experimental Alpha
Calculated Alpha

Figure 4.3

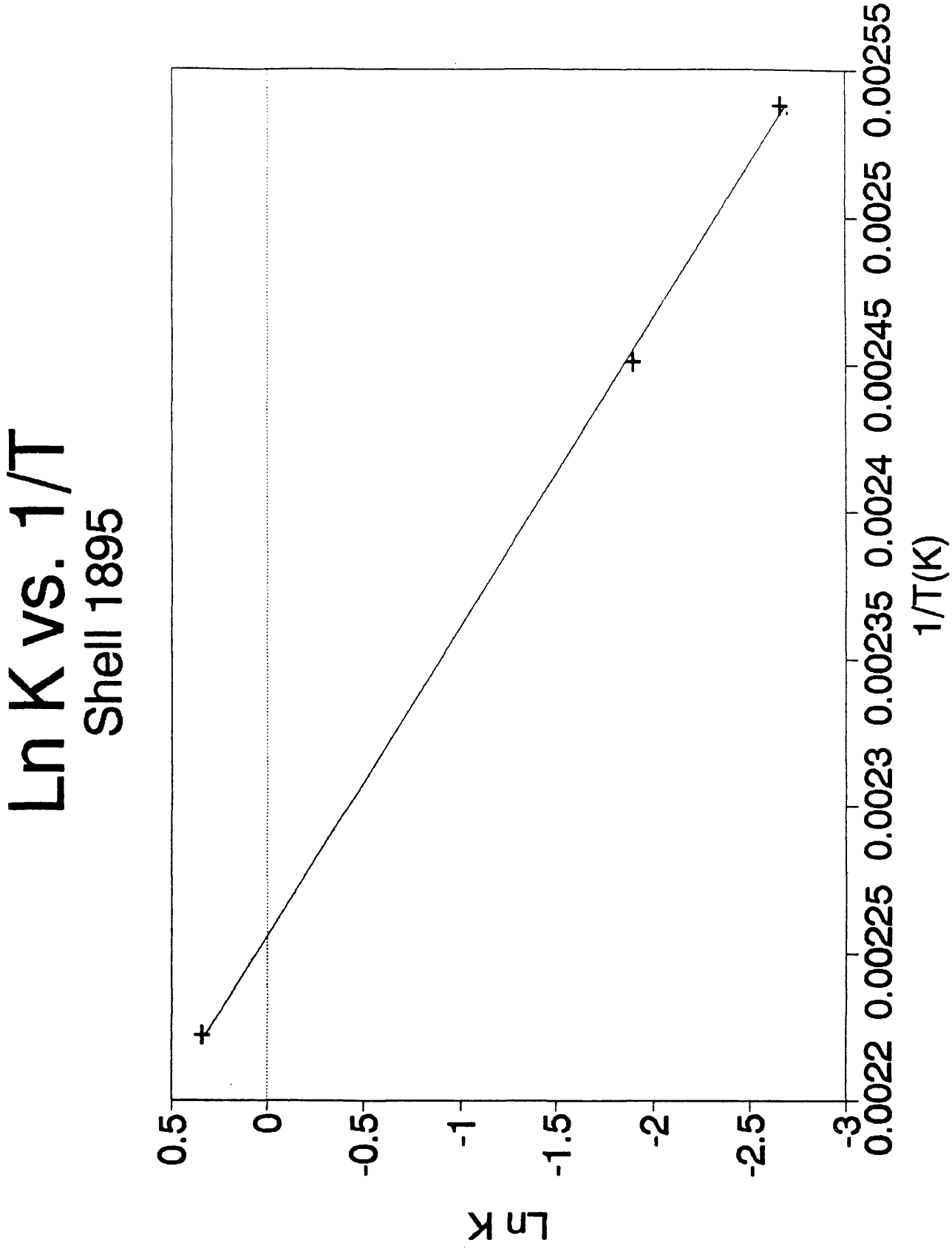
Ln K vs. 1/T
Shell 1895
Ln K
0.5
0
-0.5
-1
-1.5
-2
-2.5
-3
0.0022
0.00225
0.0023
0.00235
0.0024
0.00245
0.0025
0.00255
1/T(K)

Figure 4.4

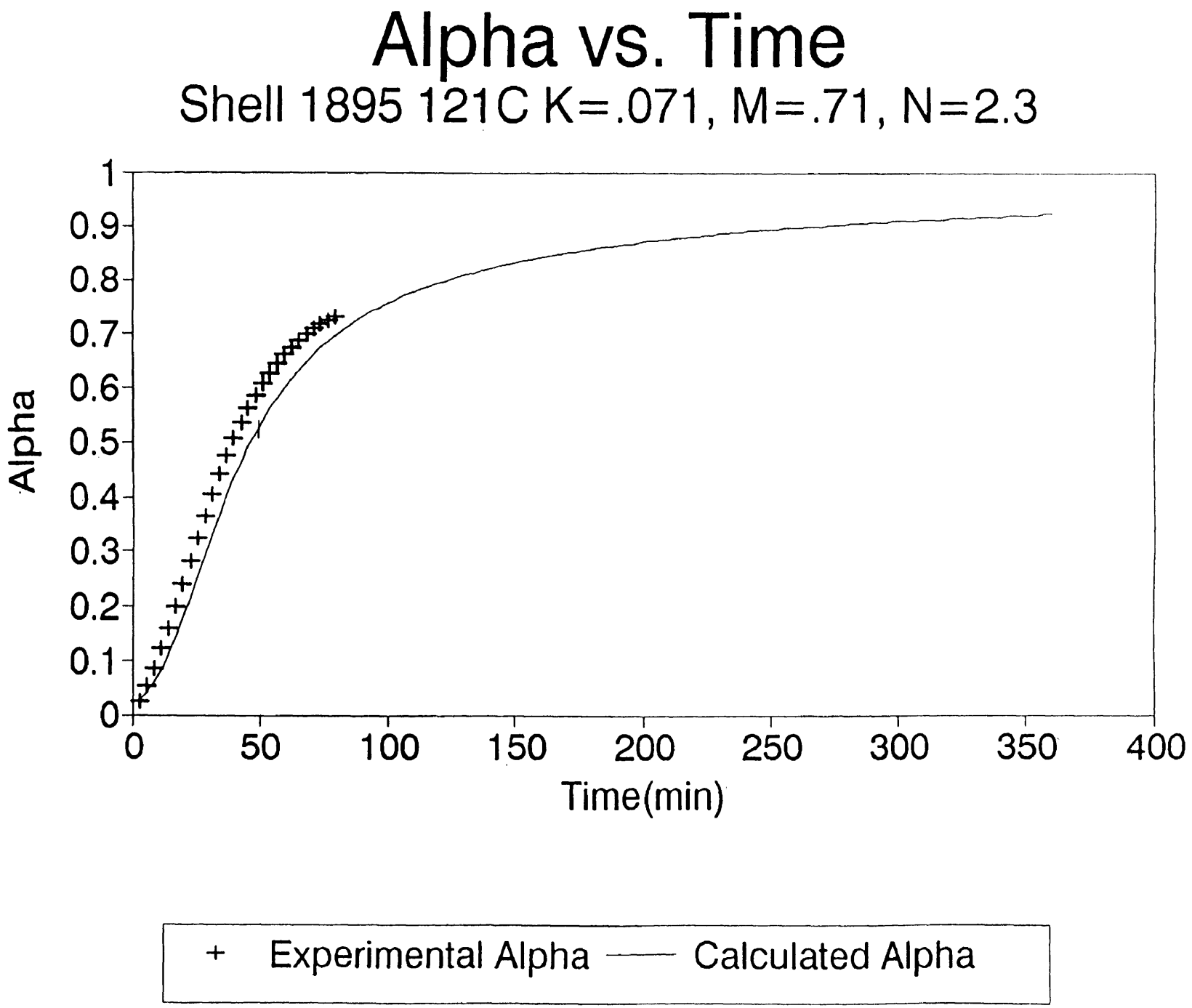
Alpha vs. Time
Shell 1895 121C K=.071, M=.71, N=2.3
Alpha
1
0.9
0.8
0.7
0.6
0.5
0.4
0.3
0.2
0.1
0
0
50
100
150
200
250
300
350
400
Time(min)
+ Experimental Alpha
Calculated Alpha

Figure 4.5

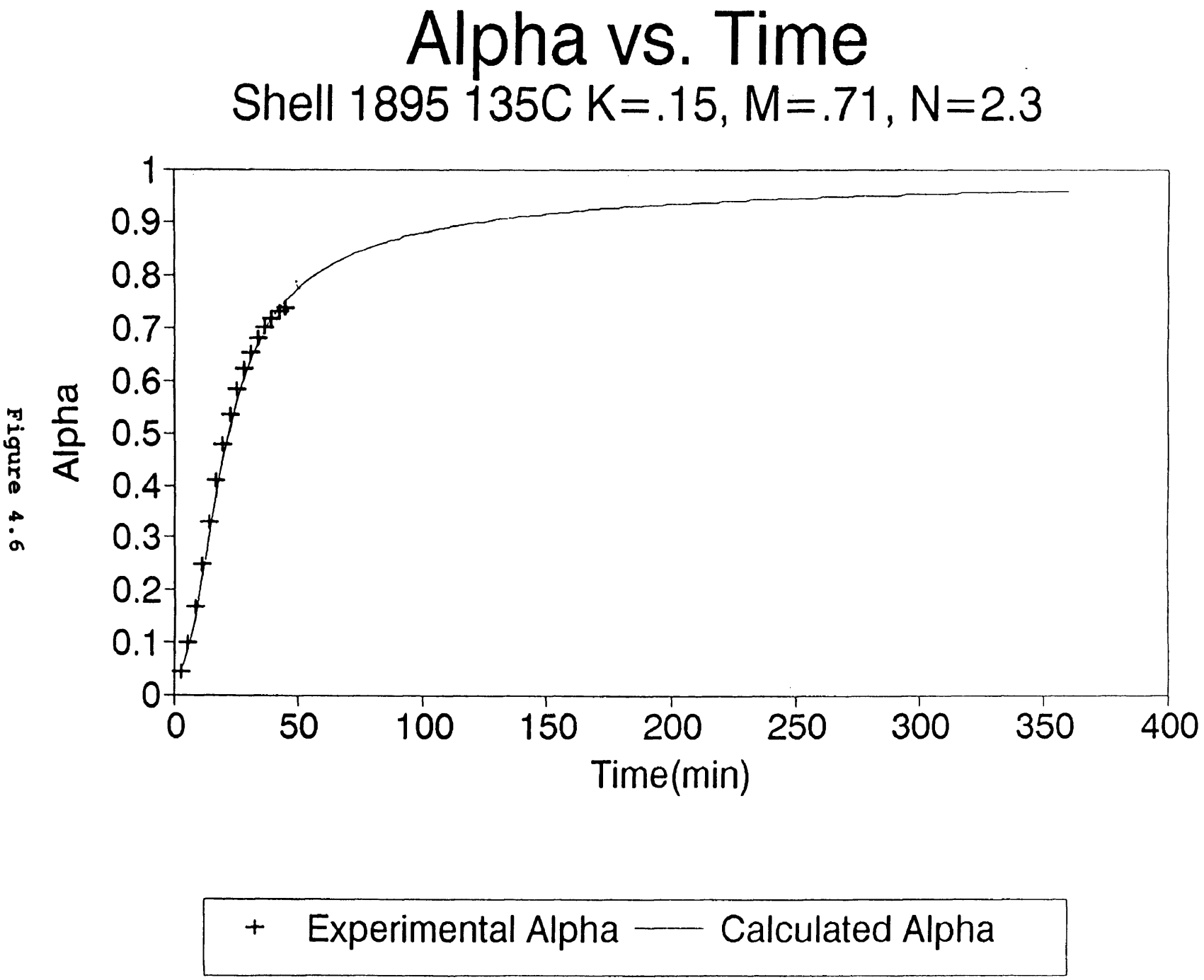
Alpha vs. Time
Shell 1895 135C K=.15, M=.71, N=2.3
Alpha
1
0.9
0.8
0.7
0.6
0.5
0.4
0.3
0.2
0.1
0
0
50
100
150
200
250
300
350
400
Time(min)
+ Experimental Alpha —— Calculated Alpha

Figure 4.6

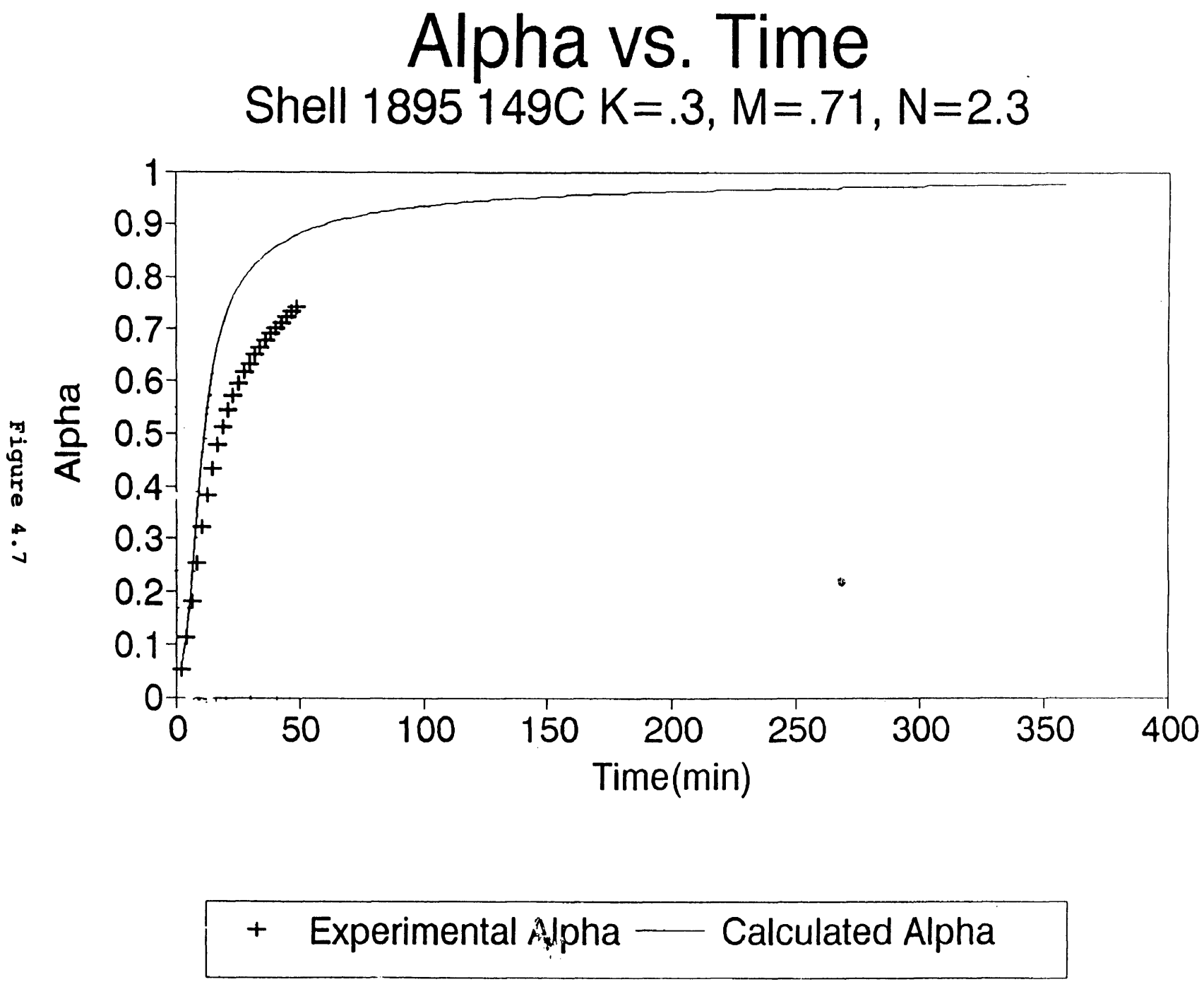
Alpha vs. Time
Shell 1895 149C K=.3, M=.71, N=2.3
Alpha
1
0.9
0.8
0.7
0.6
0.5
0.4
0.3
0.2
0.1
0
0
50
100
150
200
250
300
350
400
Time(min)
+ Experimental Alpha
Calculated Alpha

Figure 4.7

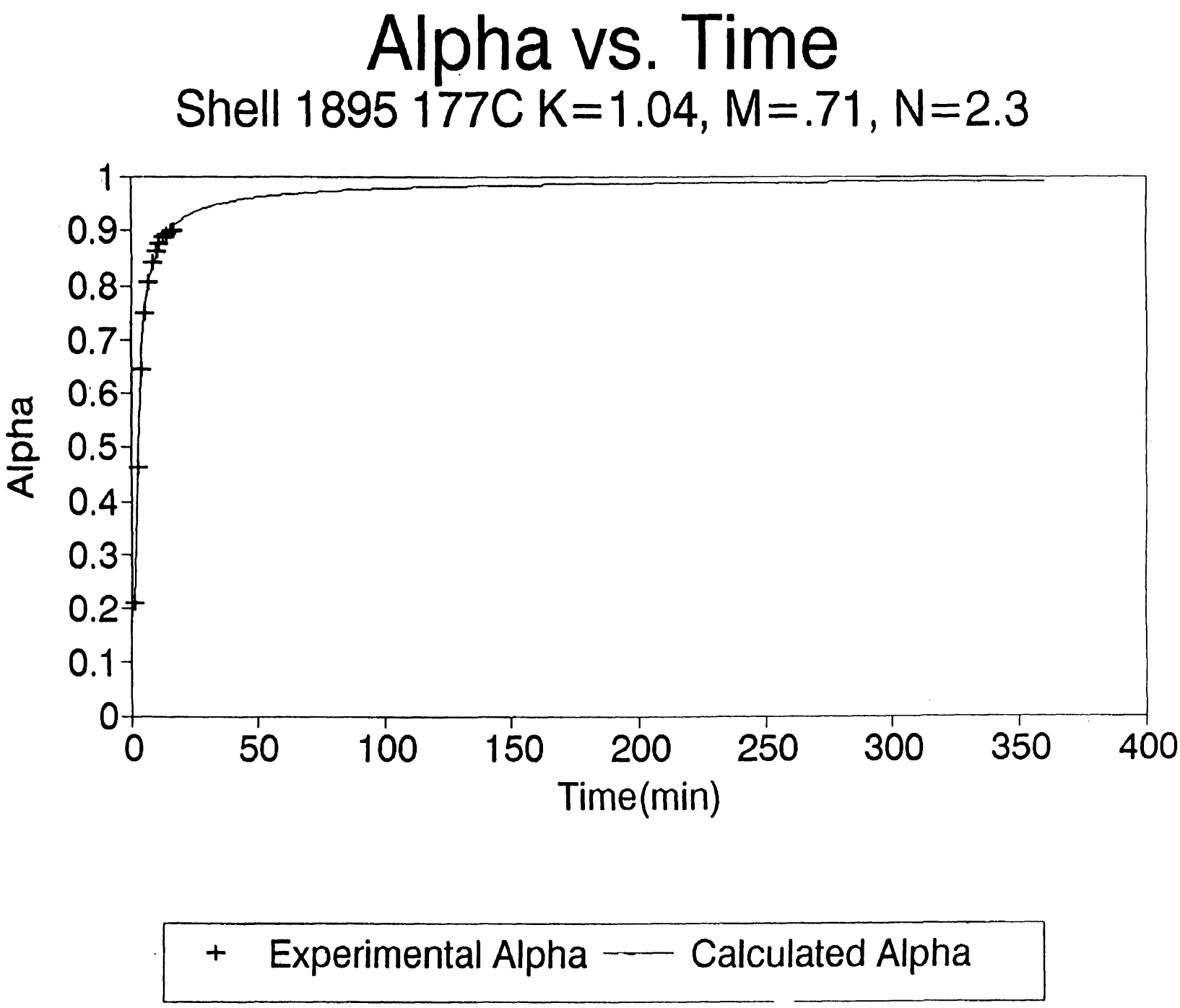
Alpha vs. Time
Shell 1895 177C K=1.04, M=.71, N=2.3
Alpha
1
0.9
0.8
0.7
0.6
0.5
0.4
0.3
0.2
0.1
0
0
50
100
150
200
250
300
350
400
Time(min)
+ Experimental Alpha
Calculated Alpha

Figure 4.8

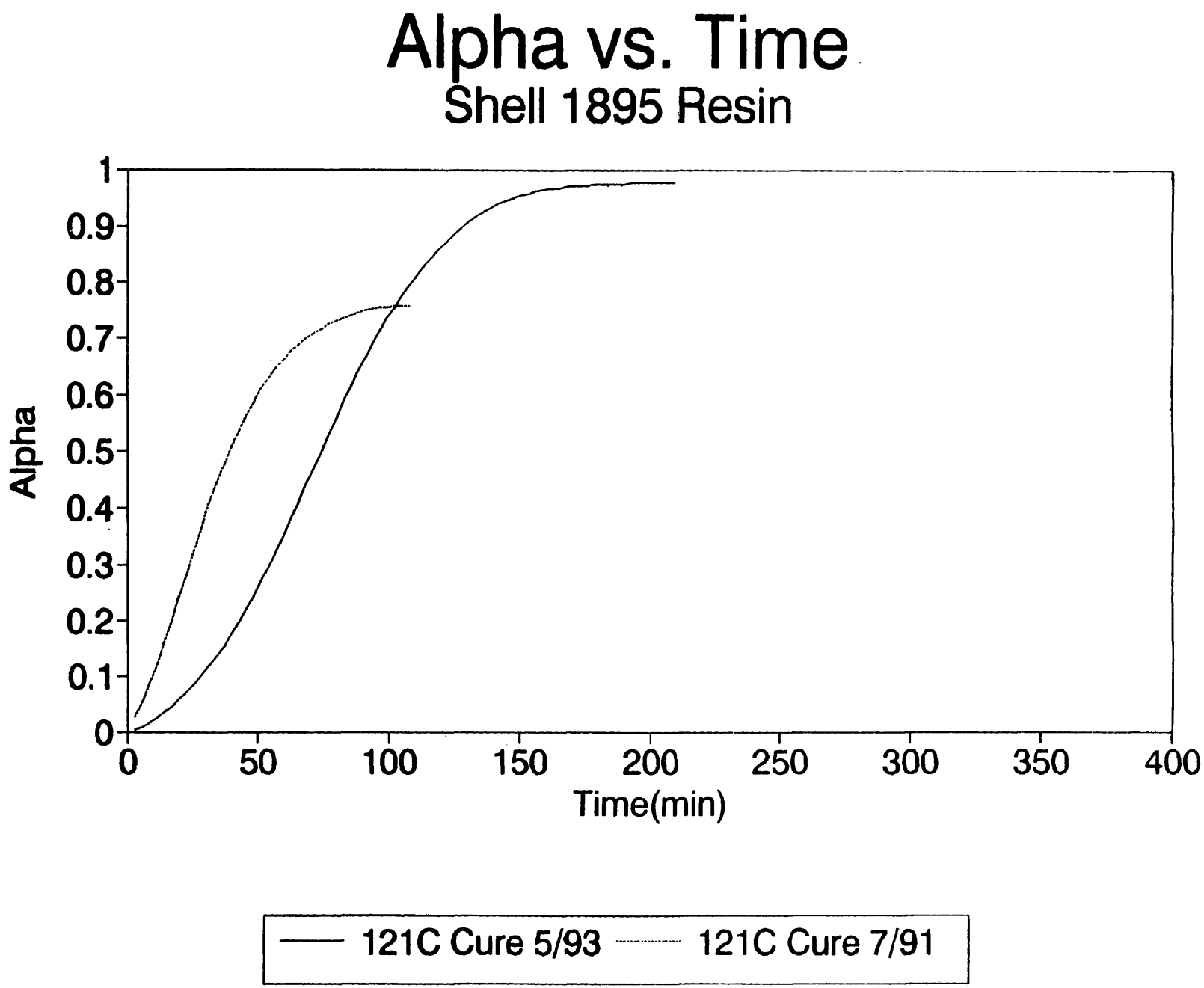
Alpha vs. Time
Shell 1895 Resin
Alpha
1
0.9
0.8
0.7
0.6
0.5
0.4
0.3
0.2
0.1
0
0
50
100
150
200
250
300
350
400
Time(min)
121C Cure 5/93
121C Cure 7/91

Figure 4.9

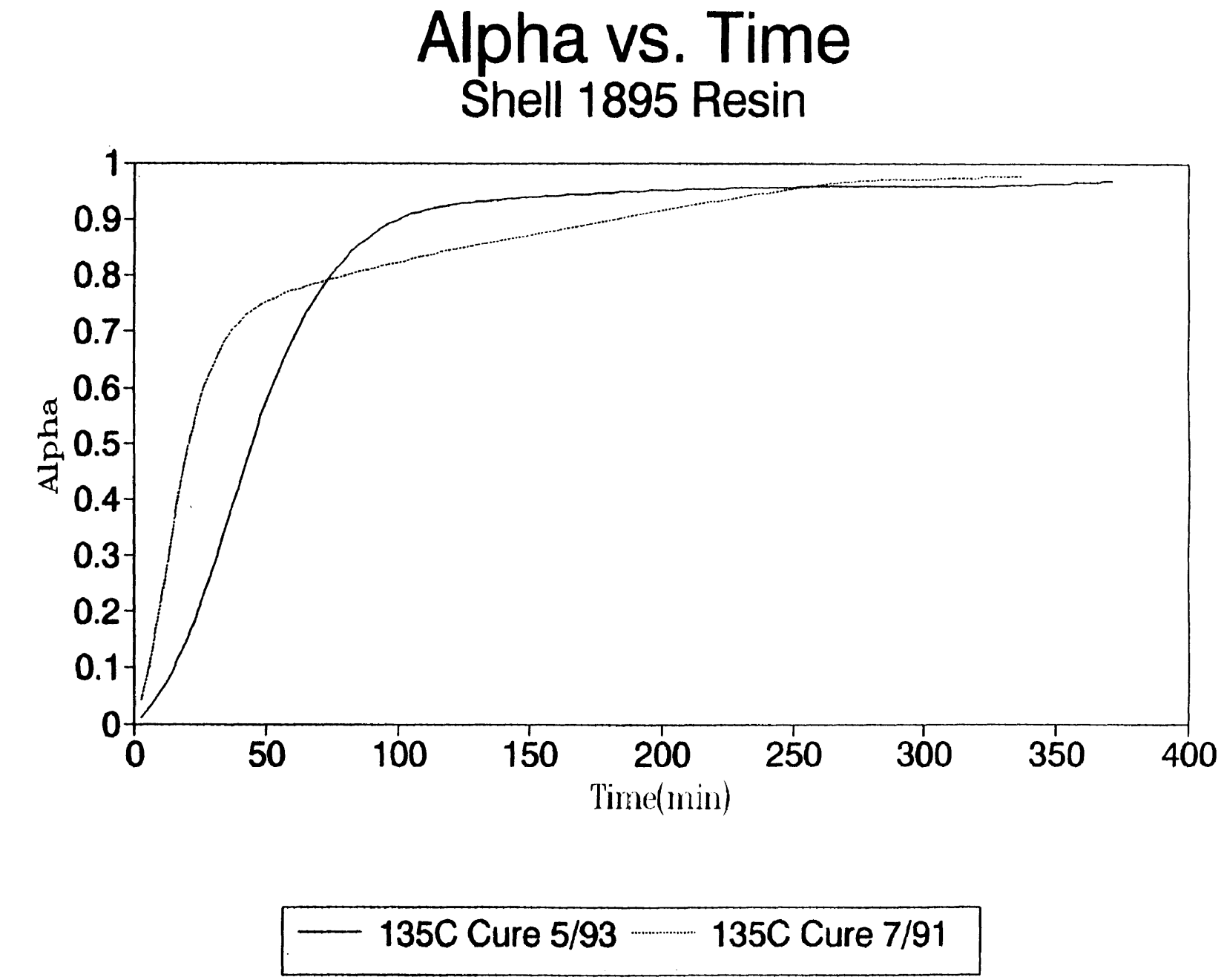
Alpha vs. Time
Shell 1895 Resin
Alpha
1
0.9
0.8
0.7
0.6
0.5
0.4
0.3
0.2
0.1
0
0
50
100
150
200
250
300
350
400
Time(min)
135C Cure 5/93
135C Cure 7/91

Figure 4.10

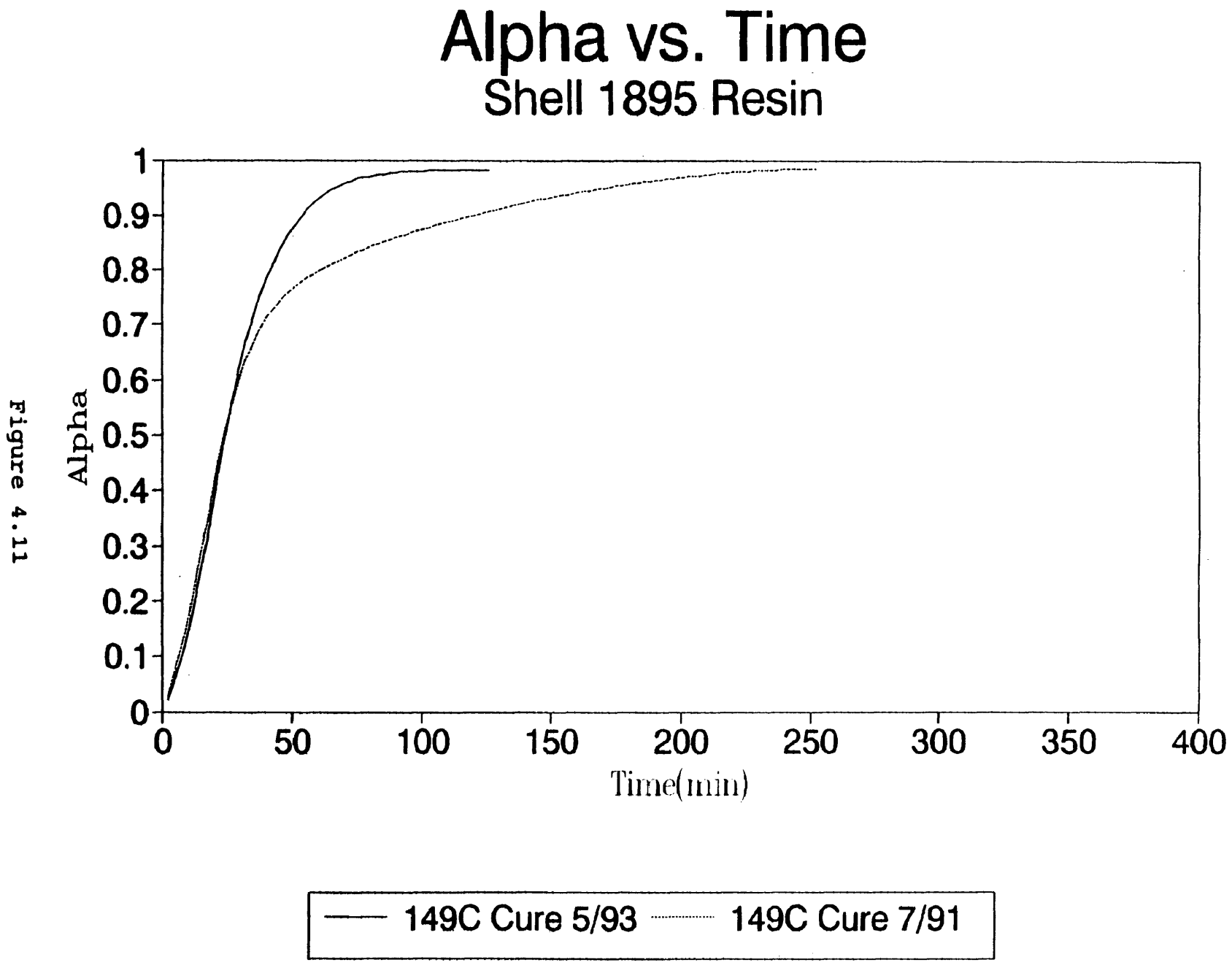
Alpha vs. Time
Shell 1895 Resin
Alpha
1
0.9
0.8
0.7
0.6
0.5
0.4
0.3
0.2
0.1
0
0
50
100
150
200
250
300
350
400
Time(min)
149C Cure 5/93
149C Cure 7/91

Figure 4.11

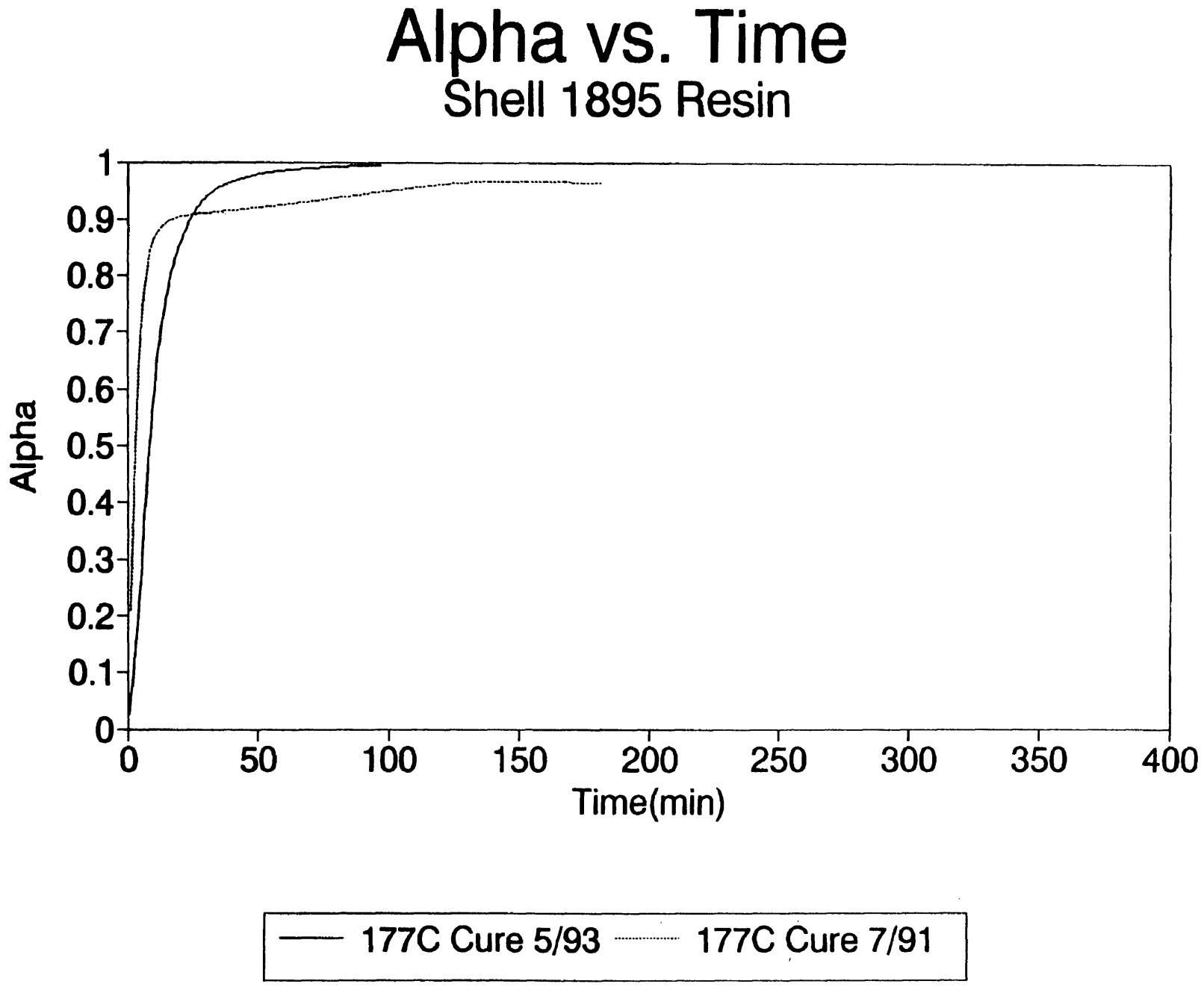
Alpha vs. Time
Shell 1895 Resin
Alpha
1
0.9
0.8
0.7
0.6
0.5
0.4
0.3
0.2
0.1
0
0
50
100
150
200
250
300
350
400
Time(min)
177C Cure 5/93
177C Cure 7/91

Figure 4.12

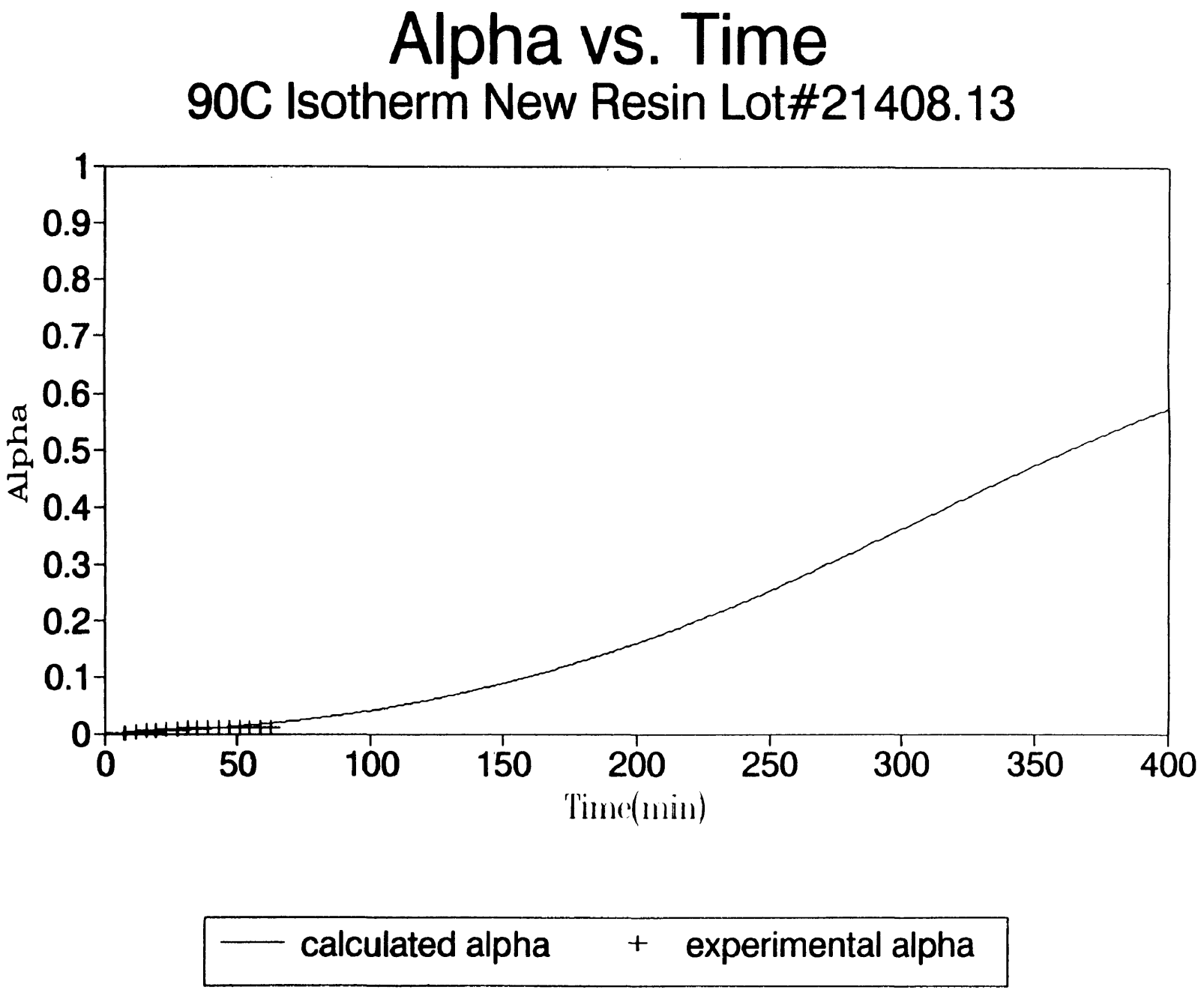
Alpha vs. Time
90C Isotherm New Resin Lot#21408.13
Alpha
1
0.9
0.8
0.7
0.6
0.5
0.4
0.3
0.2
0.1
0
0
50
100
150
200
250
300
350
400
Time(min)
calculated alpha
experimental alpha

Figure 4.13

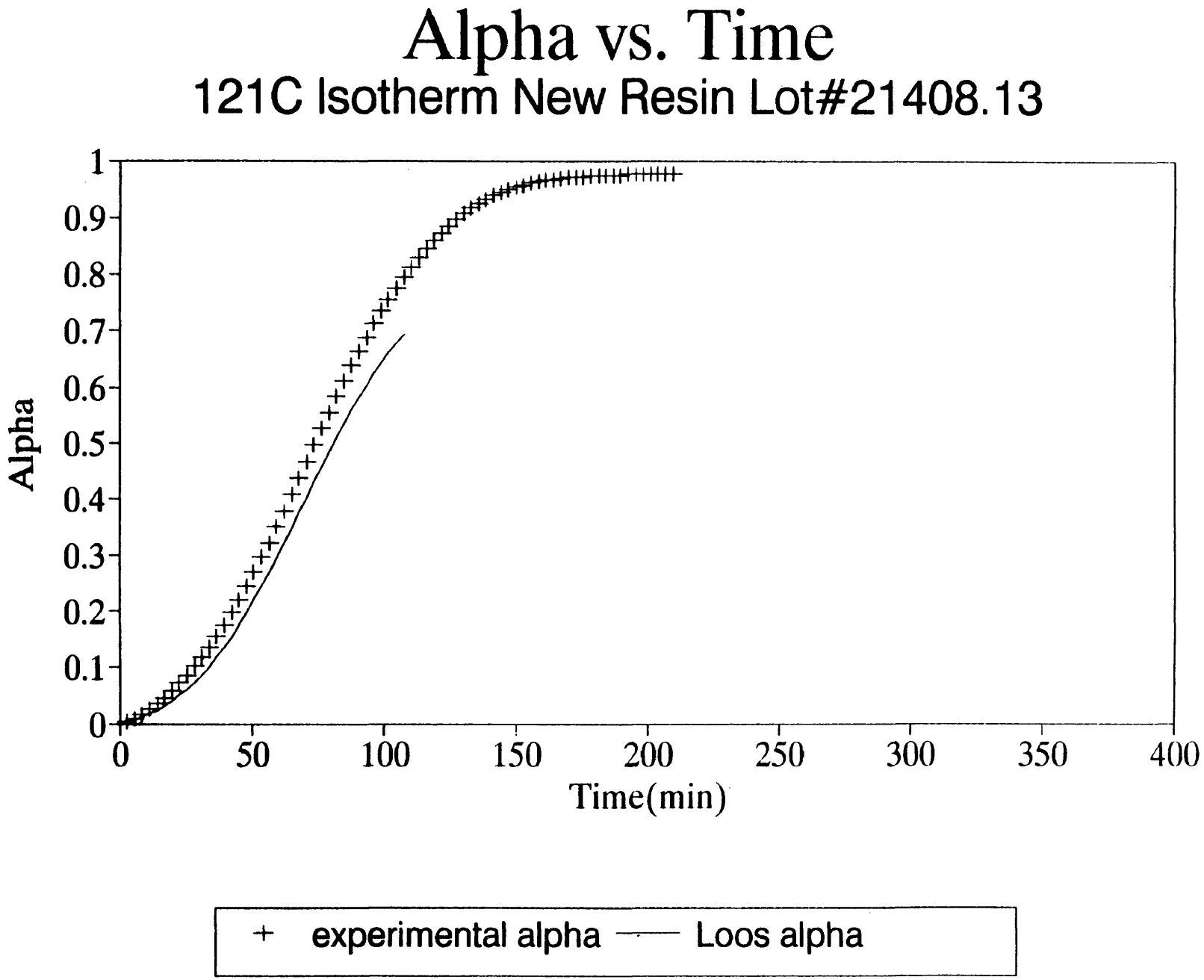
Alpha vs. Time
121C Isotherm New Resin Lot#21408.13
Alpha
1
0.9
0.8
0.7
0.6
0.5
0.4
0.3
0.2
0.1
0
0
50
100
150
200
250
300
350
400
Time(min)
experimental alpha
Loos alpha

Figure 4.14

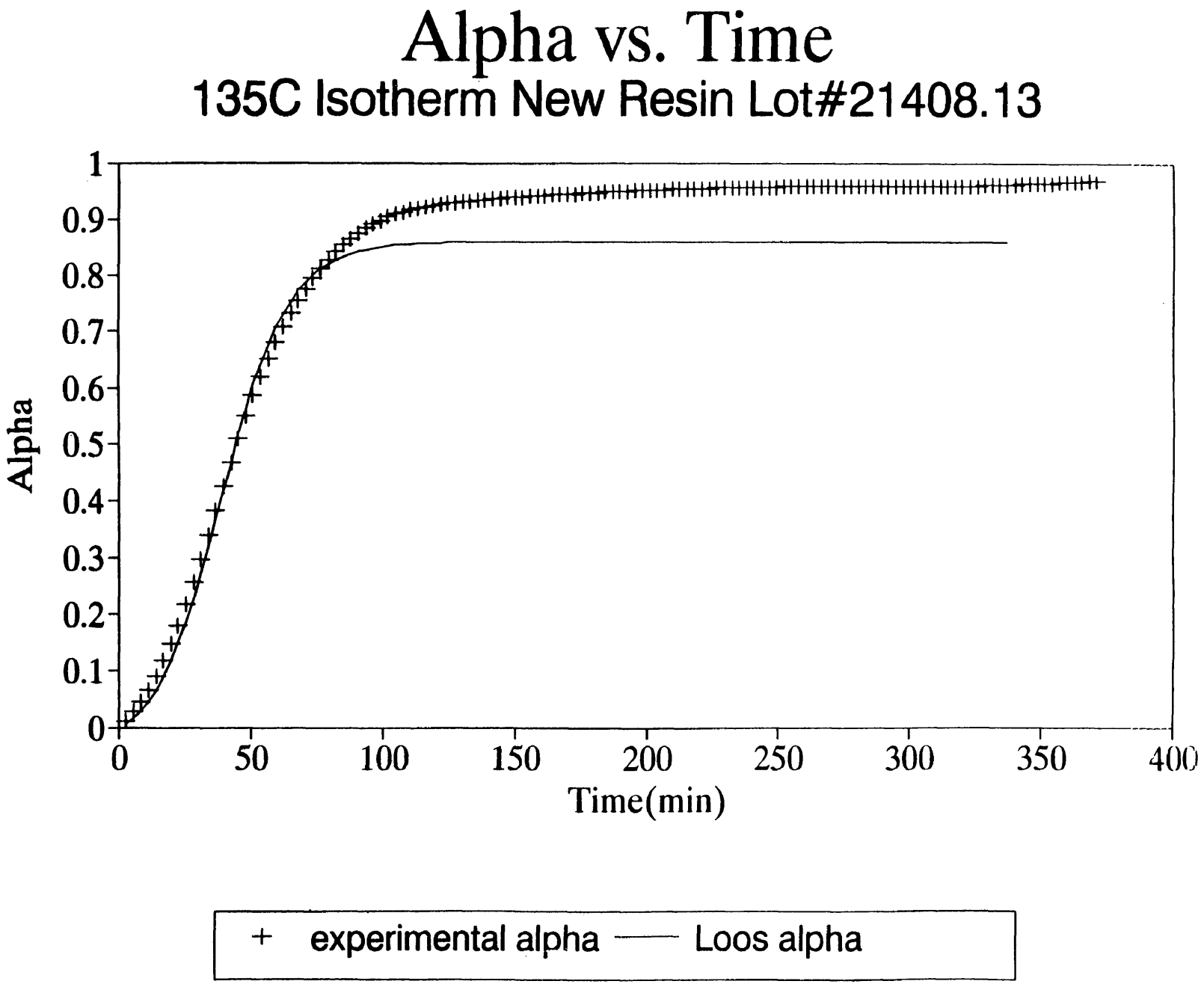
Alpha vs. Time
135C Isotherm New Resin Lot#21408.13
Alpha
1
0.9
0.8
0.7
0.6
0.5
0.4
0.3
0.2
0.1
0
0
50
100
150
200
250
300
350
400
Time(min)
+ experimental alpha
Loos alpha

Figure 4.15

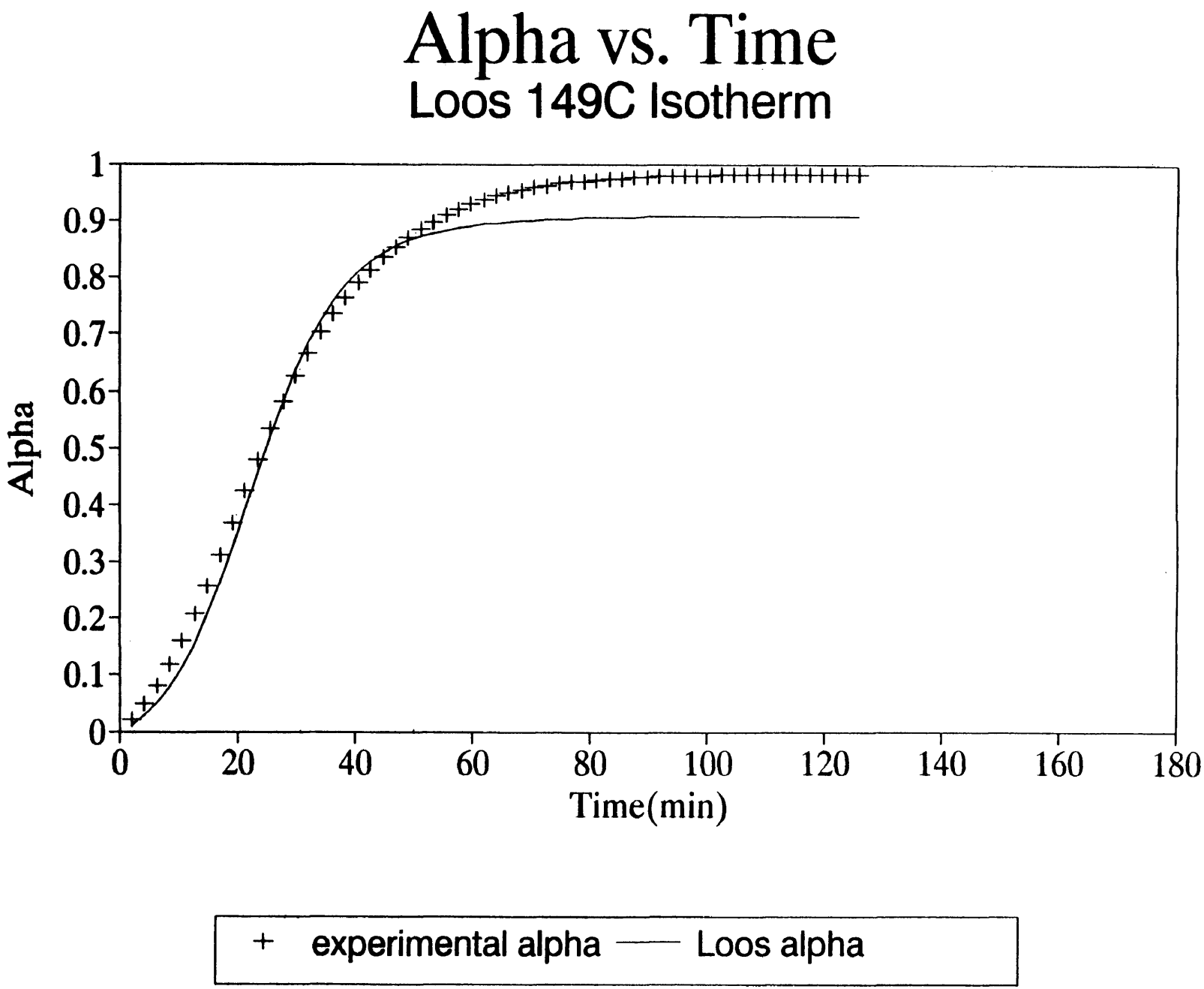
Alpha vs. Time
Loos 149C Isotherm
Alpha
1
0.9
0.8
0.7
0.6
0.5
0.4
0.3
0.2
0.1
0
0
20
40
60
80
100
120
140
160
180
Time(min)
+ experimental alpha
Loos alpha

Figure 4.16

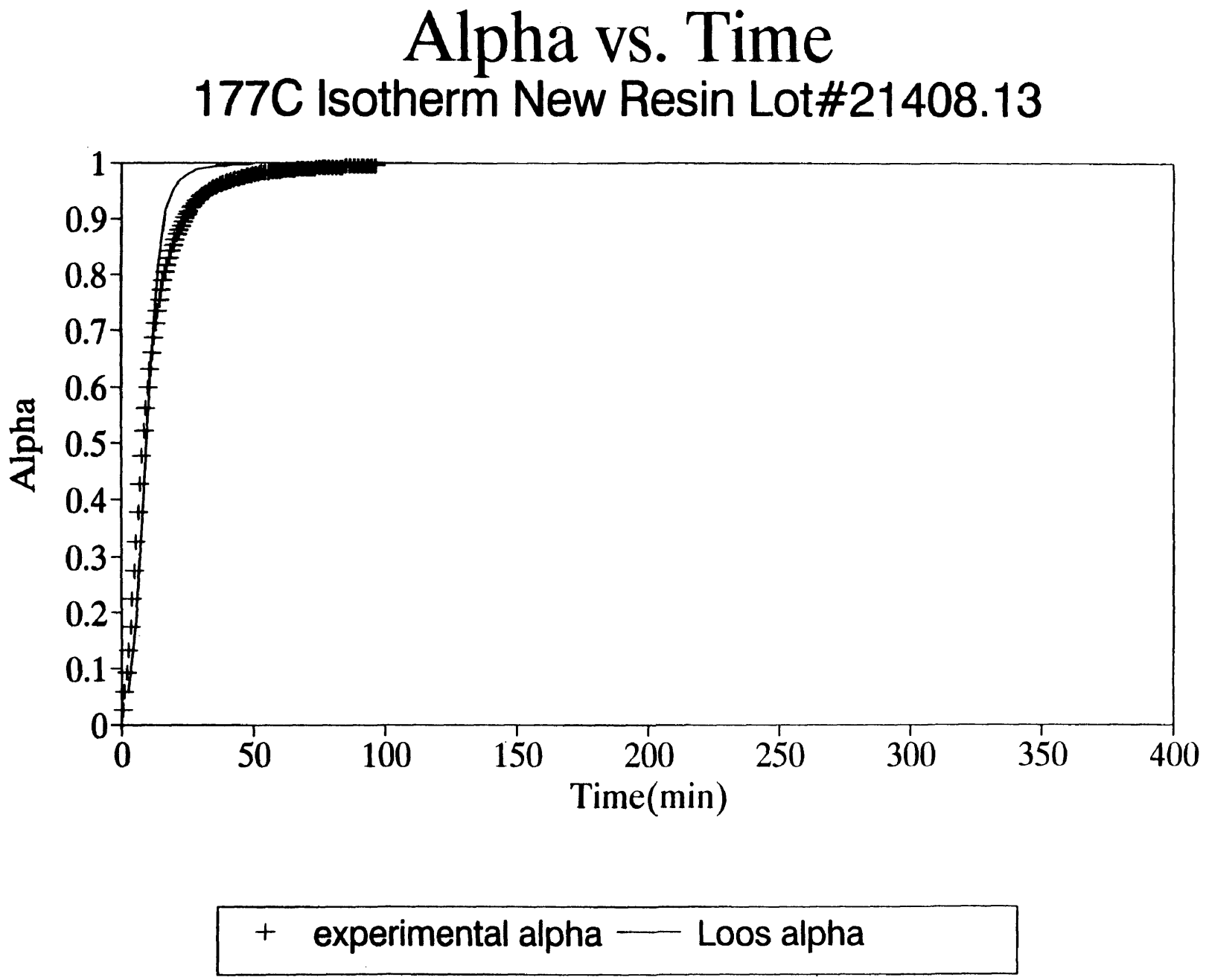
Alpha vs. Time
177C Isotherm New Resin Lot#21408.13
Alpha
1
0.9
0.8
0.7
0.6
0.5
0.4
0.3
0.2
0.1
0
0
50
100
150
200
250
300
350
400
Time(min)
+ experimental alpha
Loos alpha

Figure 4.17

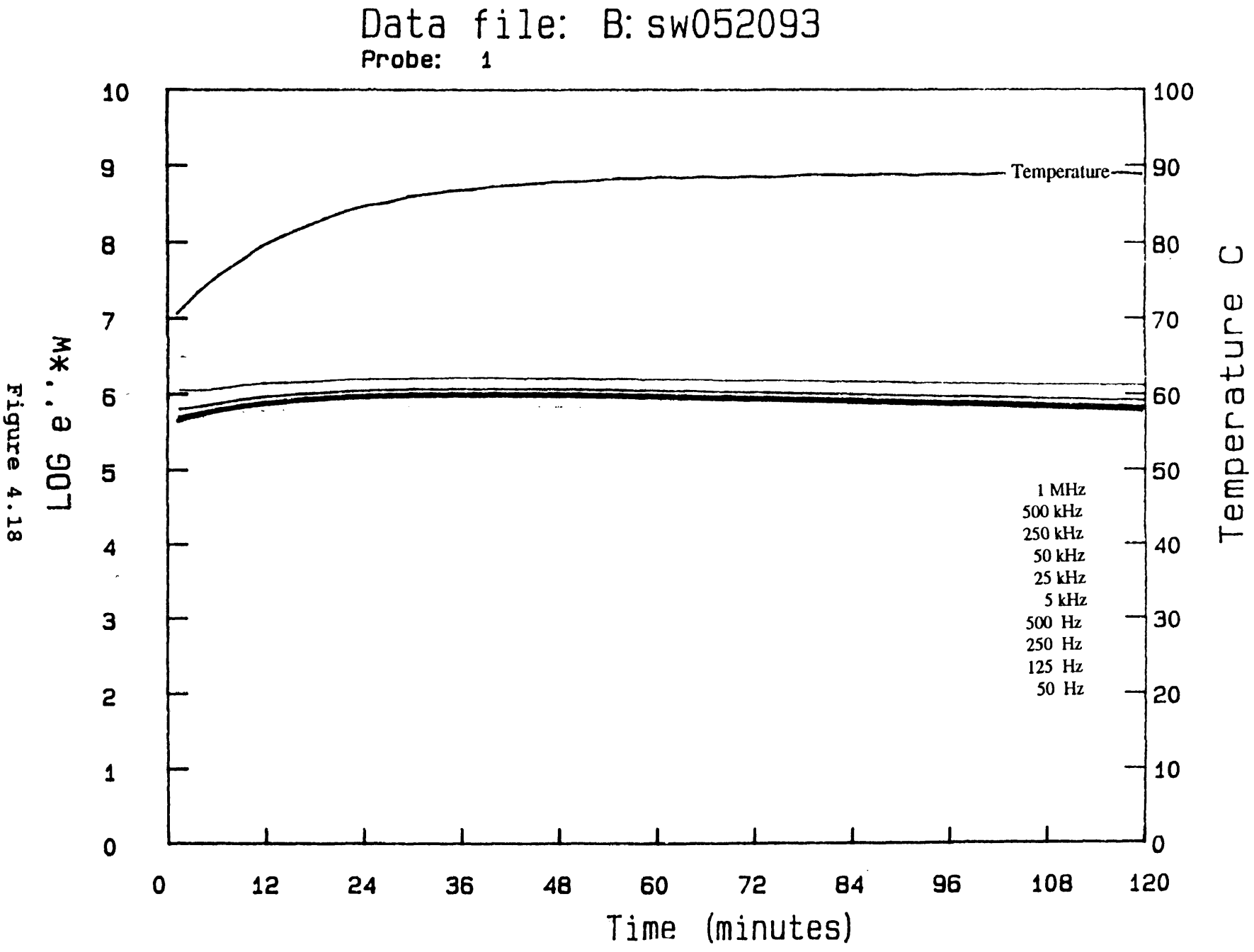
Data file: B:sw052093
Probe: 1
LOG e''*w
Temperature C
Time (minutes)
Temperature
1 MHz
500 kHz
250 kHz
50 kHz
25 kHz
5 kHz
500 Hz
250 Hz
125 Hz
50 Hz
0
1
2
3
4
5
6
7
8
9
10
0
10
20
30
40
50
60
70
80
90
100
0
12
24
36
48
60
72
84
96
108
120

Figure 4.18

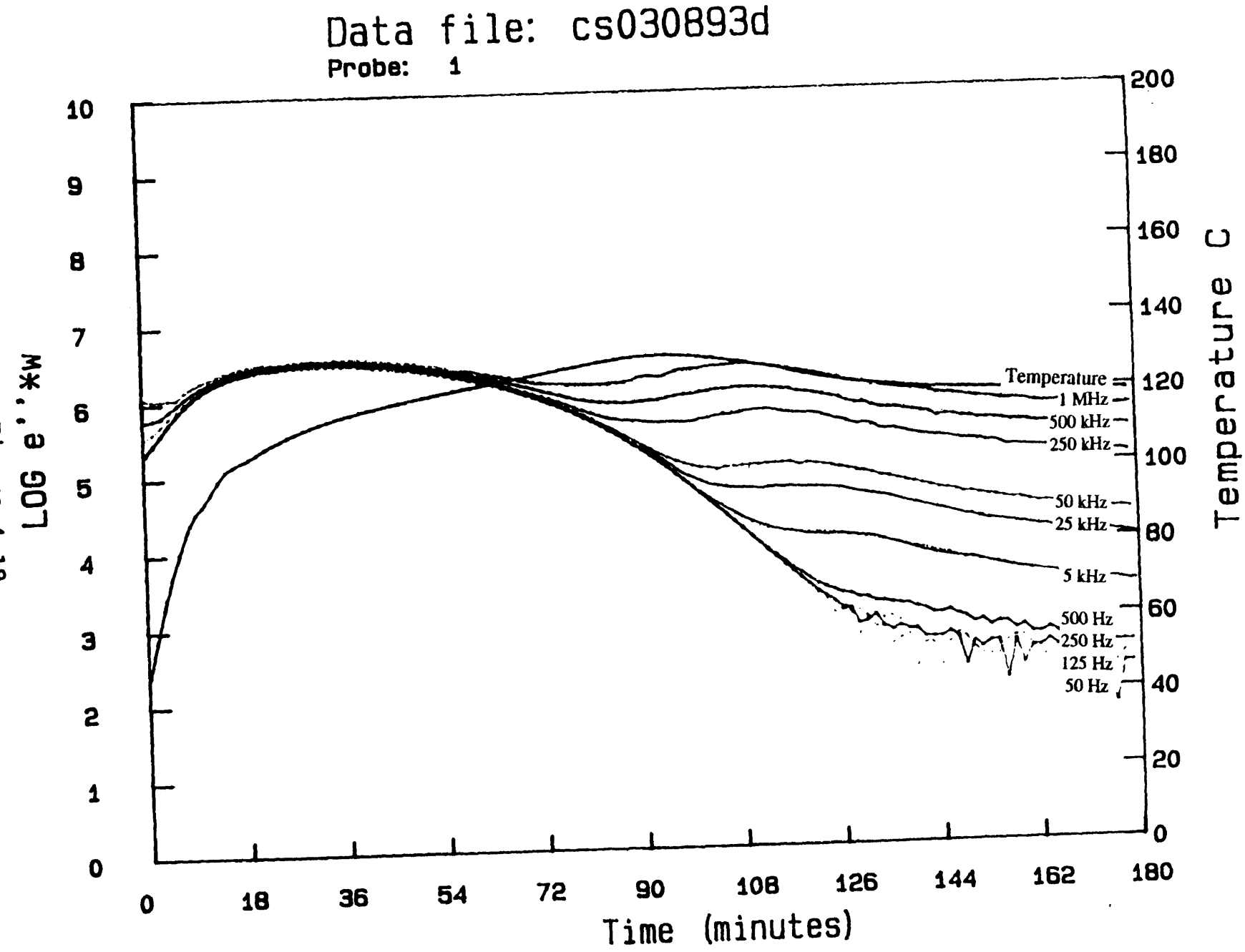
Data file: cs030893d
Probe: 1
LOG e'',*W
Temperature C
Time (minutes)
Temperature
1 MHz
500 kHz
250 kHz
50 kHz
25 kHz
5 kHz
500 Hz
250 Hz
125 Hz
50 Hz
0
18
36
54
72
90
108
126
144
162
180
0
1
2
3
4
5
6
7
8
9
10
0
20
40
60
80
100
120
140
160
180
200

Figure 4.19

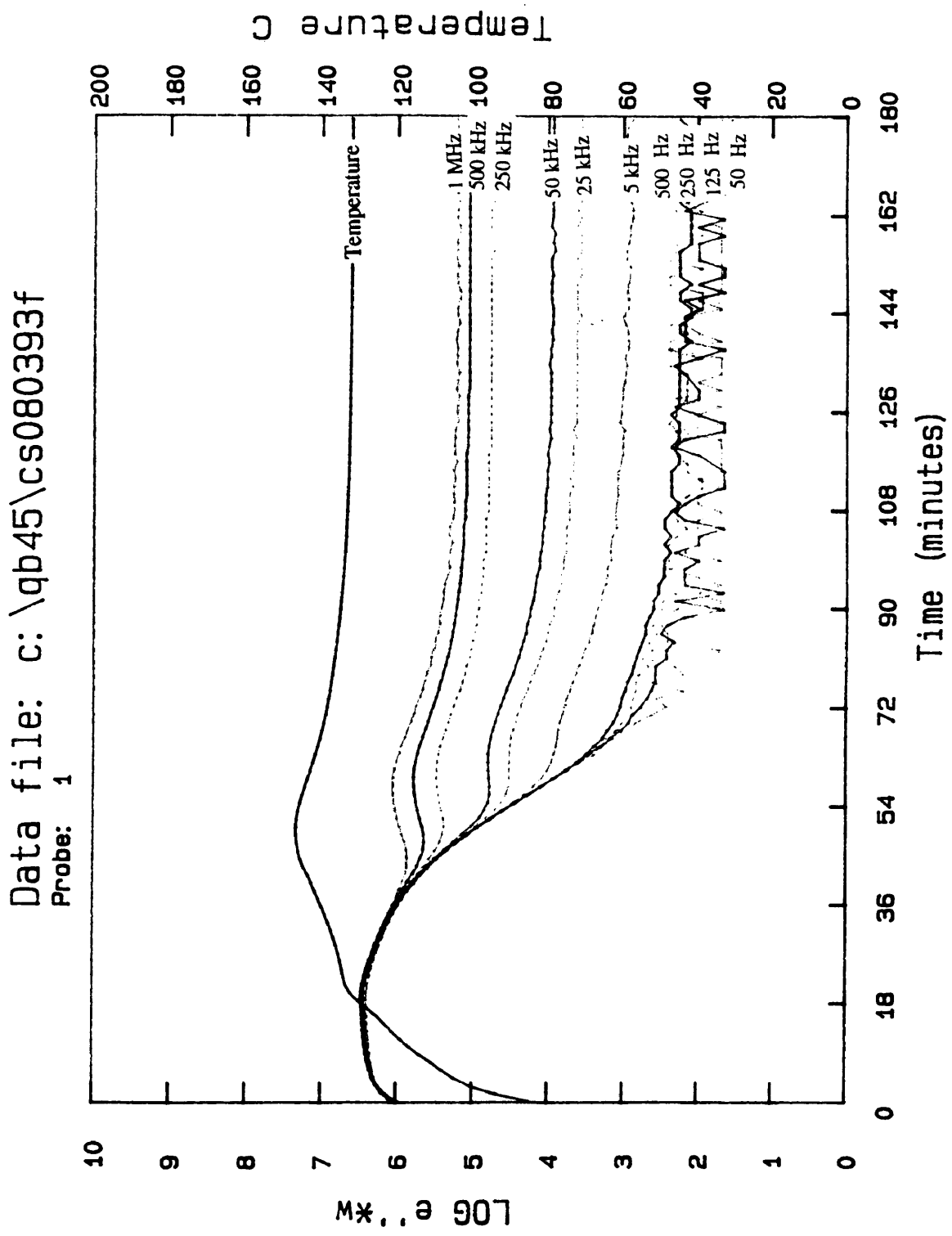
Data file: c:\qb45\cs080393f
Probe: 1
Temperature C
Log e''*W
Time (minutes)
Temperature
1 MHz
500 kHz
250 kHz
50 kHz
25 kHz
5 kHz
500 Hz
250 Hz
125 Hz
50 Hz
200
180
160
140
120
100
80
60
40
20
0
10
9
8
7
6
5
4
3
2
1
0
18
36
54
72
90
108
126
144
162
180

Figure 4.20

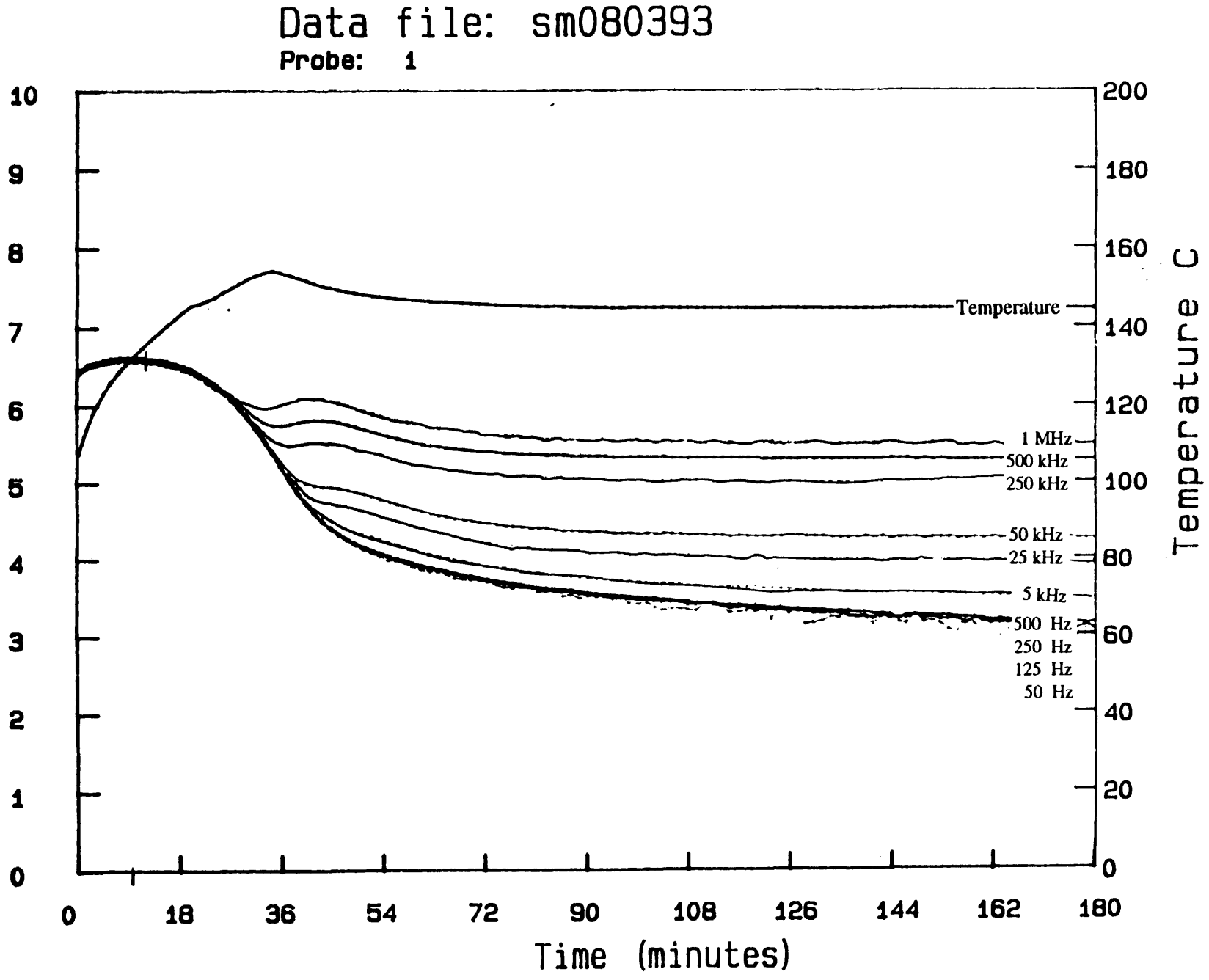
Data file: sm080393
Probe: 1
LOG e'',e* W
Temperature C
Time (minutes)
Temperature
1 MHz
500 kHz
250 kHz
50 kHz
25 kHz
5 kHz
500 Hz
250 Hz
125 Hz
50 Hz
0
1
2
3
4
5
6
7
8
9
10
0
18
36
54
72
90
108
126
144
162
180
0
20
40
60
80
100
120
140
160
180
200

Figure 4.21

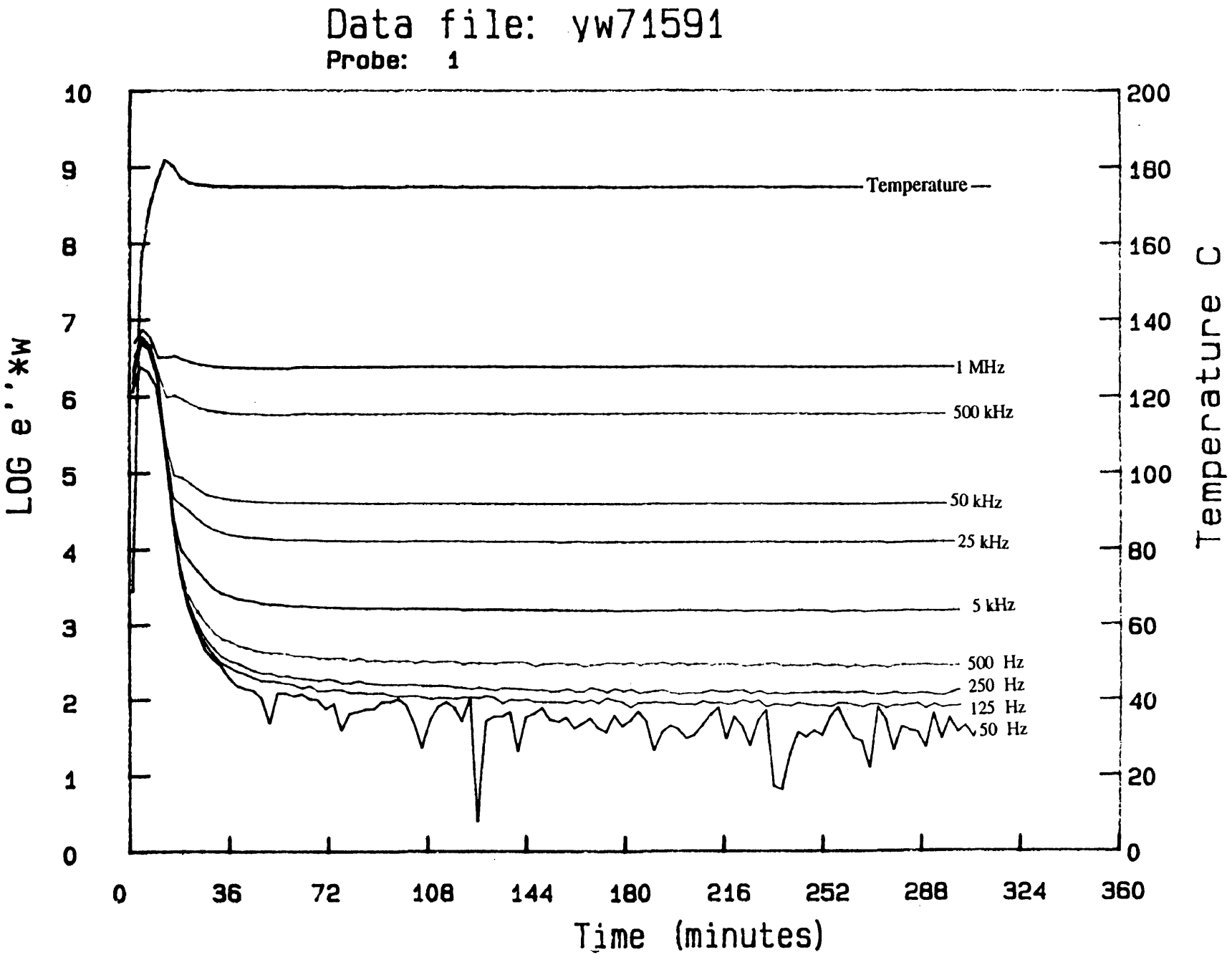
Data file: yw71591
Probe: 1
LOG e**,,e
Temperature C
Time (minutes)
Temperature
1 MHz
500 kHz
50 kHz
25 kHz
5 kHz
500 Hz
250 Hz
125 Hz
50 Hz
0
1
2
3
4
5
6
7
8
9
10
0
20
40
60
80
100
120
140
160
180
200
0
36
72
108
144
180
216
252
288
324
360

Figure 4.22

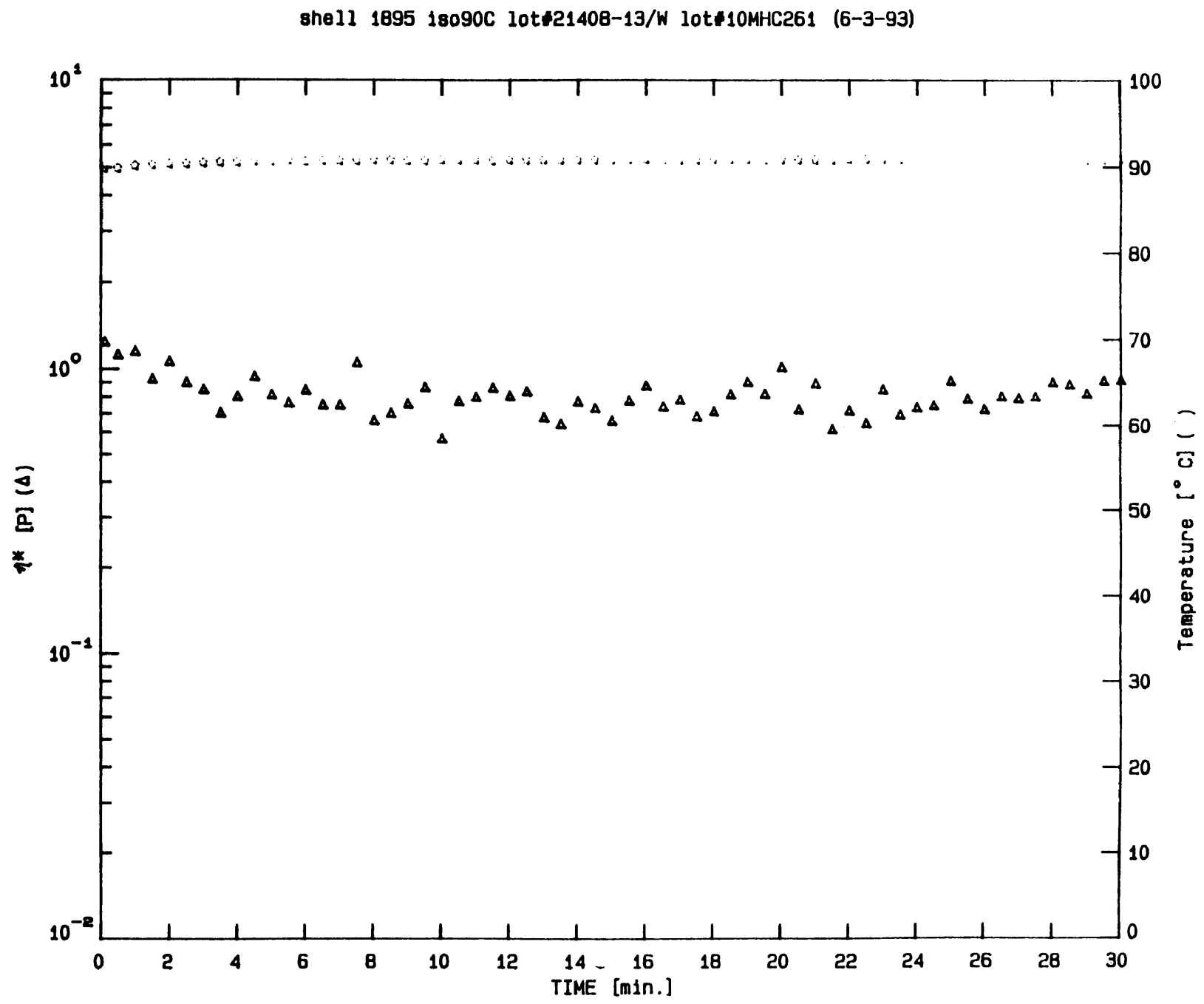
shell 1895 iso90C lot#21408-13/W lot#10MHC261 (6-3-93)
10^1
10^0
10^-1
10^-2
η* [P] (Δ)
100
90
80
70
60
50
40
30
20
10
0
Temperature [° C] ( )
0
2
4
6
8
10
12
14
16
18
20
22
24
26
28
30
TIME [min.]

Figure 4.23

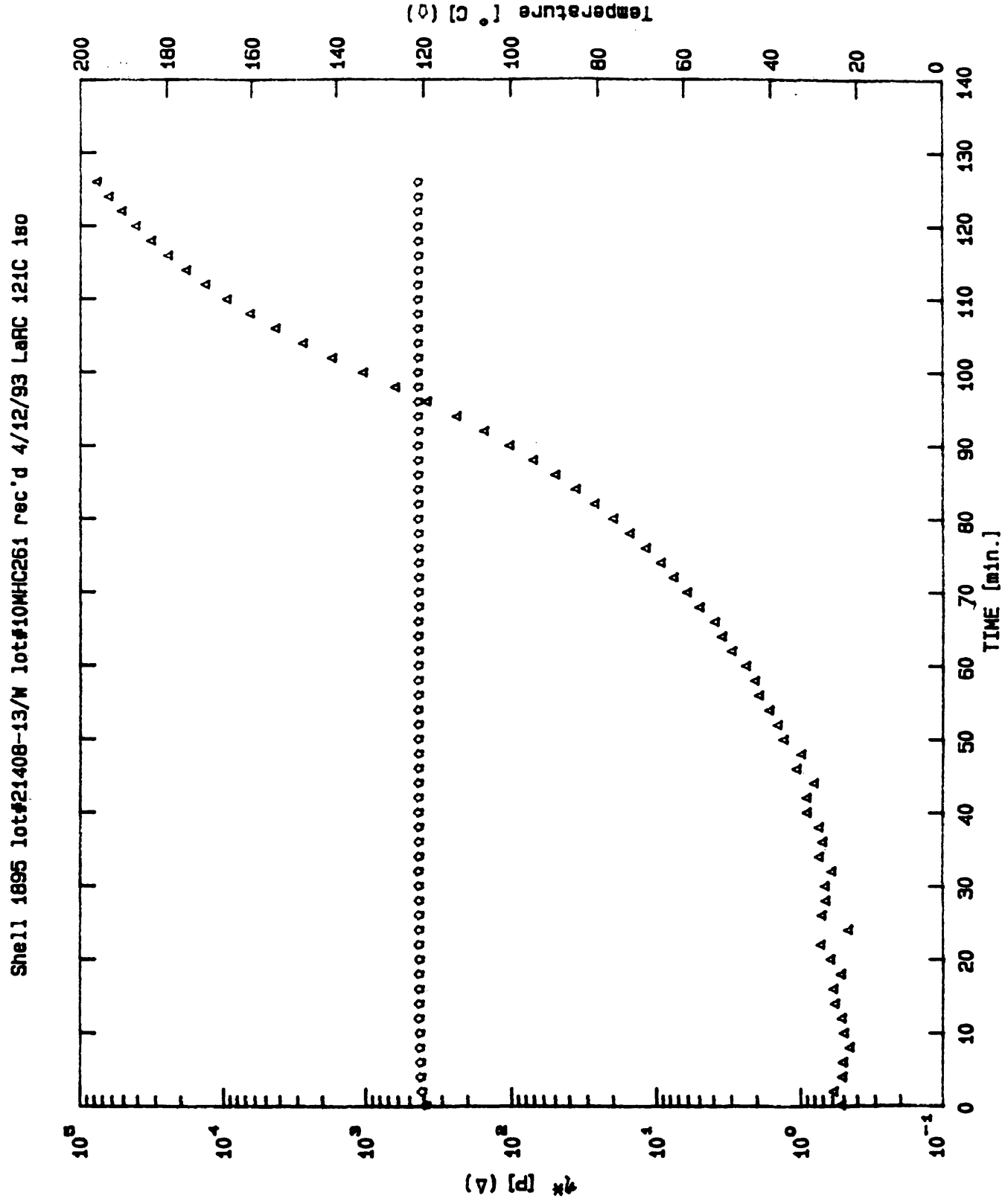
Shell 1895 lot#21408-13/W lot#10WHC261 rec'd 4/12/93 LaRC 121C iso
Temperature [° C] (O)
200
180
160
140
120
100
80
60
40
20
0
140
130
120
110
100
90
80
70
60
50
40
30
20
10
0
TIME [min.]
η* [P] (Δ)
10^5
10^4
10^3
10^2
10^1
10^0
10^-1

Figure 4.24

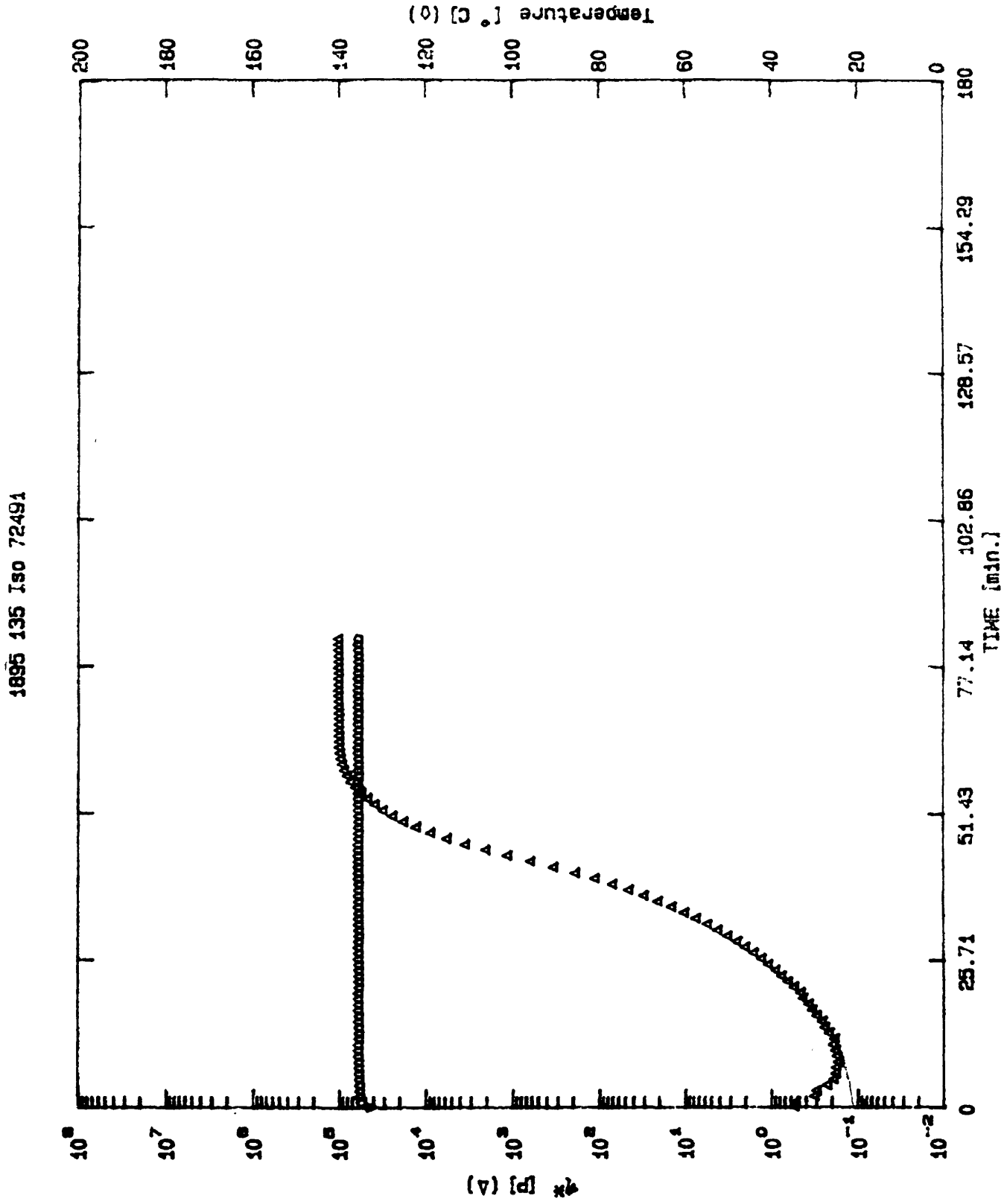
Temperature [° C] (0)
200
180
160
140
120
100
80
60
40
20
0
180
154.29
128.57
102.86
77.14
51.43
25.71
0
TIME [min.]
1895 135 Iso 72491
10^{8}
10^{7}
10^{6}
10^{5}
10^{4}
10^{3}
10^{2}
10^{1}
10^{0}
10^{-1}
10^{-2}
Φ^{*} [p] (A)

Figure 4.25

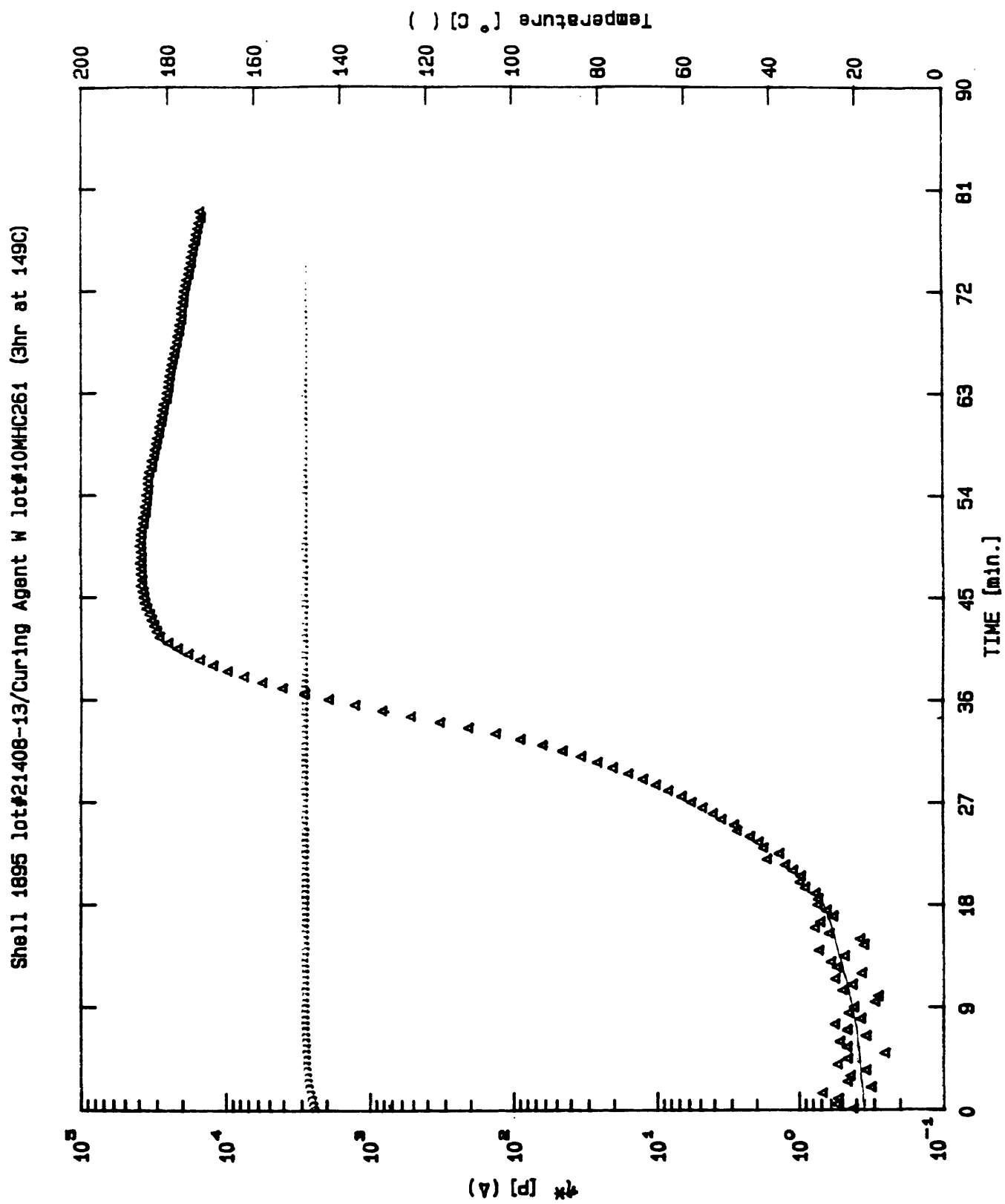
Shell 1895 lot#21408-13/Curing Agent W lot#10MHC261 (3hr at 149C)
Temperature [° C] ( )
TIME [min.]
ϕ* [p] (Å)

Figure 4.26

Temperature [° C] (O)
200
180
160
140
120
100
80
60
40
20
0
20
17.14
14.29
11.43
8.57
5.71
2.86
0
TIME [min.]
shell1895 177 iso 10%str
10^{-8}
10^{-7}
10^{-6}
10^{-5}
10^{-4}
10^{-3}
10^{-2}
10^{-1}
10^{0}
10^{-1}
10^{-2}
ϕ^* [p] (A)

Figure 4.27

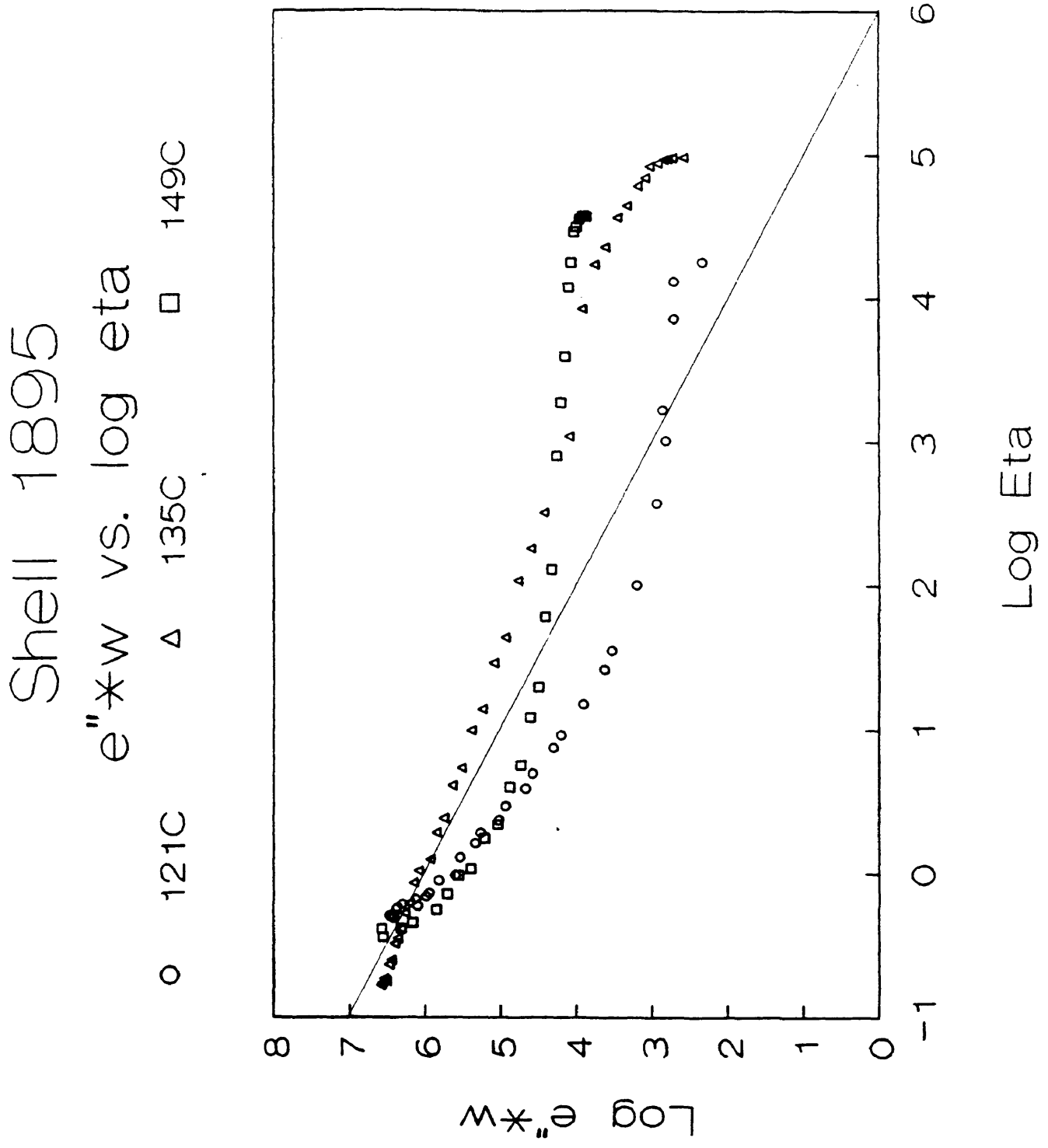
Shell 1895
e"*w vs. log eta
o 121C
Δ 135C
□ 149C
Log e"*w
Log Eta
8
7
6
5
4
3
2
1
0
-1
0
1
2
3
4
5
6

Figure 4.28

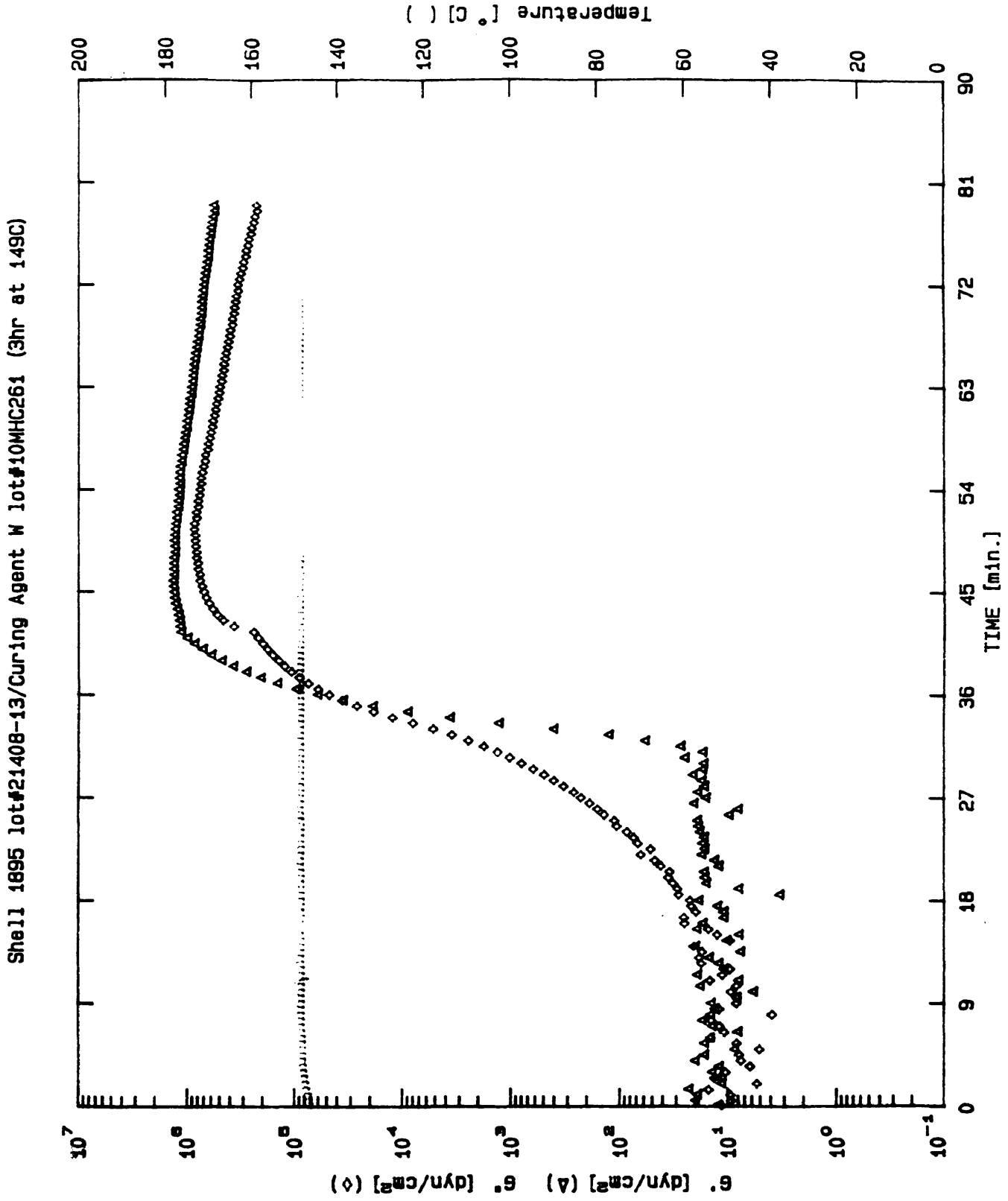
Shell 1895 lot#21408-13/Curing Agent W lot#10MHC261 (3hr at 149C)
Temperature [° C] ( )
TIME [min.]
σ' [dyn/cm²] (Δ) σ' [dyn/cm²] (◊)

Figure 4.29

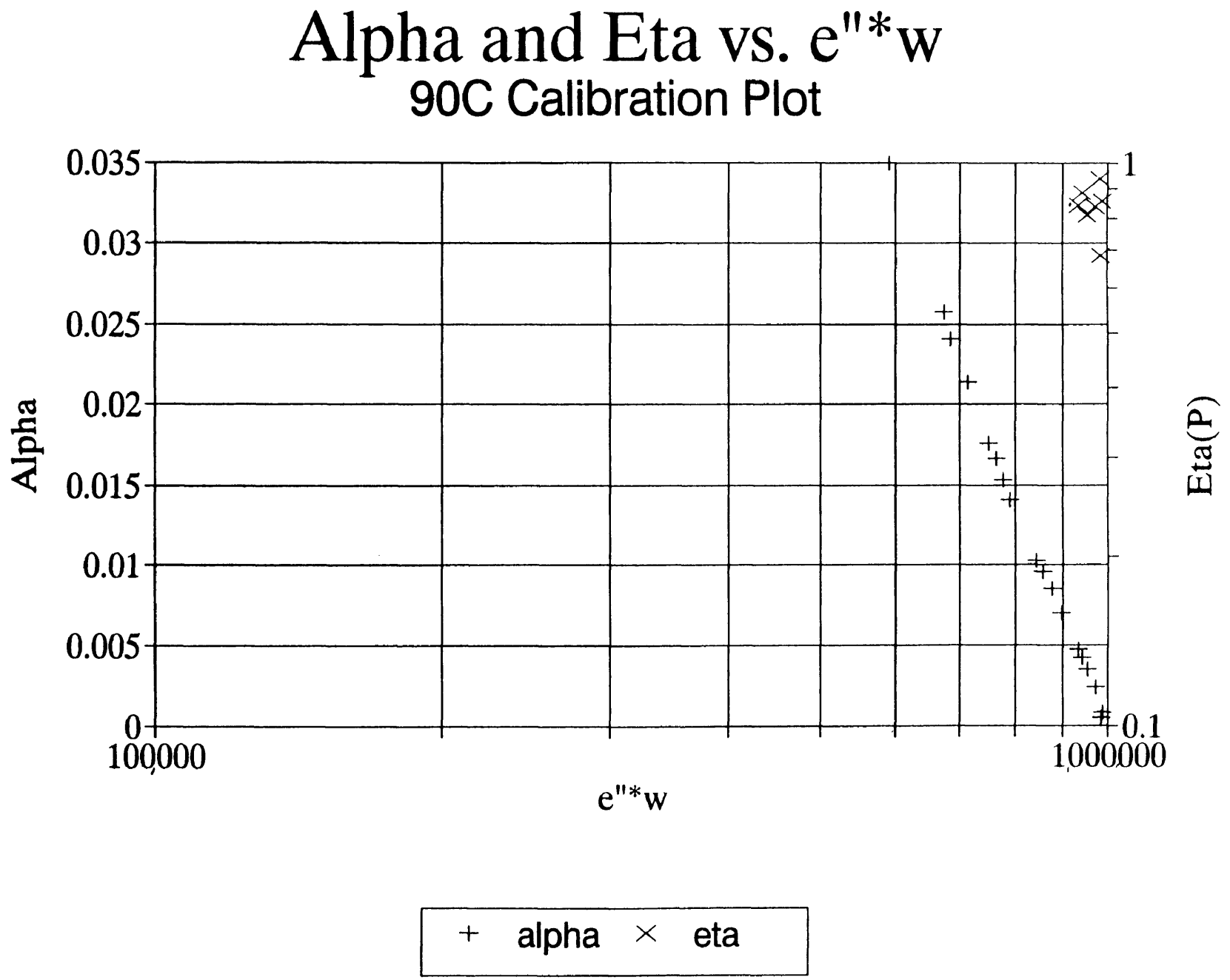
Alpha and Eta vs. e"*w
90C Calibration Plot
0.035
0.03
0.025
0.02
0.015
0.01
0.005
0
Alpha
1
0.1
Eta(P)
100000
1000000
e"*w
+ alpha × eta

Figure 4.30

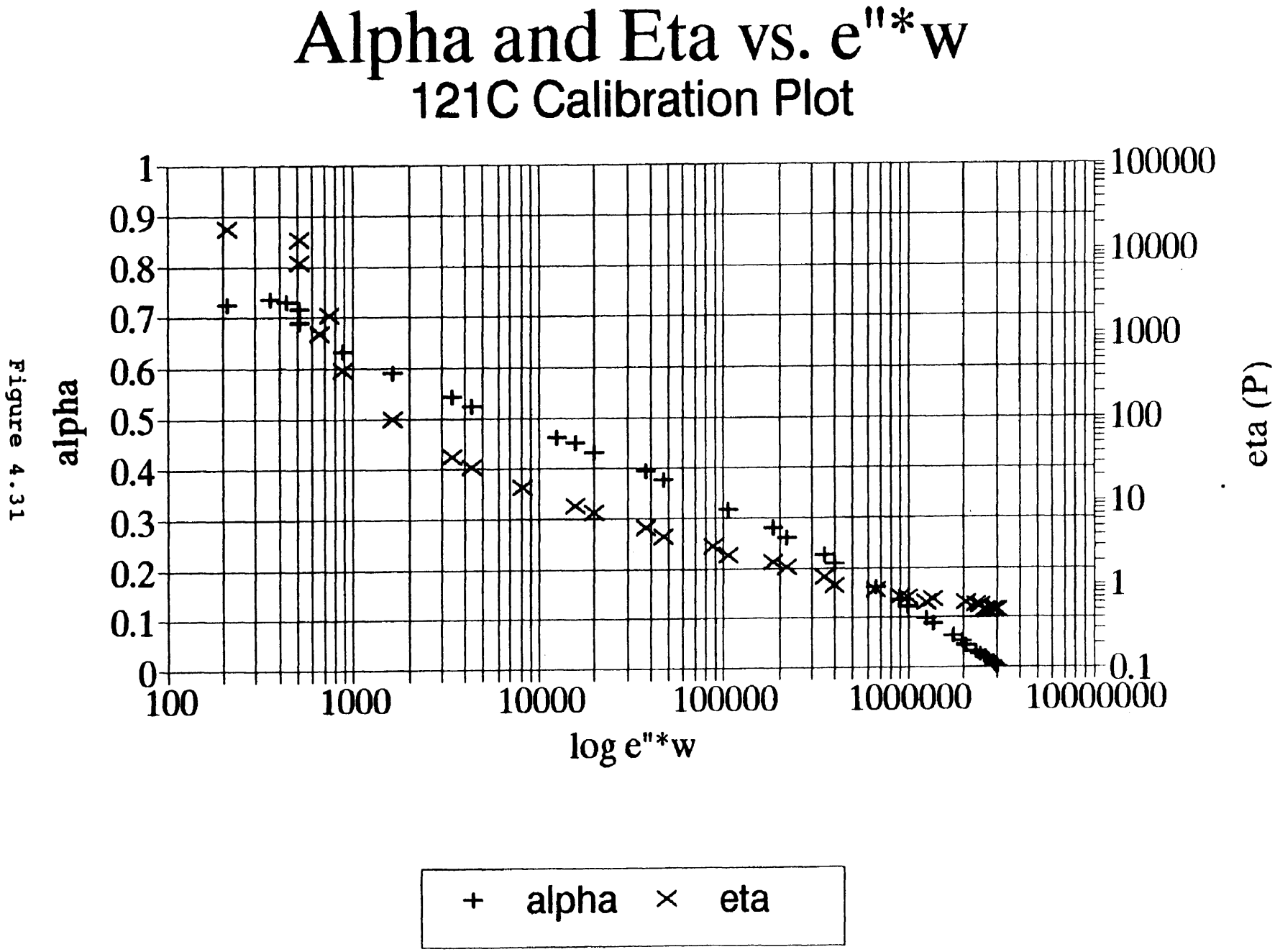
Alpha and Eta vs. e"*w
121C Calibration Plot
alpha
eta (P)
log e"*w
1
0.9
0.8
0.7
0.6
0.5
0.4
0.3
0.2
0.1
0
100000
10000
1000
100
10
1
0.1
100
1000
10000
100000
1000000
10000000
+ alpha × eta

Figure 4.31

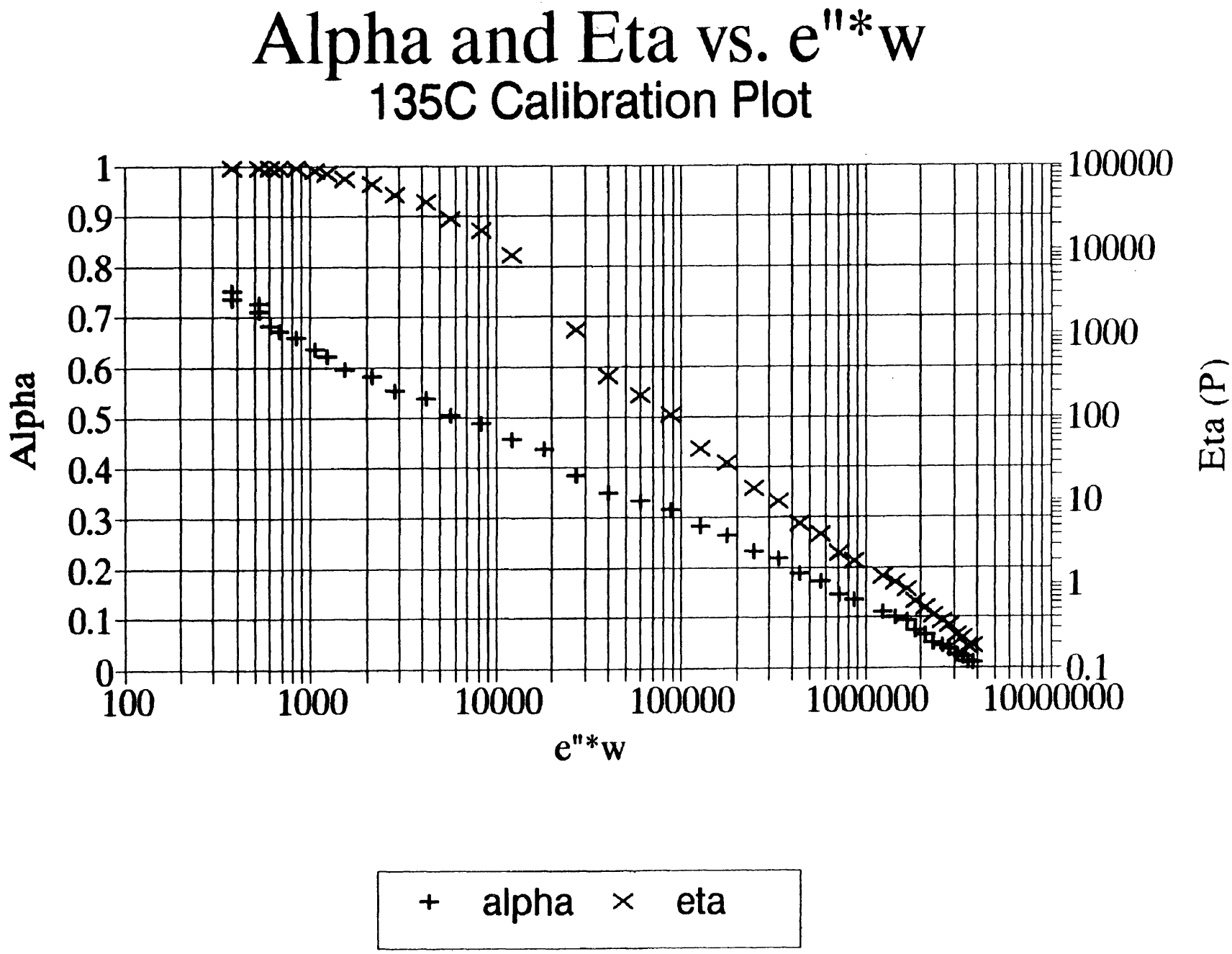
Alpha and Eta vs. e"*w
135C Calibration Plot
Alpha
Eta (P)
e"*w
1
0.9
0.8
0.7
0.6
0.5
0.4
0.3
0.2
0.1
0
100000
10000
1000
100
10
1
0.1
100
1000
10000
100000
1000000
10000000
+ alpha × eta

Figure 4.32

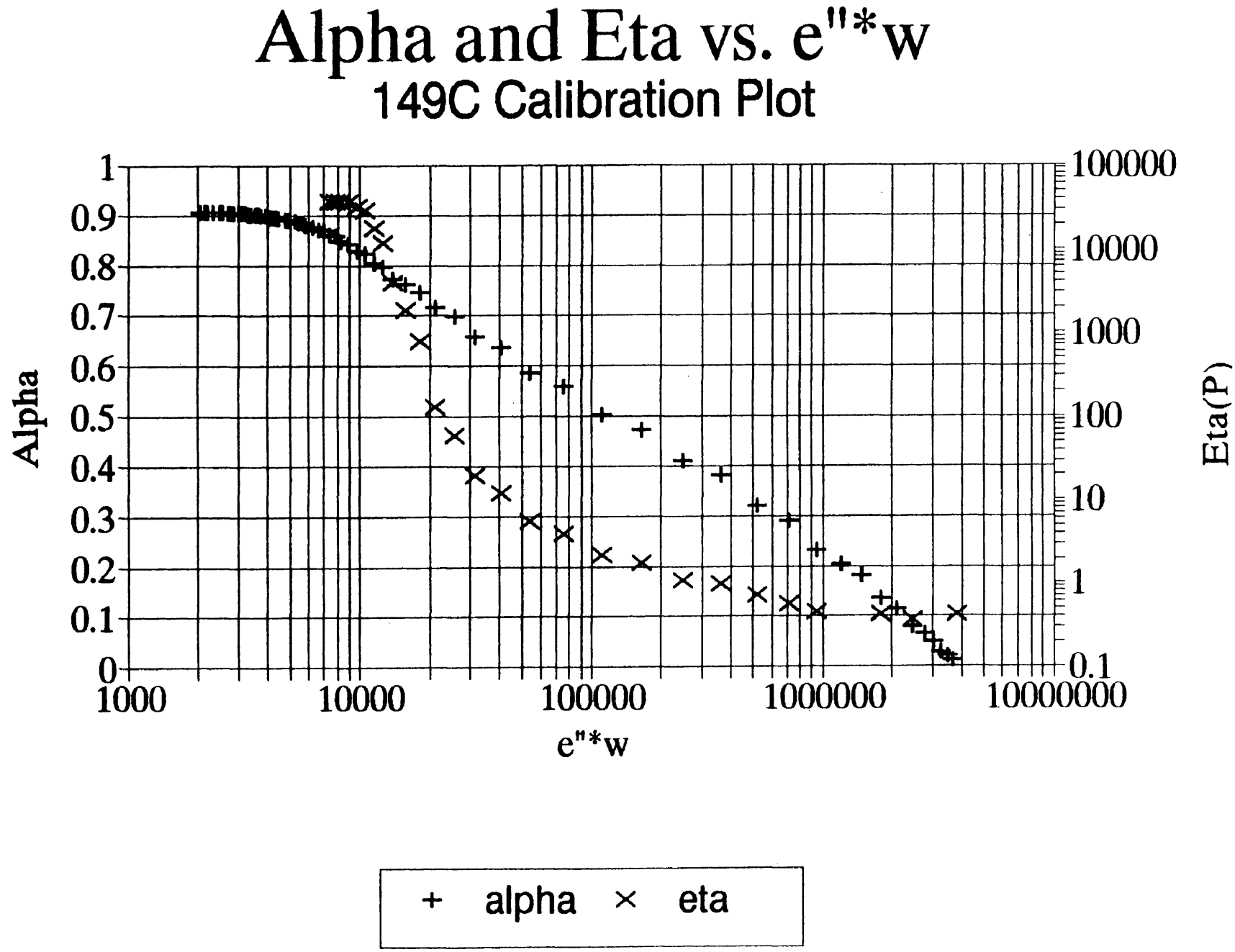
Alpha and Eta vs. e"*w
149C Calibration Plot
Alpha
Eta(P)
e"*w
1
0.9
0.8
0.7
0.6
0.5
0.4
0.3
0.2
0.1
0
100000
10000
1000
100
10
1
0.1
1000
10000
100000
1000000
10000000
+ alpha × eta

Figure 4.33

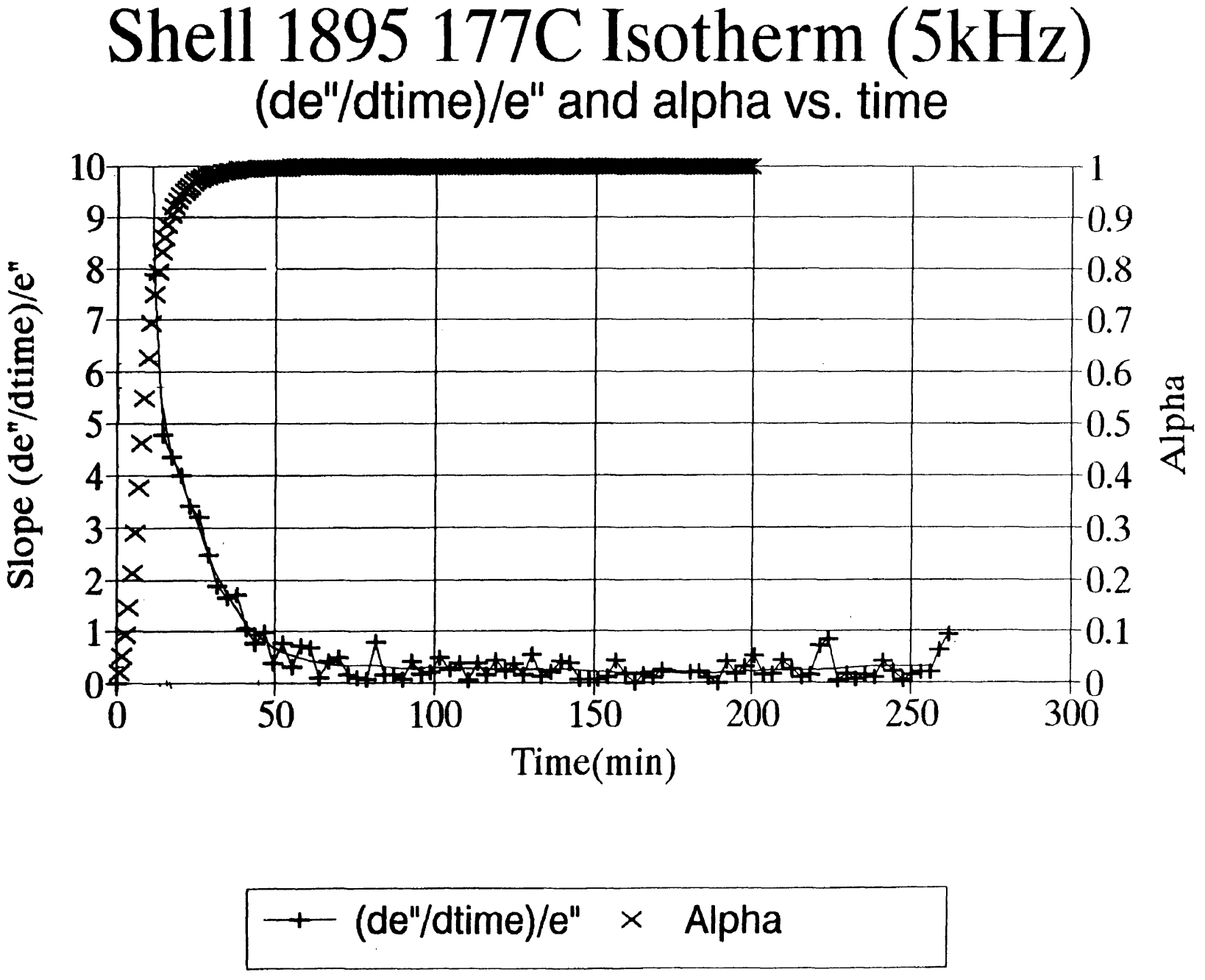
Shell 1895 177C Isotherm (5kHz)
(de"/dtime)/e" and alpha vs. time
Slope (de"/dtime)/e"
Alpha
Time(min)
0
1
2
3
4
5
6
7
8
9
10
0
0.1
0.2
0.3
0.4
0.5
0.6
0.7
0.8
0.9
1
0
50
100
150
200
250
300
(de"/dtime)/e"
Alpha

Figure 4.34

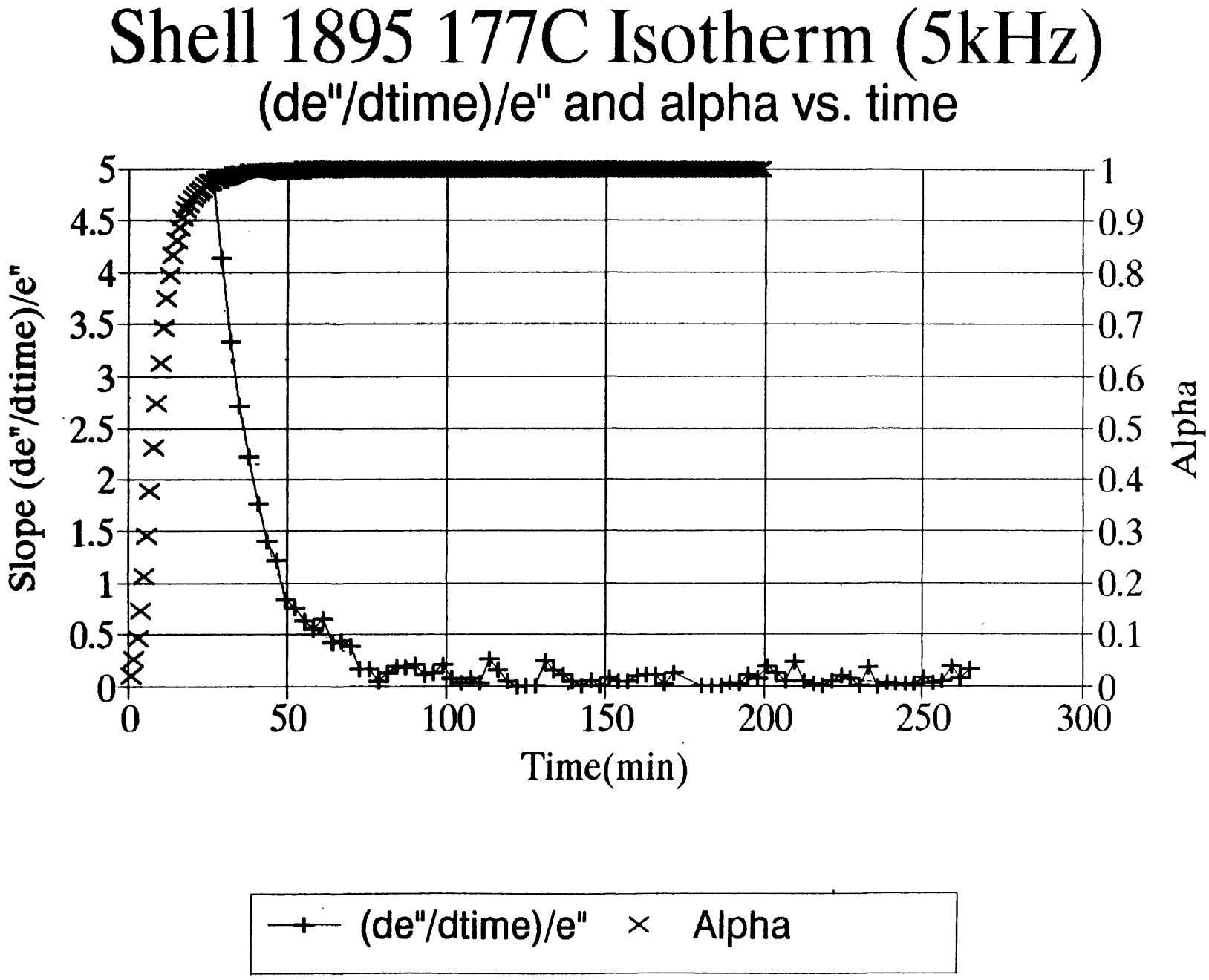
Shell 1895 177C Isotherm (5kHz)
(de"/dtime)/e" and alpha vs. time
Slope (de"/dtime)/e"
Alpha
Time(min)
0
0.5
1
1.5
2
2.5
3
3.5
4
4.5
5
0
0.1
0.2
0.3
0.4
0.5
0.6
0.7
0.8
0.9
1
0
50
100
150
200
250
300
(de"/dtime)/e"
Alpha

Figure 4.35

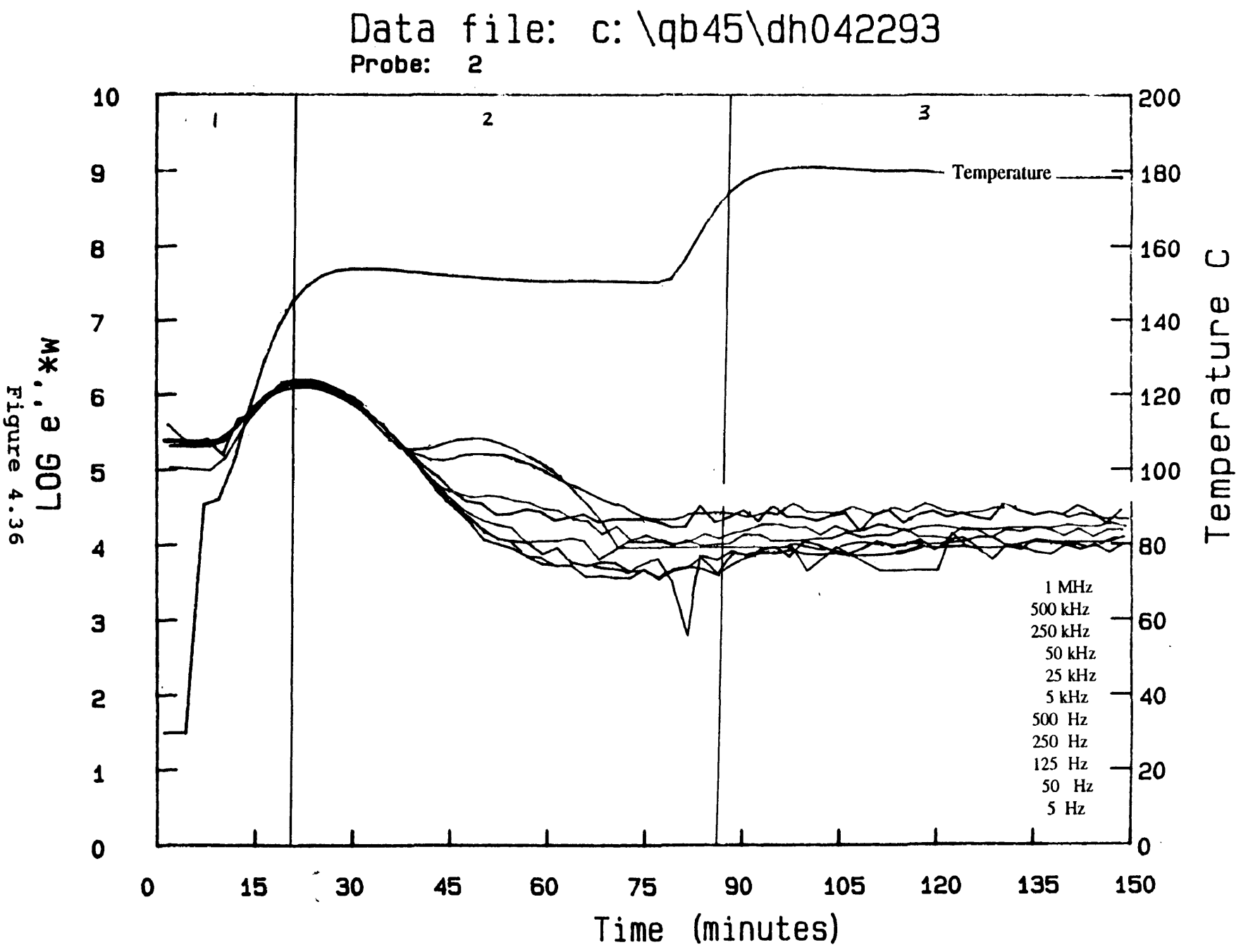
Data file: c:\qb45\dh042293
Probe: 2
1
2
3
Temperature
1 MHz
500 kHz
250 kHz
50 kHz
25 kHz
5 kHz
500 Hz
250 Hz
125 Hz
50 Hz
5 Hz
LOG e''*W
Temperature C
Time (minutes)
0
15
30
45
60
75
90
105
120
135
150
0
1
2
3
4
5
6
7
8
9
10
0
20
40
60
80
100
120
140
160
180
200

Figure 4.36

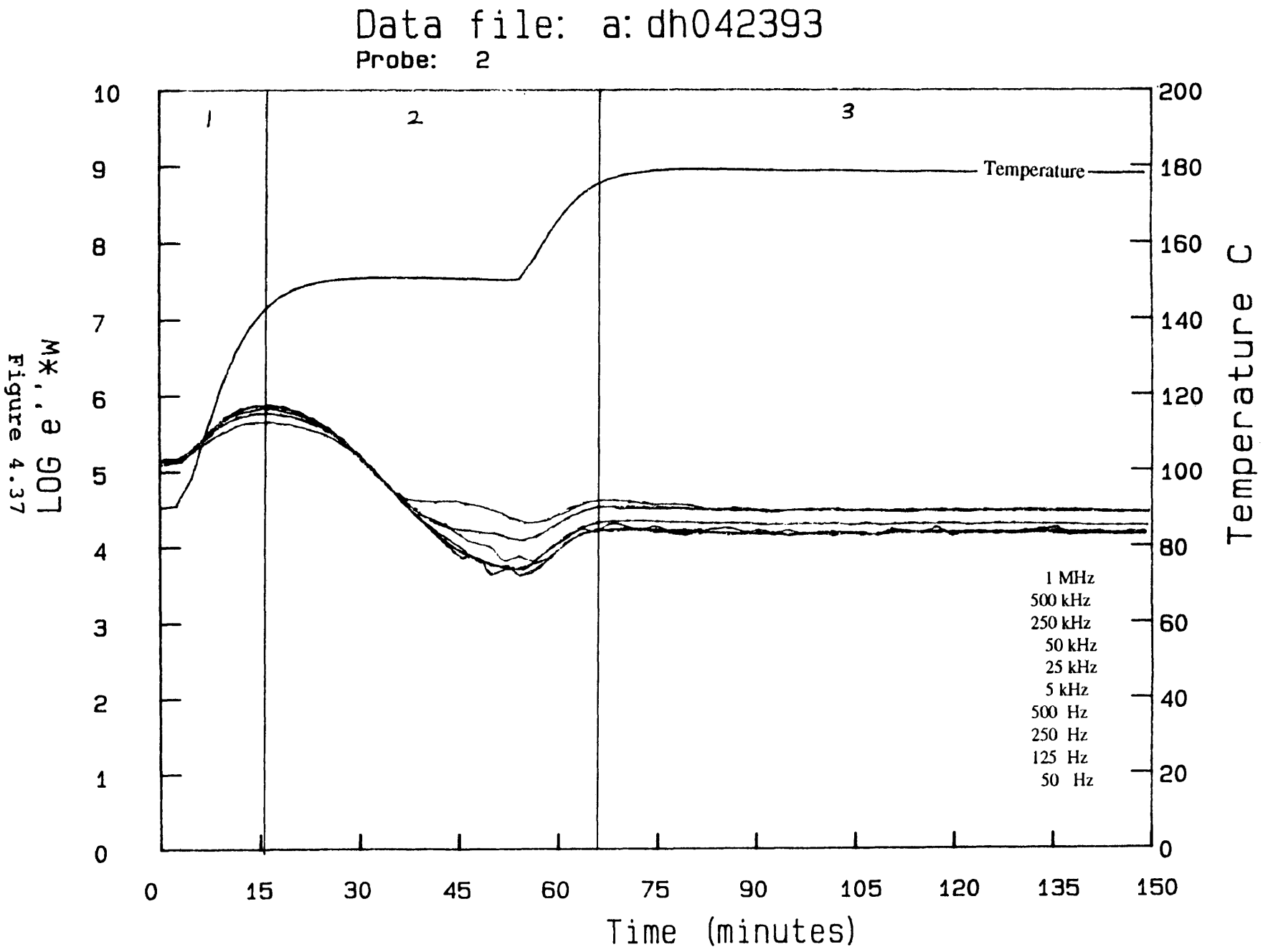
Data file: a:dh042393
Probe: 2
1
2
3
Temperature
1 MHz
500 kHz
250 kHz
50 kHz
25 kHz
5 kHz
500 Hz
250 Hz
125 Hz
50 Hz
LOG e'',e*W
Temperature C
Time (minutes)
0
15
30
45
60
75
90
105
120
135
150
0
1
2
3
4
5
6
7
8
9
10
0
20
40
60
80
100
120
140
160
180
200

Figure 4.37

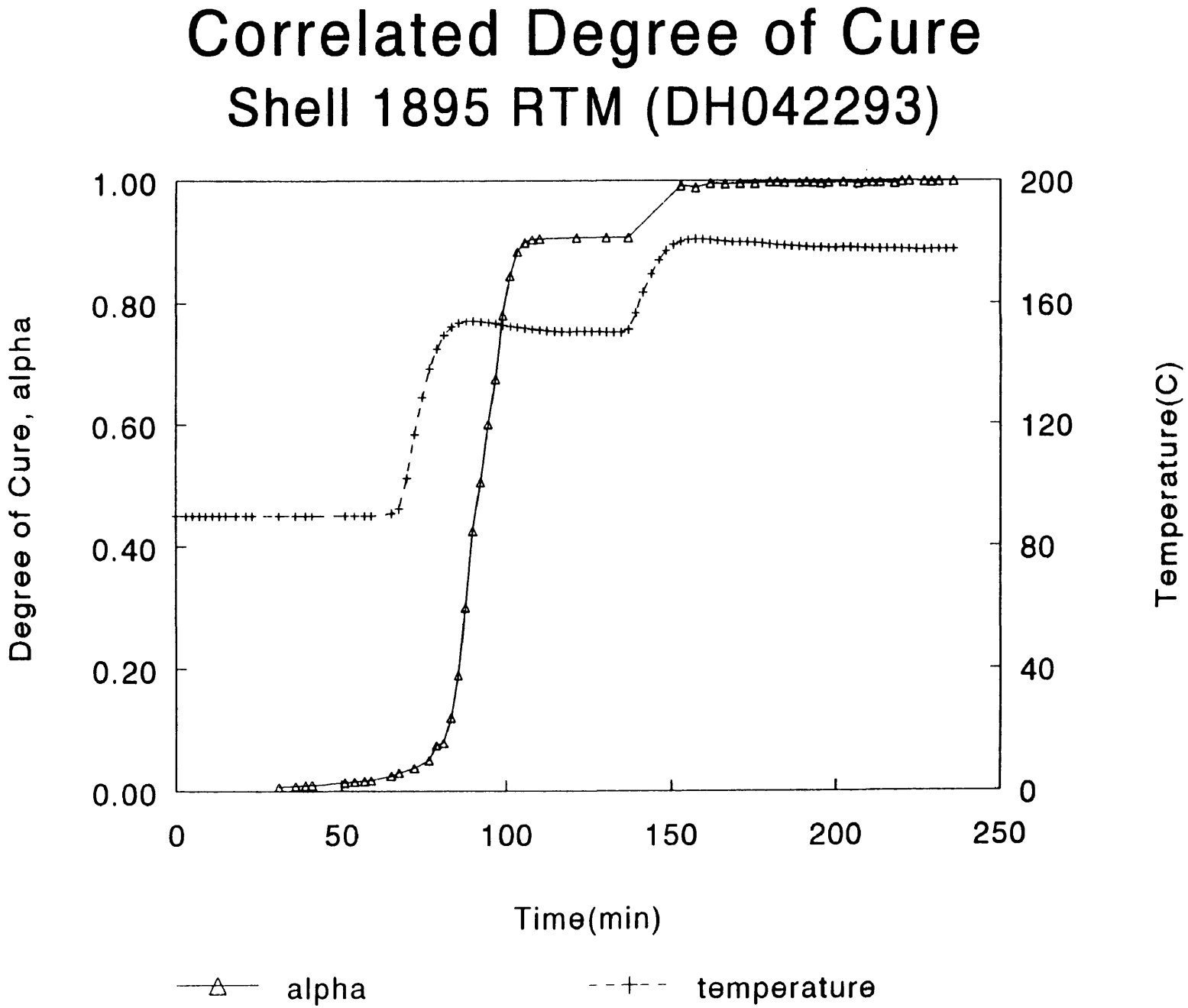
Correlated Degree of Cure
Shell 1895 RTM (DH042293)
Degree of Cure, alpha
Temperature(C)
Time(min)
1.00
0.80
0.60
0.40
0.20
0.00
200
160
120
80
40
0
0
50
100
150
200
250
alpha
temperature

Figure 4.38

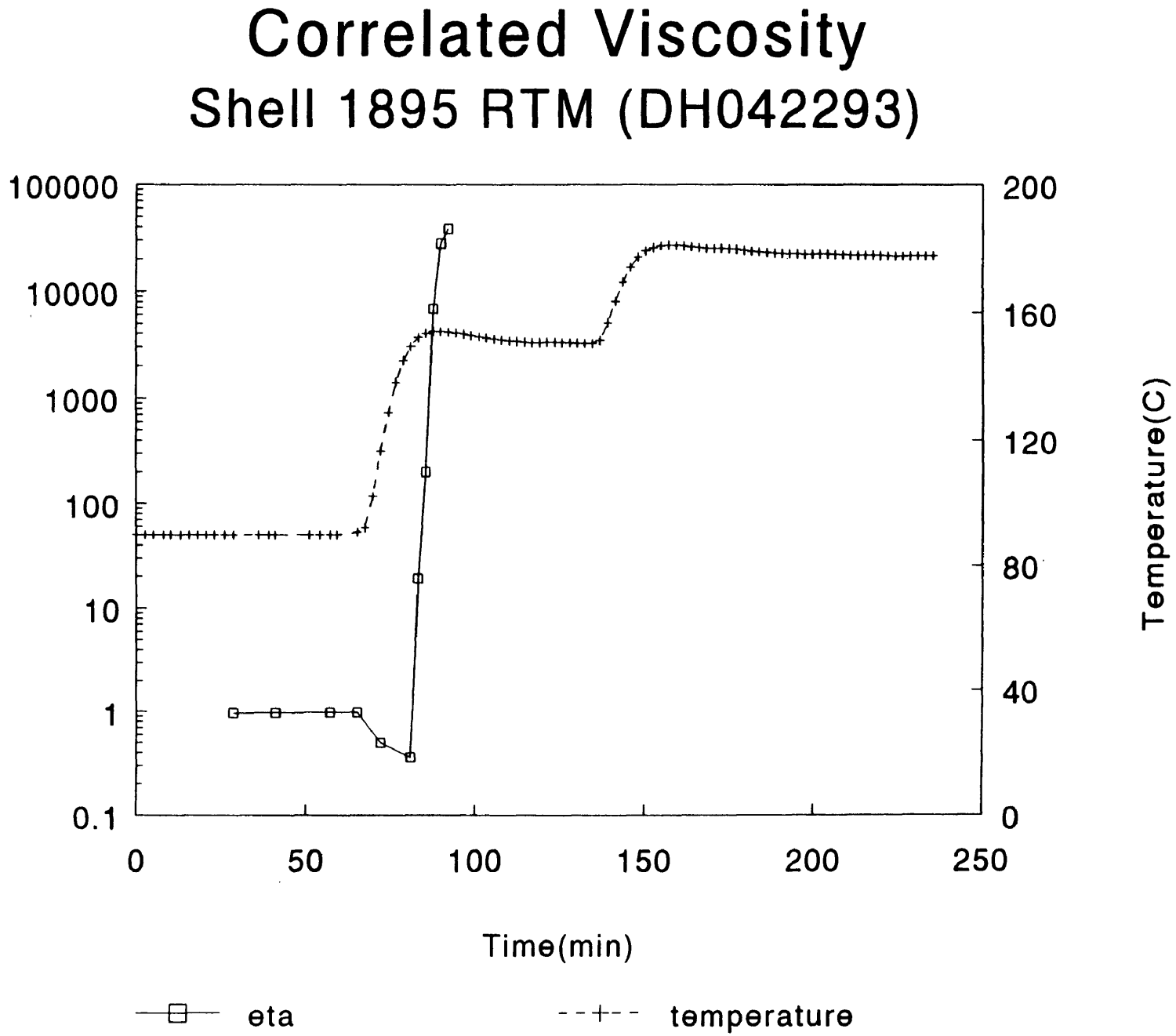
Correlated Viscosity
Shell 1895 RTM (DH042293)
100000
10000
1000
100
10
1
0.1
Eta(P)
200
160
120
80
40
0
Temperature(C)
0
50
100
150
200
250
Time(min)
eta
temperature

Figure 4.39

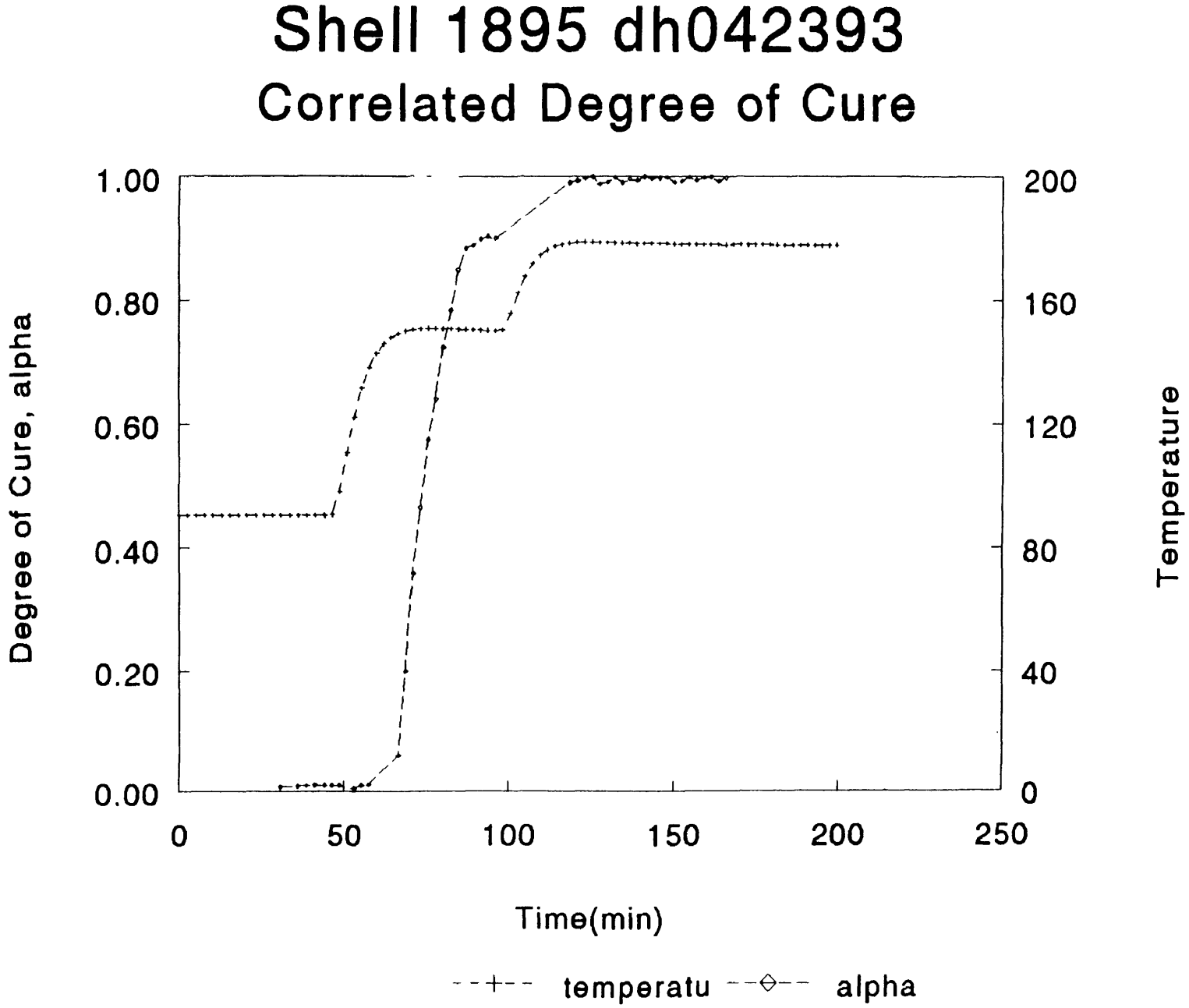
Shell 1895 dh042393
Correlated Degree of Cure
Degree of Cure, alpha
Temperature
1.00
0.80
0.60
0.40
0.20
0.00
200
160
120
80
40
0
0
50
100
150
200
250
Time(min)
temperatu
alpha

Figure 4.40

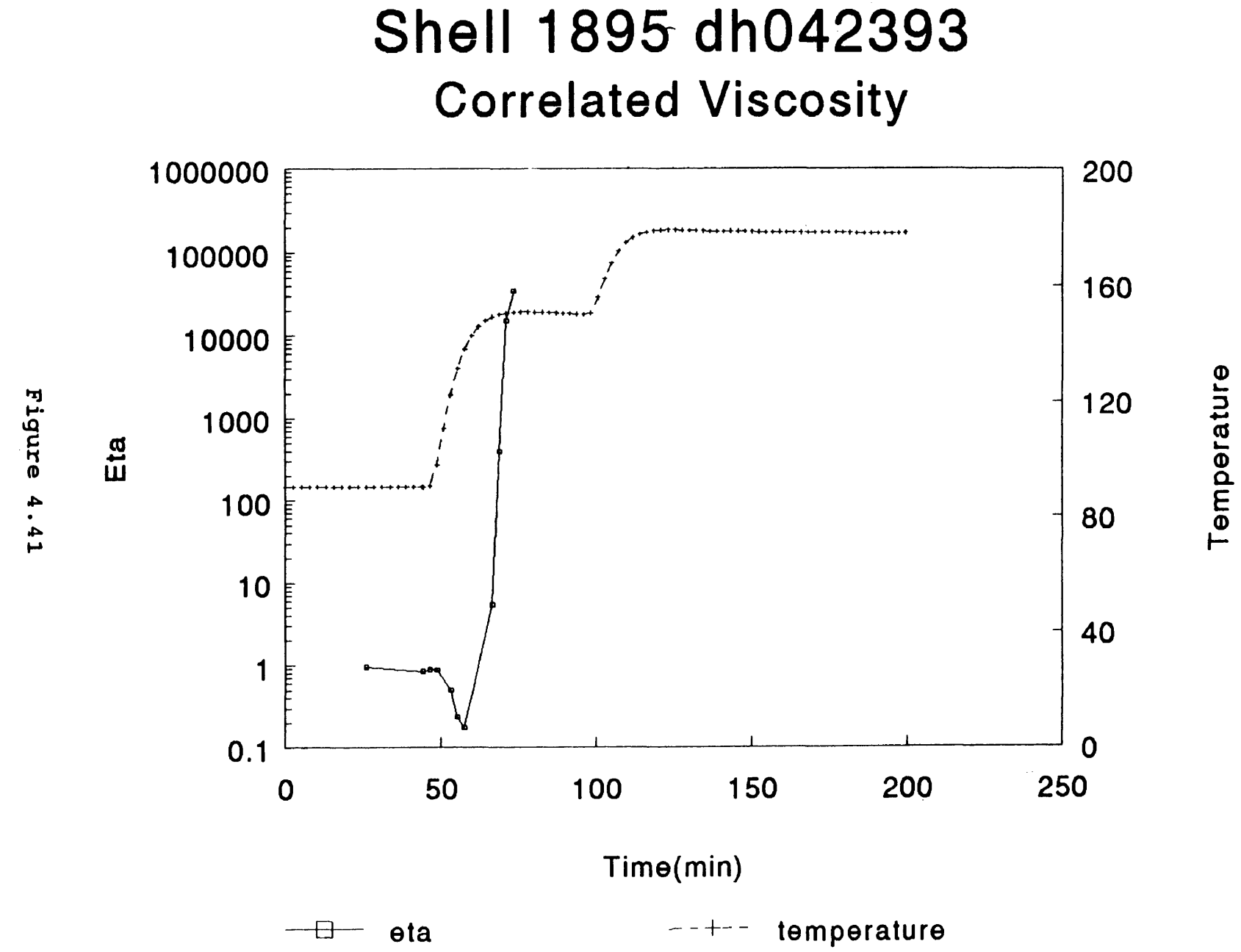
Shell 1895 dh042393
Correlated Viscosity
Eta
1000000
100000
10000
1000
100
10
1
0.1
0
50
100
150
200
250
Time(min)
200
160
120
80
40
0
Temperature
eta
temperature

Figure 4.41

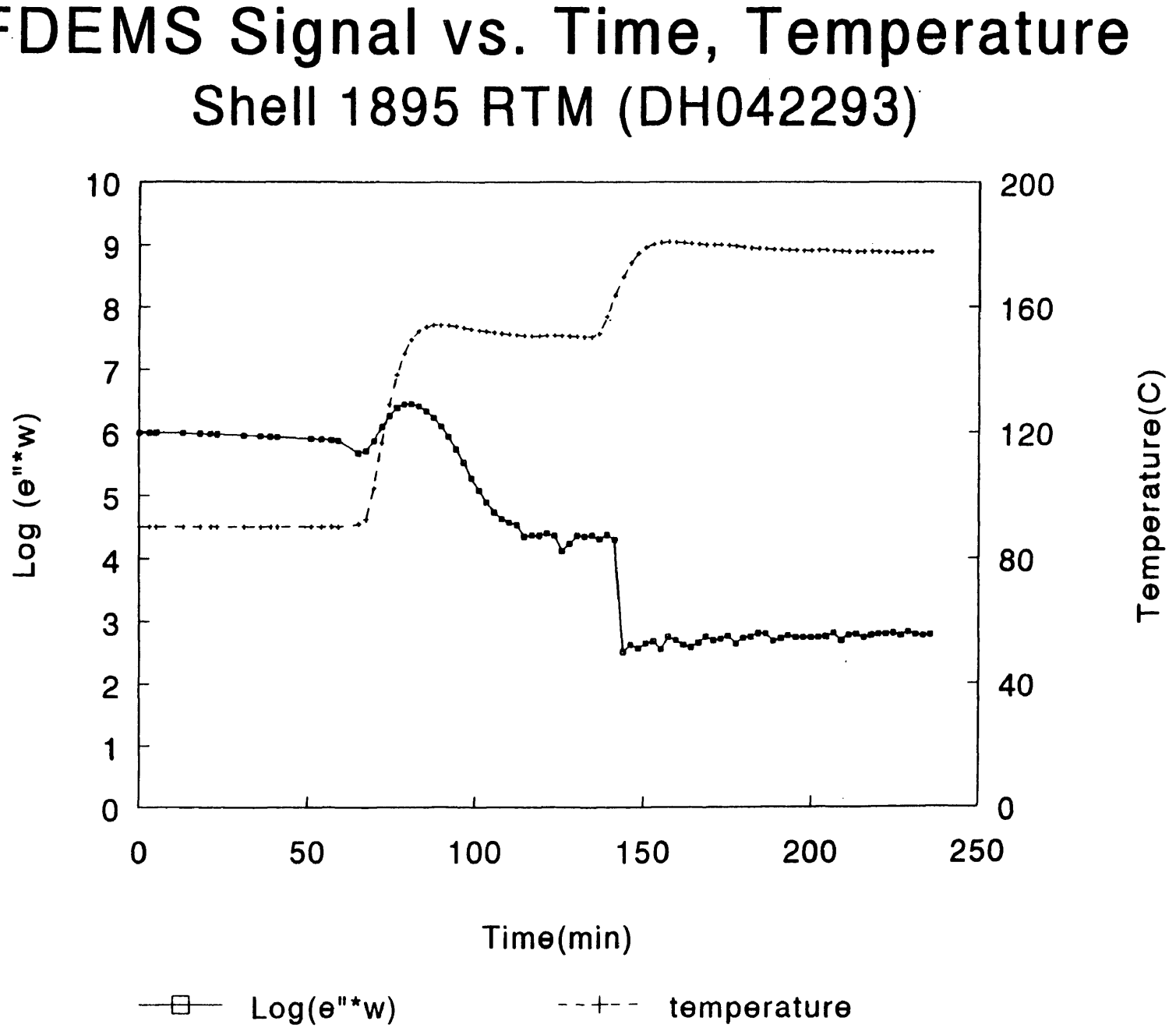
FDEMS Signal vs. Time, Temperature
Shell 1895 RTM (DH042293)
Log (e"*w)
Temperature(C)
Time(min)
0
1
2
3
4
5
6
7
8
9
10
0
40
80
120
160
200
0
50
100
150
200
250
Log(e"*w)
temperature

Figure 4.42

Chapter IV References

1. Kissinger, H. E., "Reaction Kinetics in Differential Thermal Analysis," *Analytical Chemistry*.

2. Cole, K. C., "A New Approach to Modeling the Cure Kinetics of Epoxy Amine Thermosetting Resins. 1. Mathmatical Development," *Macromolecules*, Vol. 24, 1991.

3. Mijovic, J., Fishbain, A., Wijaya, J., "Mechanistic Modeling of Epoxy-Amine Kinetics. 1. Model Compound Study," *Macromolecules*, Vol. 25, 1992.

4. Tully, Patricia, Masters Thesis, "Dielectric and Kinetic Analysis of Thermosetting Polyester Resin," College of William and Mary, 1989.

5. Wilkinson, Leland, **SYSTAT: The System for Statistics**, Evanston, IL, SYSTAT, Inc., 1989.

6. Winter, H. H., "Can the Gel Point of a Crosslinking Polymer be Detected by the G'-G" Crossover?", *Polymer Engineering and Science*, Vol. 27, No. 22, 1987.

Chapter V

Characterization of PR500 Resin

The PR500 resin system was characterized thermally, dielectrically and rheometrically. Temperature ramps and isothermal cures were performed on the DSC, rheometer, and FDEMS instrumentation as discussed in previous chapters.

Reaction Kinetics

The Differential Scanning Calorimeter was employed to analyze the kinetic behavior of the resin as it polymerized. Initially, a temperature sweep was conducted on the DSC from 50°C to 300°C at a rate of 2°C/minute. The results from this experiment indicated that there was no reaction before 150°C. The manufacturer suggests that the higher temperatures are necessary to decrease the viscosity in order to activate the catalyst. Below 150°C the catalyst is preserved in the viscous resin and is unable to react. The DSC ramp in Fig. 5.1 distinguishes the onset of reaction at around 150°C and the reaction completion at 250°C. By integrating the exothermic peak from 150°C to 250°C, the total heat generated by the polymerization reaction was

estimated at 272 J/g.

Isothermal DSC cures were conducted on the neat resin for temperatures from 160°C to 200°C consistent with the rheometric and dielectric data. Immediately following the isothermal cure, a rapid ramp of the cured resin was performed to reveal the residual heat of the reaction. An isothermal cure at a temperature below T_g would reach a maximum degree of cure and the reramp then would advance the resin to full cure. The 160°C isotherm therefore would have a lower heat of reaction and a higher residual heat than a higher temperature isotherm.

Once all the experimental data was collected, the values of the degree of cure, α, and the change in alpha over the change in time, $d\alpha/dt$, were calculated. The experimental alphas were determined from the change in heat flow at a particular time over the sum of the heat of reaction and the residual heat. The change in alpha over the change in time, $d\alpha/dt$, is the rate of polymerization[1,2].

Analogous to the Shell RSL 1895 kinetic analysis, SYSTAT® determined that the autocatalytic model

[5-1] $$d\alpha/dt = k\ \alpha^m\ (1-\alpha)^n$$

rendered the best fit of the experimental data. Estimation of the parameters using a program to test the various combinations of k, m and n produced specific models for the individual isotherms. The temperature dependence of the rate constants was determined using the Arrhenius equation.

[5-2] $k = A\ e^{-(B/T)}$ or $\ln k = \ln A - B/T$

The natural log of the rate constant, k, was graphed versus the inverse temperature. The linear relation of the rate constant with inverse temperature produced values of A and B of 2.08 $x10^5$ min^- and 6714.9 K^-, respectively. Since the reaction orders m and n from the individual isotherms were quite close, the values of m and n were averaged to 0.43 and 1.08, respectively.

The resulting kinetic model for the PR500 resin system was

[5-3] $d\alpha/dt = (2.08 \times 10^5\ e^{-6714.9/T})\ \alpha^{.43}\ (1-\alpha)^{1.08}$

Theoretical alpha values predicted by this kinetic model provided excellent agreement with experimental values. This is shown in the 160°, 180° and 200°C alpha versus time plots in Figures 5.2, 5.3, and 5.4. This final kinetic model for PR500 will predict the degree of cure at any time and temperature in the polymerization reaction. Furthermore, the advancement of the degree of cure predicted by this model will be the basis for future correlations.

Correlation of Degree of Cure and Viscosity

The correlation between log η and log $\epsilon''*\omega$ was obtained by performing a series of isothermal Rheometer and FDEMS experiments to measure the viscosity and dielectric loss, ϵ'', of the resin as a function of time (Fig. 5.5 - Fig.

5.12). In correlating the results, only the isotherms at 160°, 170°, and 180°C were considered. A frequency of 125 Hz was selected for the dielectric data in order to best characterize the ionic mobility of the resin as it cured.

After the appropriate corrections, as discussed in chapter VI, were made to η and ϵ'' experimental data, the viscosity and $\epsilon''*\omega$ were correlated with respect to time and temperature (Fig. 5.13 - Fig. 5.15).

In the calibration plot combining the 160°, 170° and 180°C correlations, the log of $\epsilon''*\omega$ is inversely related to the viscosity η up to the gel point at approximately 2.4 Poise (Fig. 5.16). Table 5.1 shows the gel points for the individual isotherms determined by the crossing over of G′ and G″ measurements.

Temperature	Gel Point(min)
160°C	---
170°C	49.8
180°C	36.6

Table 5.1

The gel point of a crosslinking system designates the point where the reaction has the possibility of forming an infinite network[3]. Since the loss factor ϵ'' is dominated by ionic mobility in the overlapping frequencies, an inverse relation exists between $\epsilon''*\omega$ and η so long as the material is fluid. As the resin becomes highly crosslinked

polarization effects dominate the reaction and the points on the calibration plot begin to scatter with the increasing viscosity.

Correlations also were made relating α, log η and log $\epsilon''*\omega$ for the individual isotherms. The procedures used for Shell 1895 development resin were also used to construct the calibration plots for PR500 resin system. Figures 5.17 through 5.19 show the calibration plots for the 160°, 170°, and 180°C isothermal data.

For the high temperature cure at 190° and 200°C a third type of calibration plot was constructed to determine the shut-off criteria for the RTM process. Similar to the 177°C calibration plot for Shell 1895, a five-point method was used to calculate the slopes, $(d\epsilon''/dt)/\epsilon''$ and $(d\epsilon'/dt)/\epsilon'$. The values of ϵ'' and ϵ' were taken at a higher frequency of 5 kHz for the 190°C data and 250kHz for the 200°C data where the dielectric loss remains constant after an initial drop. Figure 5.20 and 5.21 shows the normalized rate of change, $(d\epsilon''/dt)/\epsilon''$, and theoretical alpha graphed versus time. This calibration plot was then compared with the graph obtained using ϵ' in the slope equation (Fig. 5.22 and Fig. 5.23). The second method clearly produced a more sensitive measure of the end of the curing reaction.

In Figures 5.22 and 5.23, the degree of cure increases rapidly to 0.96 and then gradually approaches 1. The DSC, therefore, is not as accurate as the ϵ' and ϵ'' measurements

in the later stages of the cure. When the slope of $\epsilon'*\omega$ becomes less than 0.005, the resin has reached full cure resulting in the shutdown of the RTM process.

DSC Data File: pramp
Sample Weight: 8.700 mg
Fri Jun 25 18:45:16 1993
pr500 lot214a3r NASALaRC

PERKIN-ELMER
7 Series Thermal Analysis System

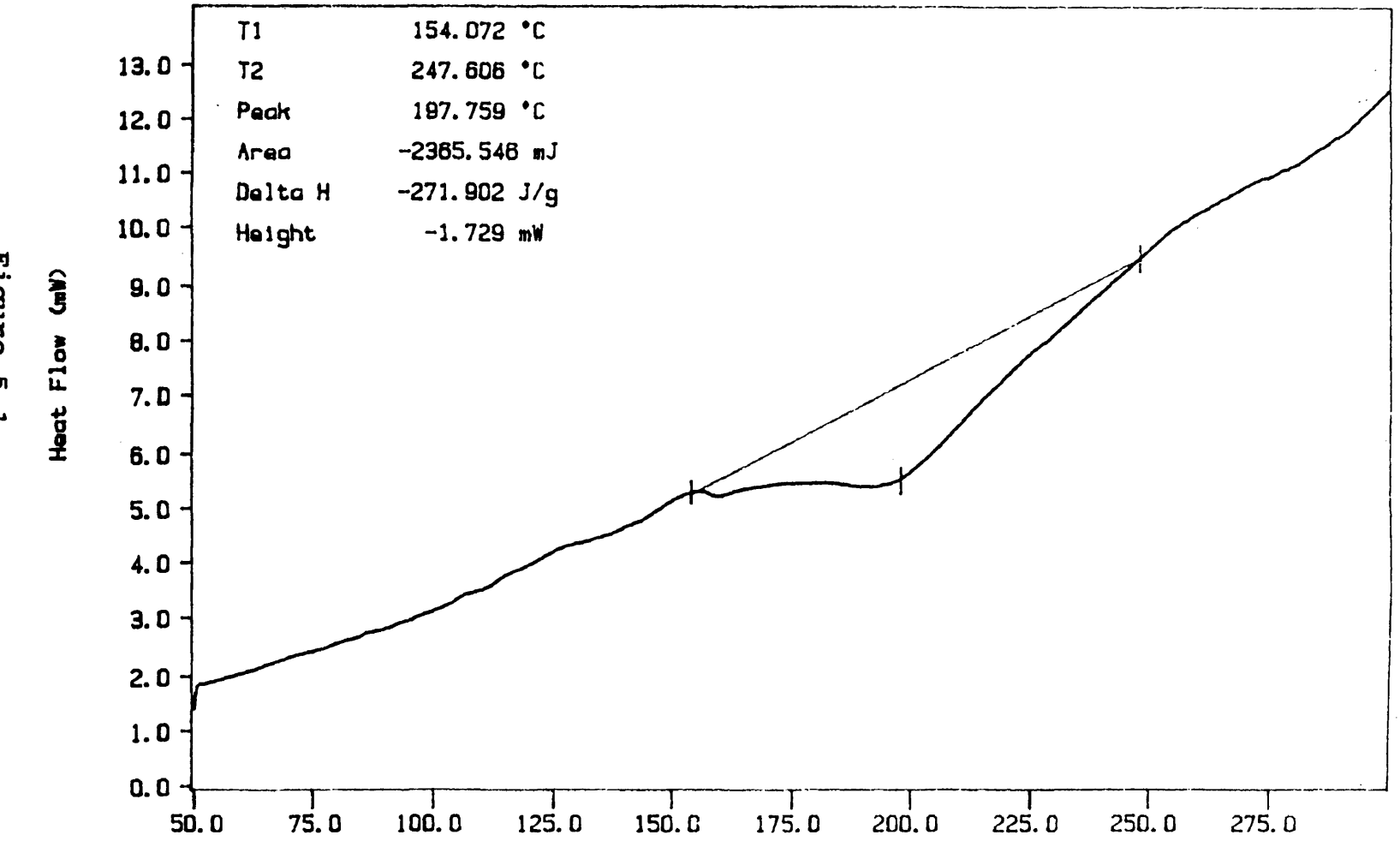

Figure 5.1

Alpha vs. Time

PR500 lot#214A3R rec'd 2/25/93 @LaRC

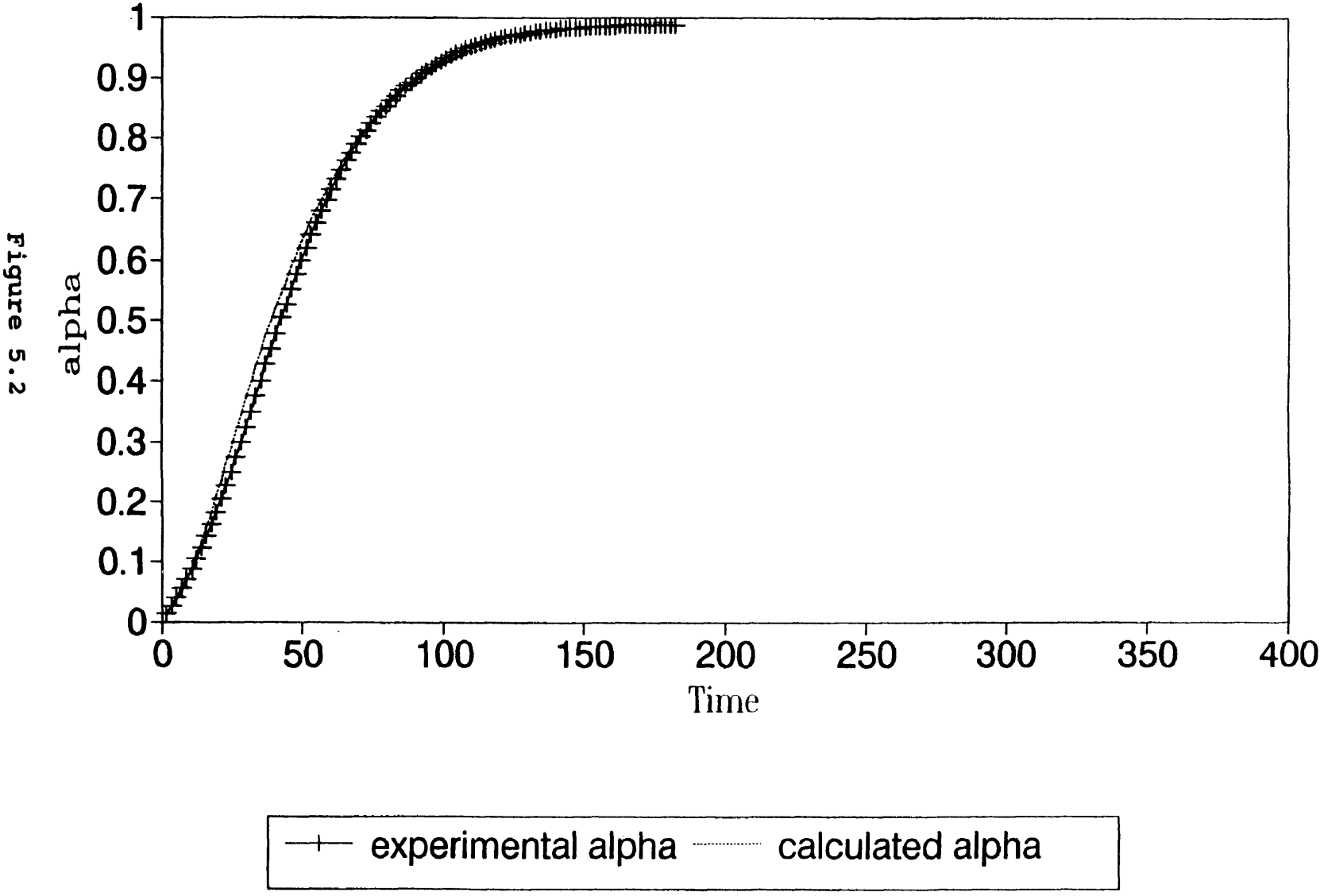

Figure 5.2

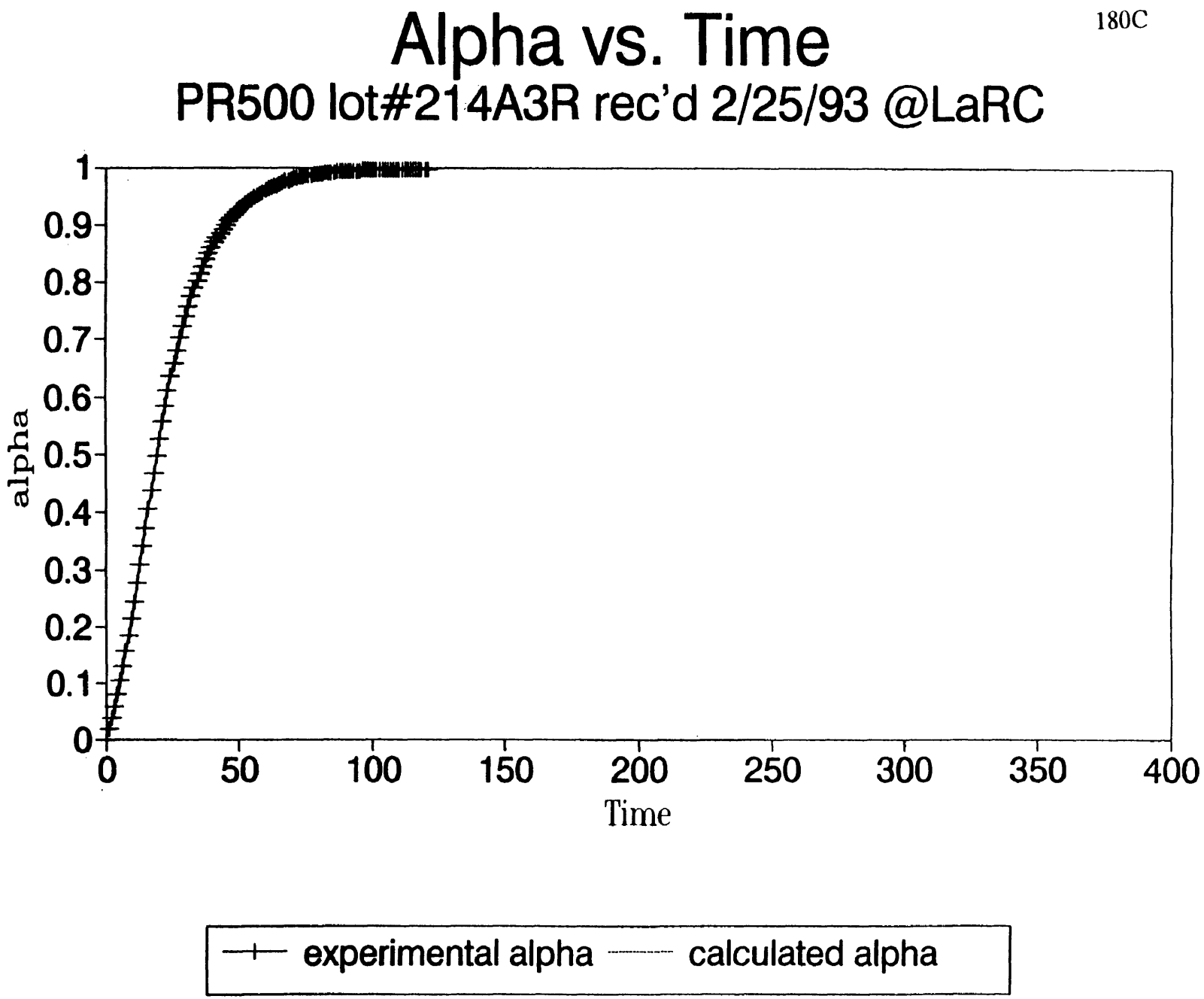
Alpha vs. Time
PR500 lot#214A3R rec'd 2/25/93 @LaRC
180C
alpha
1
0.9
0.8
0.7
0.6
0.5
0.4
0.3
0.2
0.1
0
0
50
100
150
200
250
300
350
400
Time
experimental alpha
calculated alpha

Figure 5.3

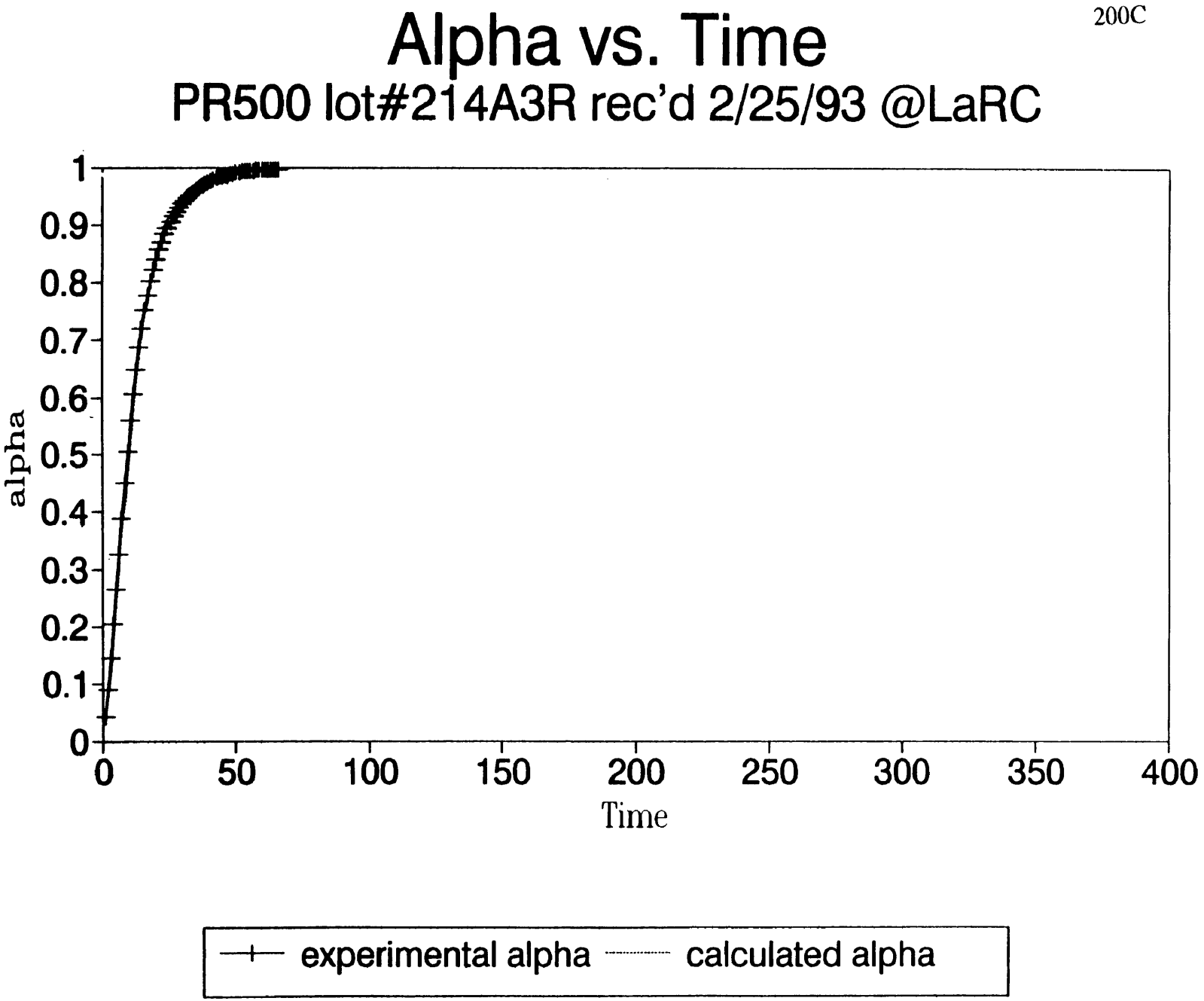
Alpha vs. Time
PR500 lot#214A3R rec'd 2/25/93 @LaRC
alpha
1
0.9
0.8
0.7
0.6
0.5
0.4
0.3
0.2
0.1
0
0
50
100
150
200
250
300
350
400
Time
experimental alpha
calculated alpha

Figure 5.4

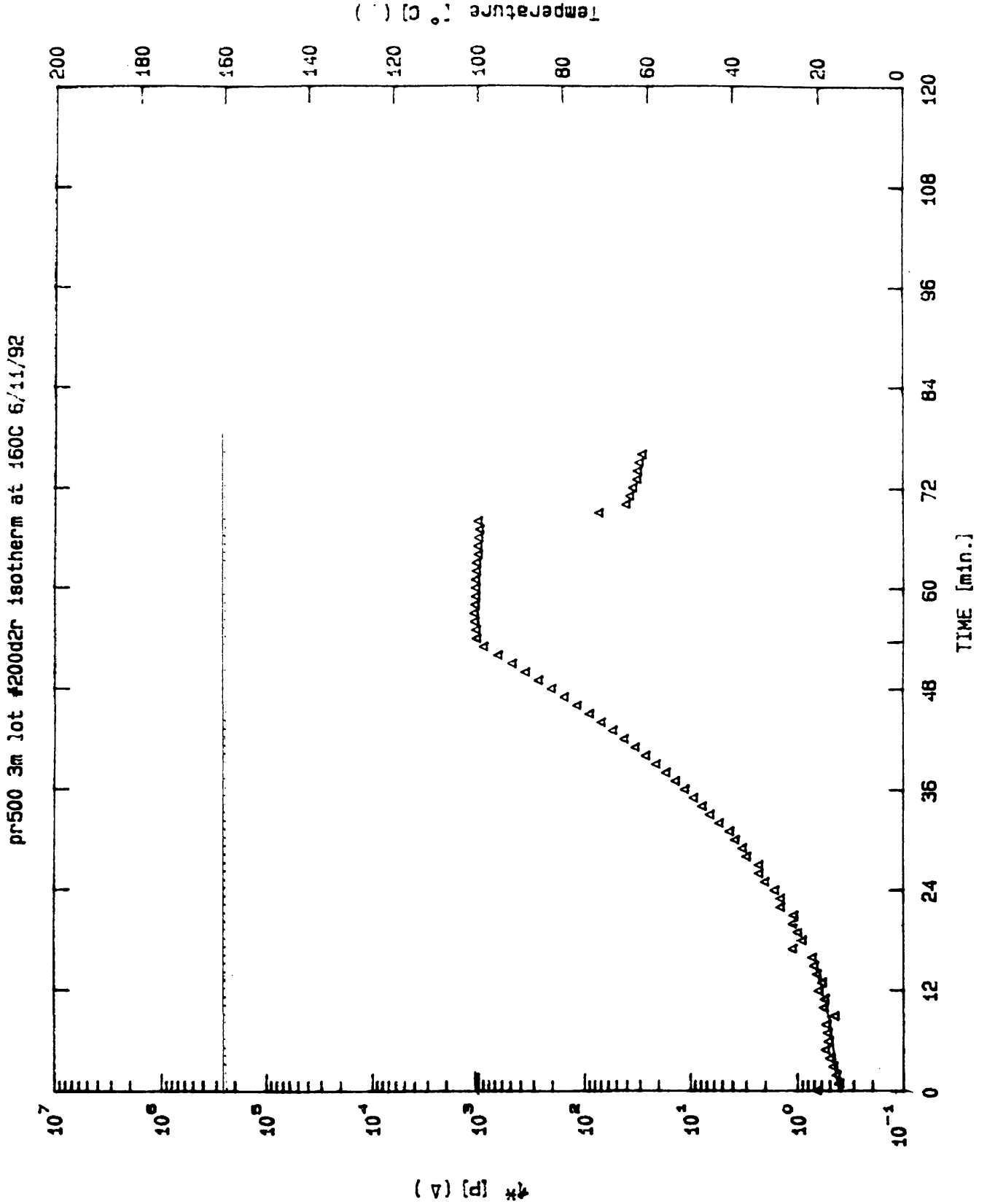
pr500 3m lot #200d2r isotherm at 160C 6/11/92
Temperature [° C] ( )
TIME [min.]
φ* [p] (Δ)

Figure 5.5

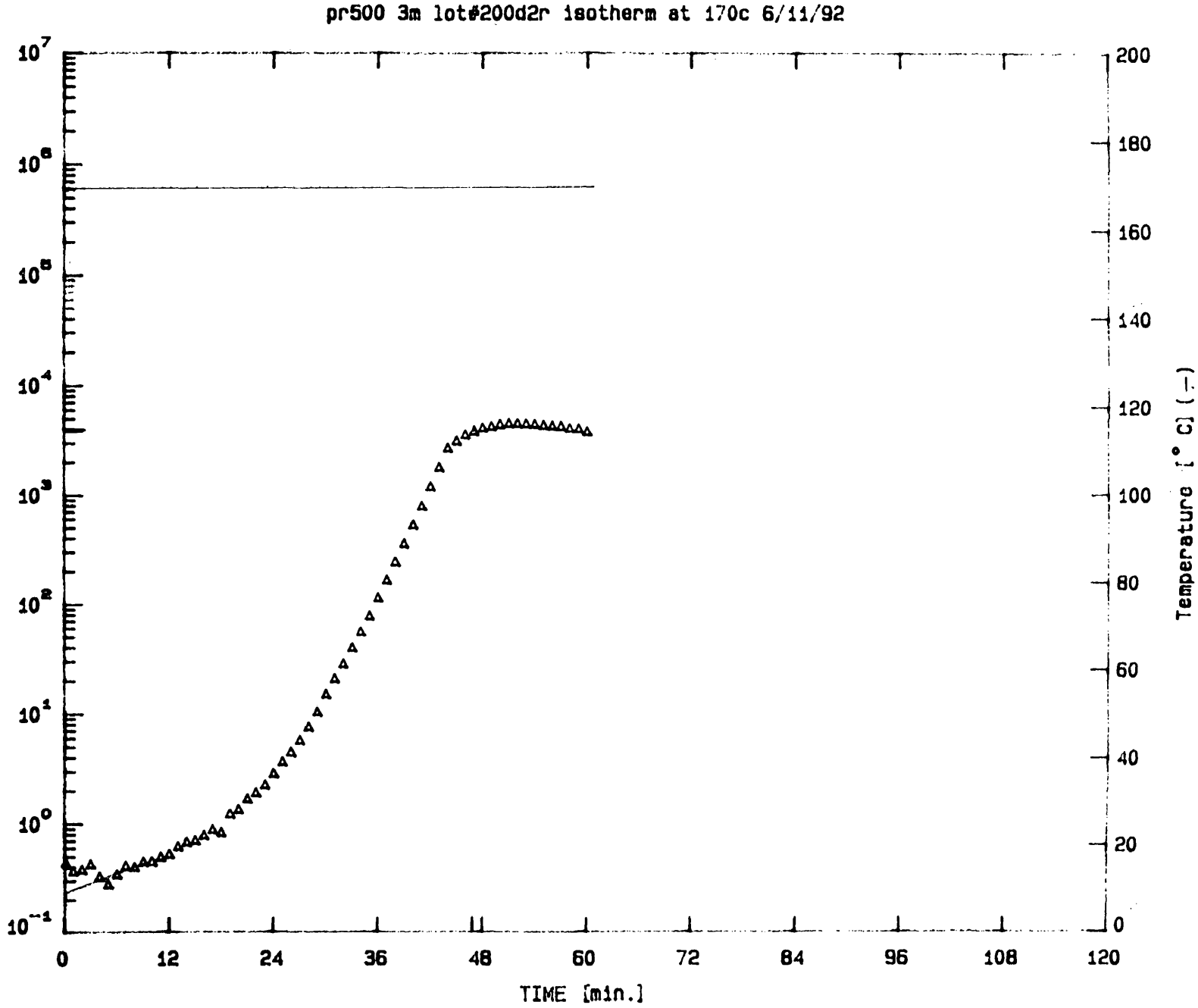
pr500 3m lot#200d2r isotherm at 170c 6/11/92
1* [P] (Δ)
Temperature [° C] (—)
TIME [min.]
10^{7}
10^{6}
10^{5}
10^{4}
10^{3}
10^{2}
10^{1}
10^{0}
10^{-1}
200
180
160
140
120
100
80
60
40
20
0
0
12
24
36
48
60
72
84
96
108
120

Figure 5.6

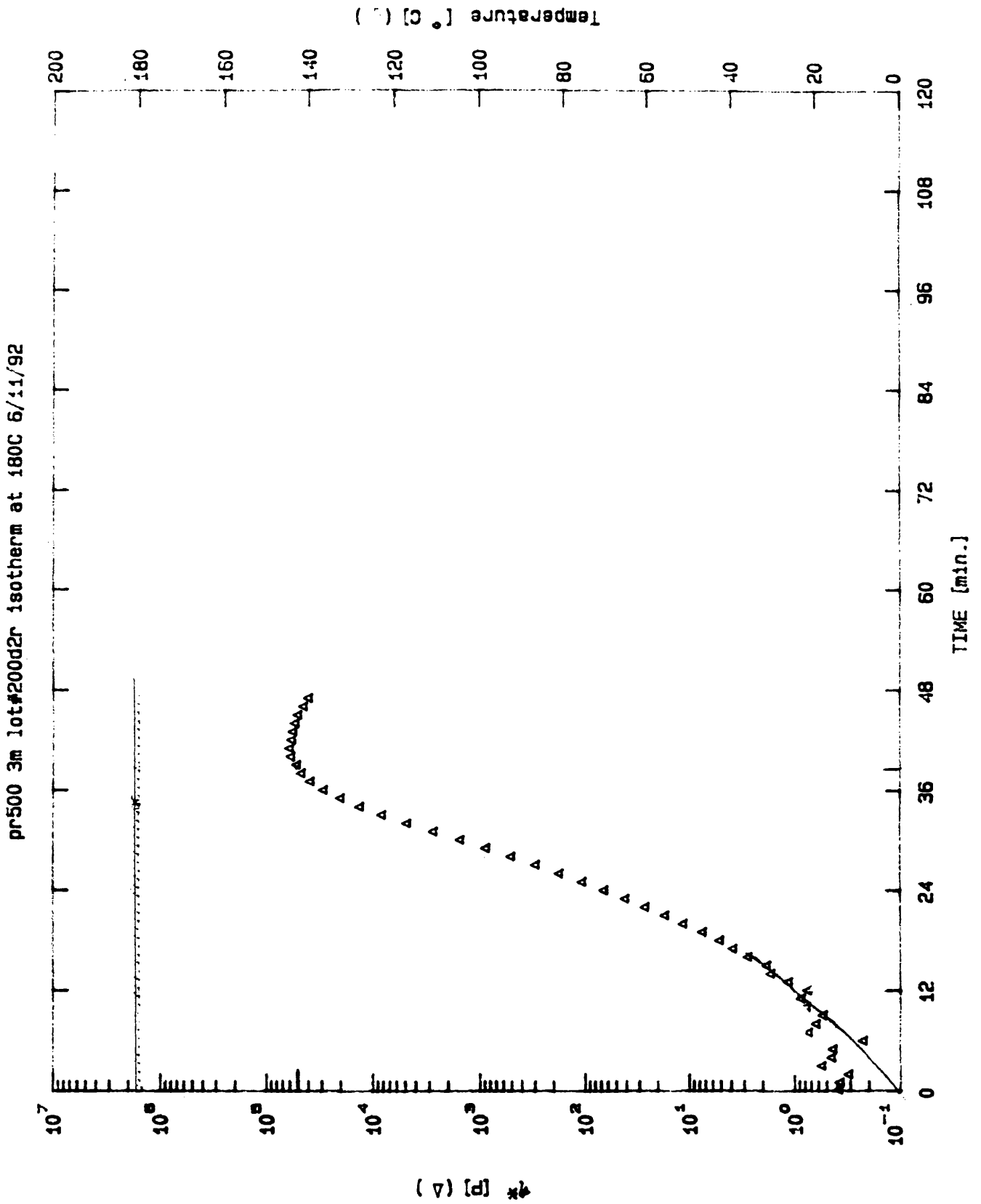
pr500 3m lot#200d2r isotherm at 180C 6/11/92
Temperature [° C] ( )
TIME [min.]
dp/dt [p] (Δ)

Figure 5.7

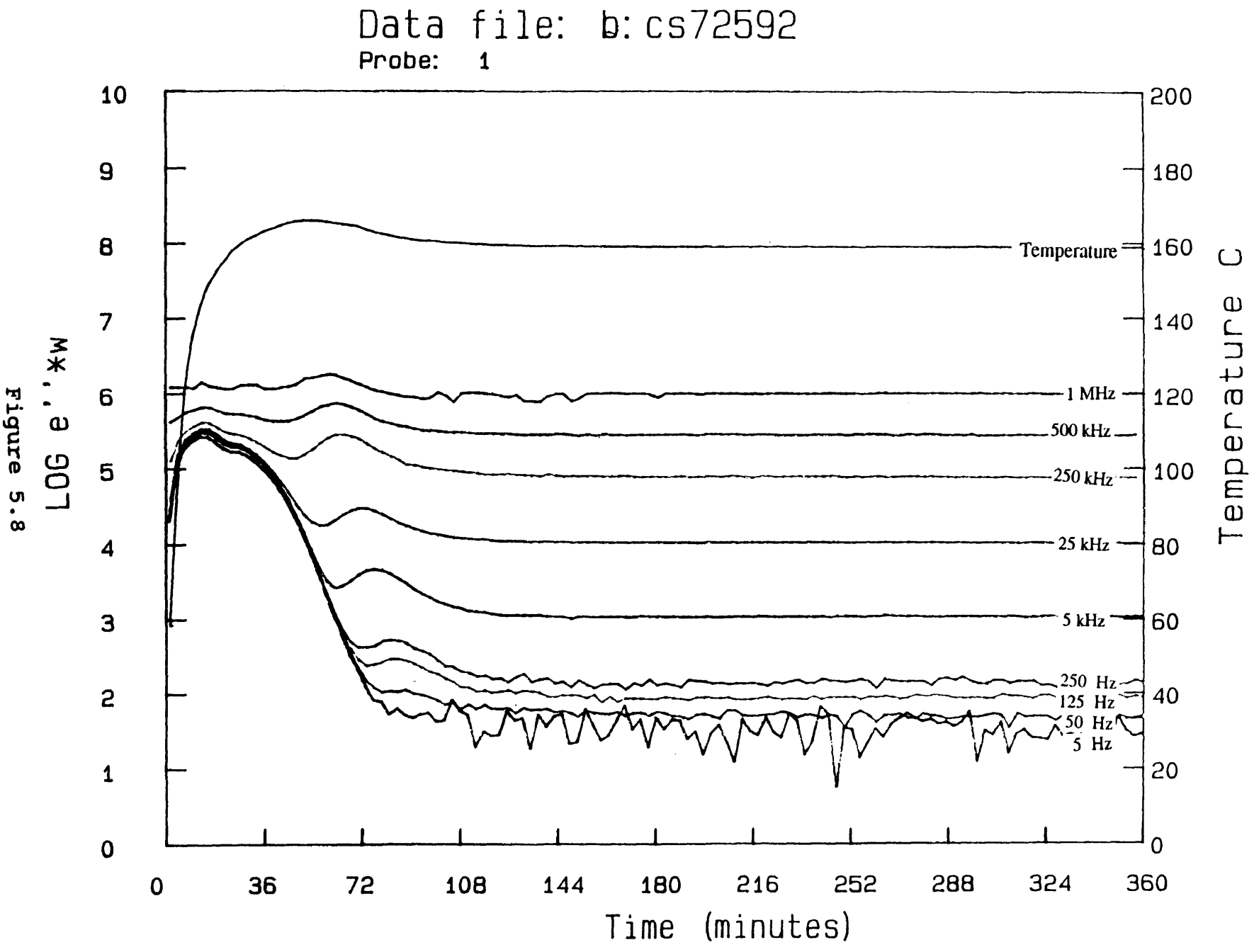
Data file: b:cs72592
Probe: 1
LOG e''*w
Temperature C
Time (minutes)
Temperature
1 MHz
500 kHz
250 kHz
25 kHz
5 kHz
250 Hz
125 Hz
50 Hz
5 Hz
0
1
2
3
4
5
6
7
8
9
10
0
20
40
60
80
100
120
140
160
180
200
0
36
72
108
144
180
216
252
288
324
360

Figure 5.8

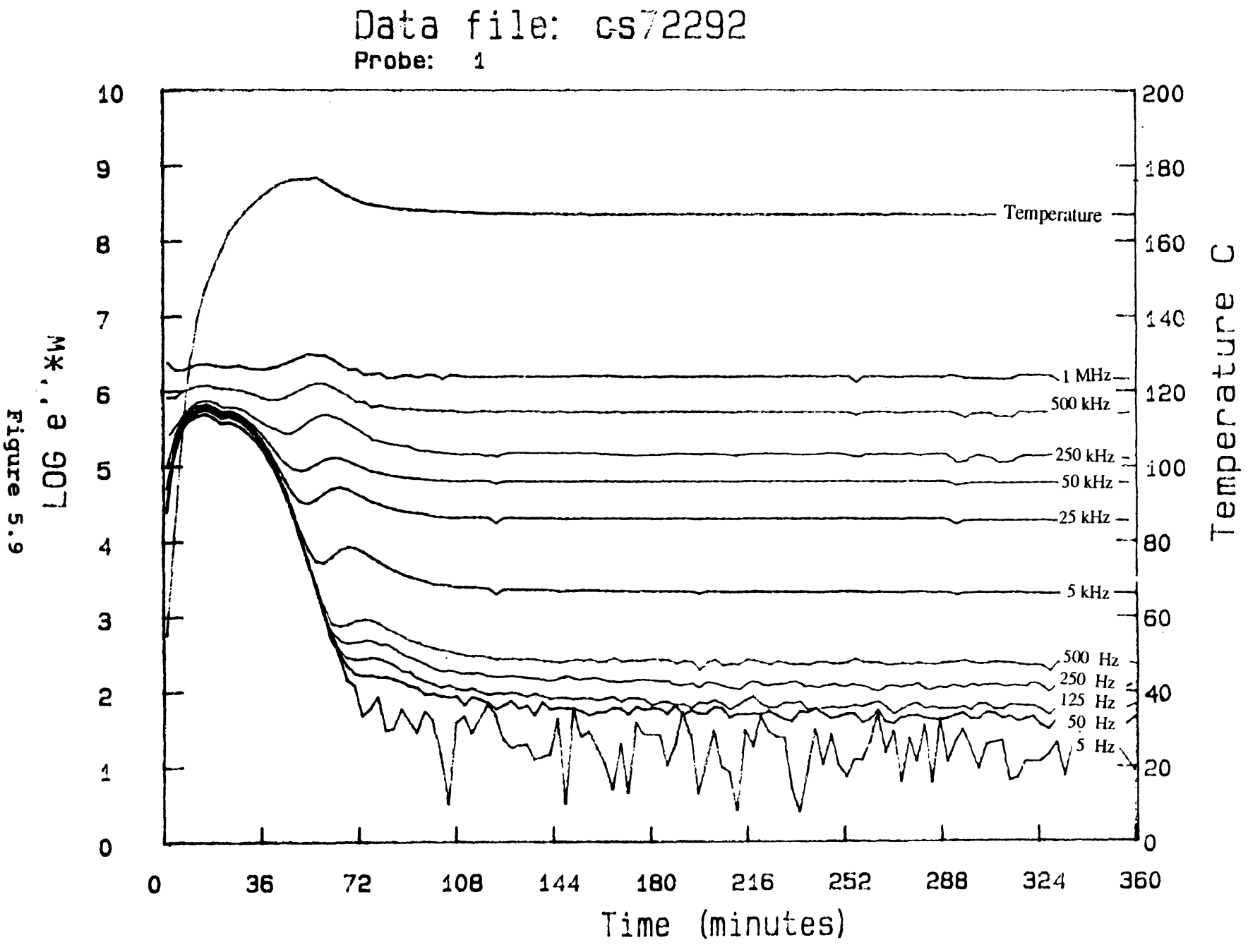
Data file: cs72292
Probe: 1
LOG e'' *w
Temperature C
Time (minutes)
Temperature
1 MHz
500 kHz
250 kHz
50 kHz
25 kHz
5 kHz
500 Hz
250 Hz
125 Hz
50 Hz
5 Hz
0
1
2
3
4
5
6
7
8
9
10
0
20
40
60
80
100
120
140
160
180
200
0
36
72
108
144
180
216
252
288
324
360

Figure 5.9

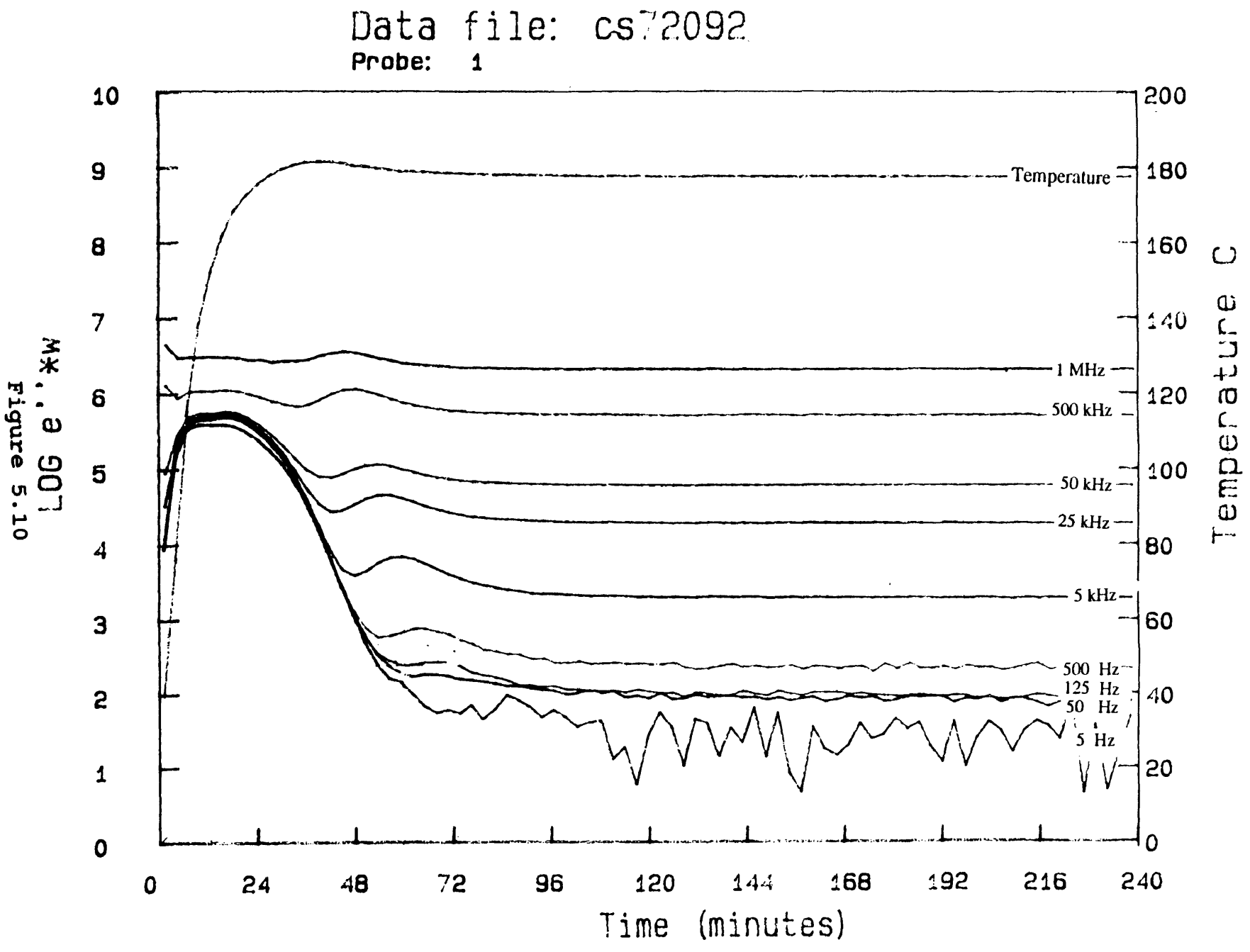
Data file: cs72092
Probe: 1
LOG e'',e* w
Temperature C
Time (minutes)
Temperature
1 MHz
500 kHz
50 kHz
25 kHz
5 kHz
500 Hz
125 Hz
50 Hz
5 Hz
0
24
48
72
96
120
144
168
192
216
240
0
1
2
3
4
5
6
7
8
9
10
0
20
40
60
80
100
120
140
160
180
200

Figure 5.10

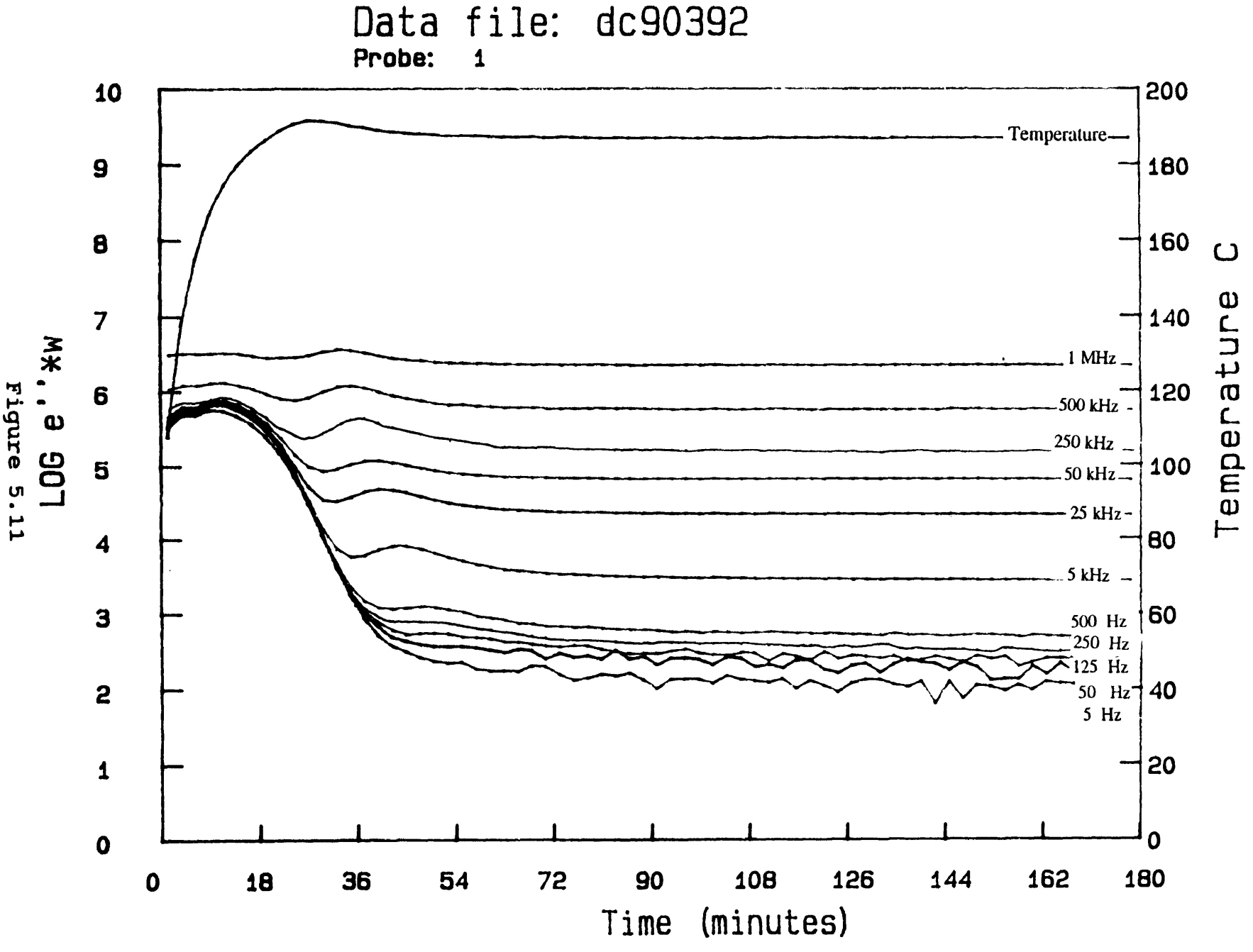
Data file: dc90392
Probe: 1
LOG e''*W
Temperature C
Time (minutes)
Temperature
1 MHz
500 kHz
250 kHz
50 kHz
25 kHz
5 kHz
500 Hz
250 Hz
125 Hz
50 Hz
5 Hz
0
1
2
3
4
5
6
7
8
9
10
0
18
36
54
72
90
108
126
144
162
180
0
20
40
60
80
100
120
140
160
180
200

Figure 5.11

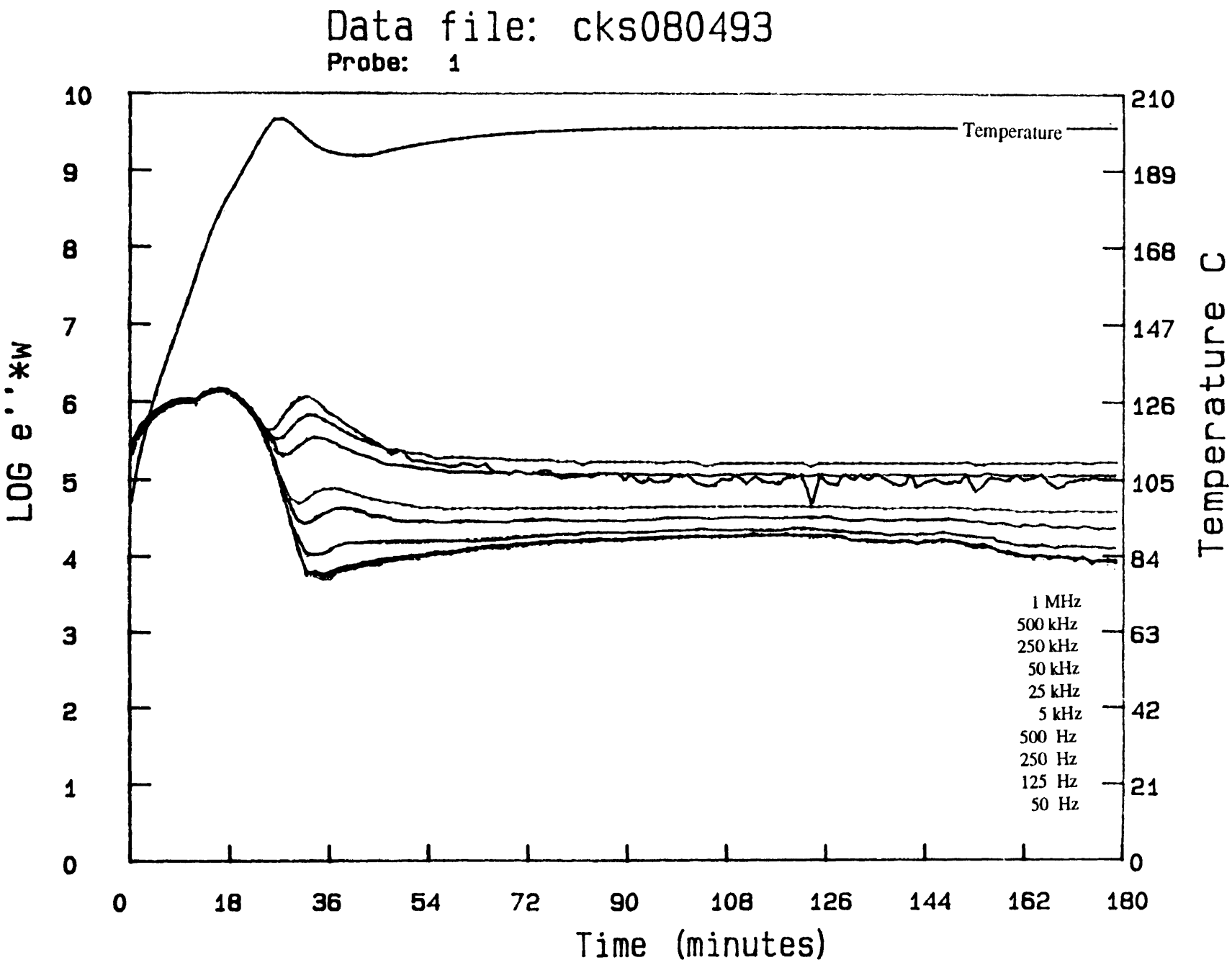
Data file: cks080493
Probe: 1
LOG e'',e*,w
Temperature C
Time (minutes)
Temperature
1 MHz
500 kHz
250 kHz
50 kHz
25 kHz
5 kHz
500 Hz
250 Hz
125 Hz
50 Hz
0
1
2
3
4
5
6
7
8
9
10
0
18
36
54
72
90
108
126
144
162
180
0
21
42
63
84
105
126
147
168
189
210

Figure 5.12

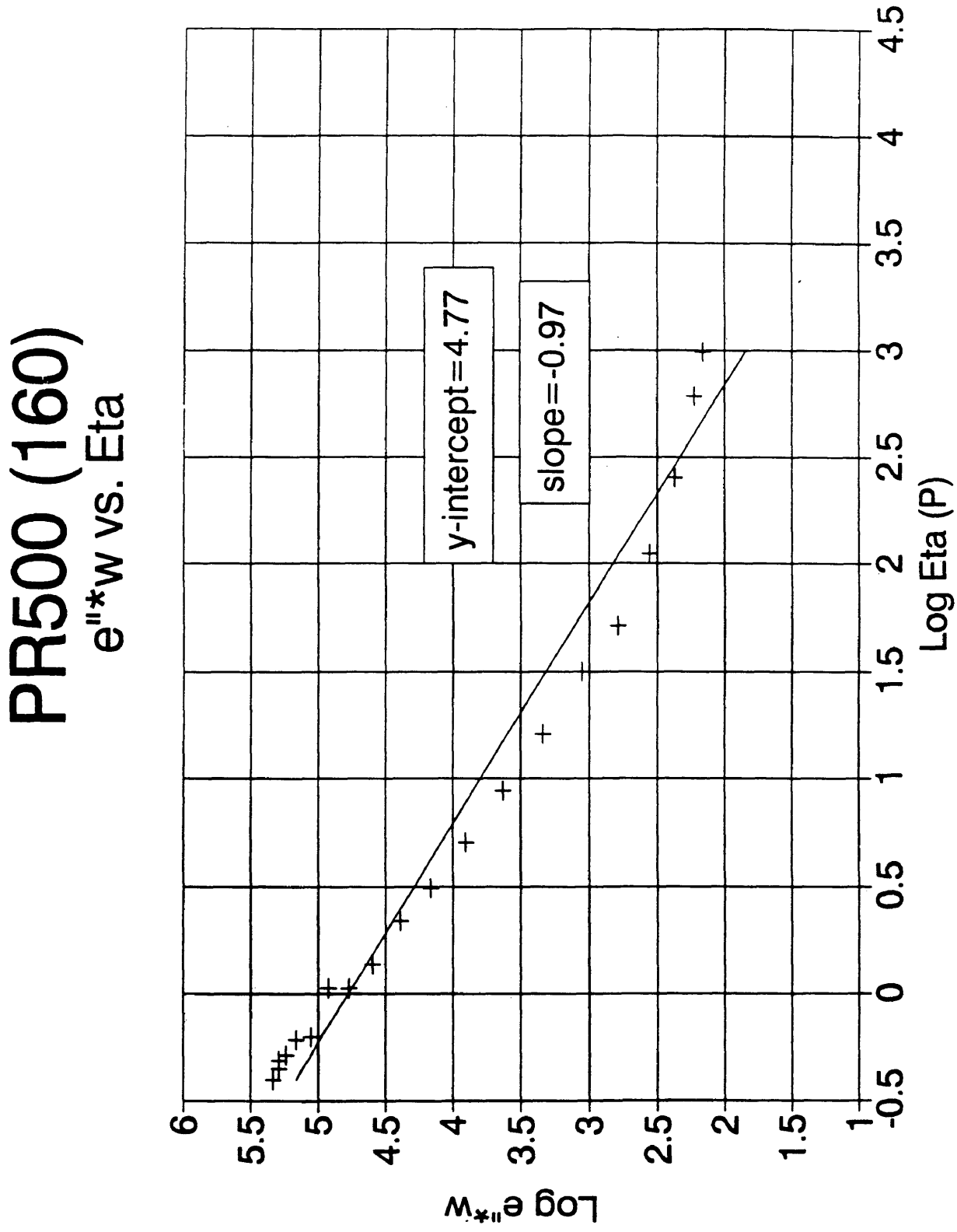
PR500 (160)
e"*w vs. Eta
y-intercept=4.77
slope=-0.97
Log e"*w
Log Eta (P)
6
5.5
5
4.5
4
3.5
3
2.5
2
1.5
1
-0.5
0
0.5
1
1.5
2
2.5
3
3.5
4
4.5

Figure 5.13

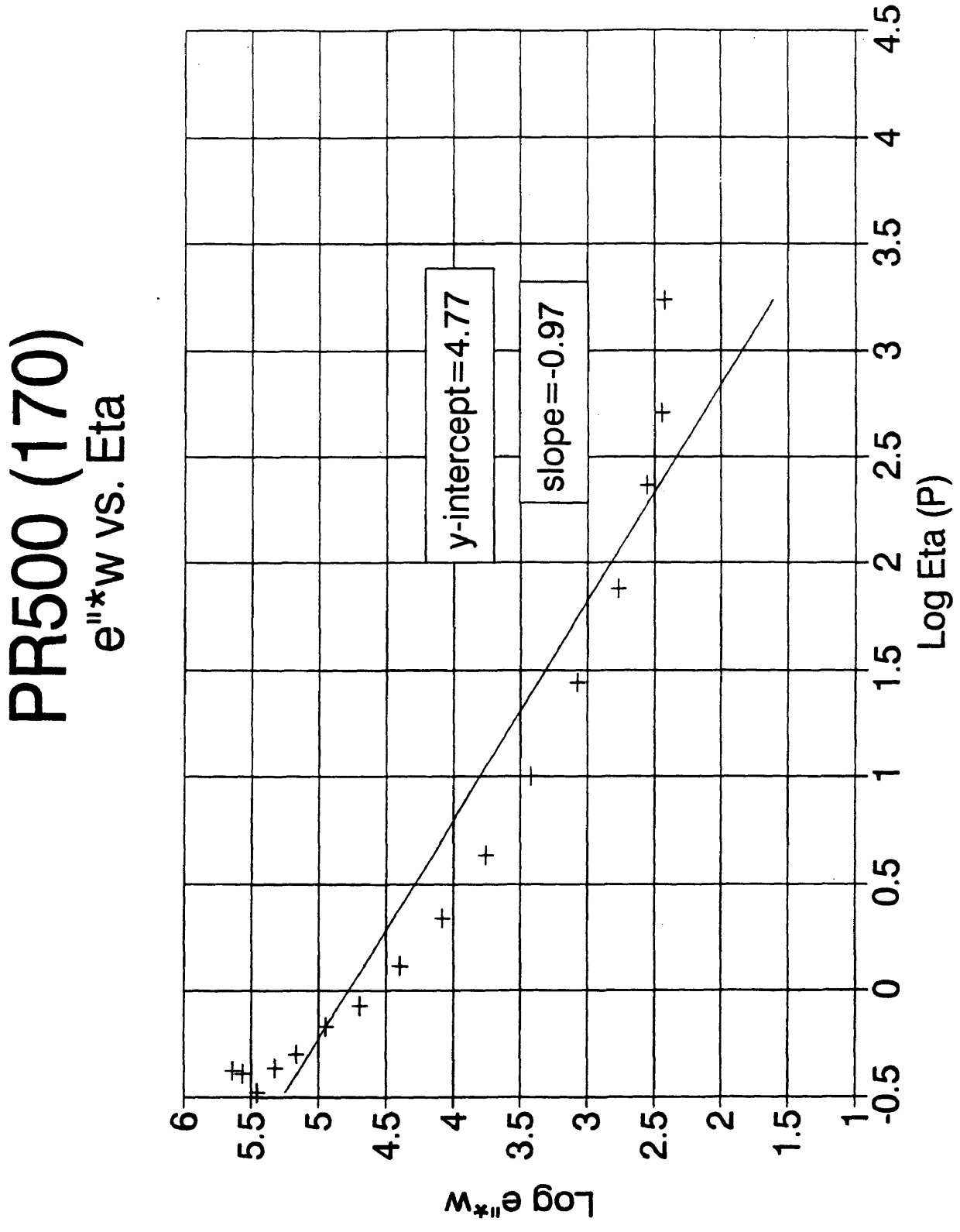
PR500 (170)
e"*w vs. Eta
y-intercept=4.77
slope=-0.97
Log e"*w
Log Eta (P)
6
5.5
5
4.5
4
3.5
3
2.5
2
1.5
1
-0.5
0
0.5
1
1.5
2
2.5
3
3.5
4
4.5

Figure 5.14

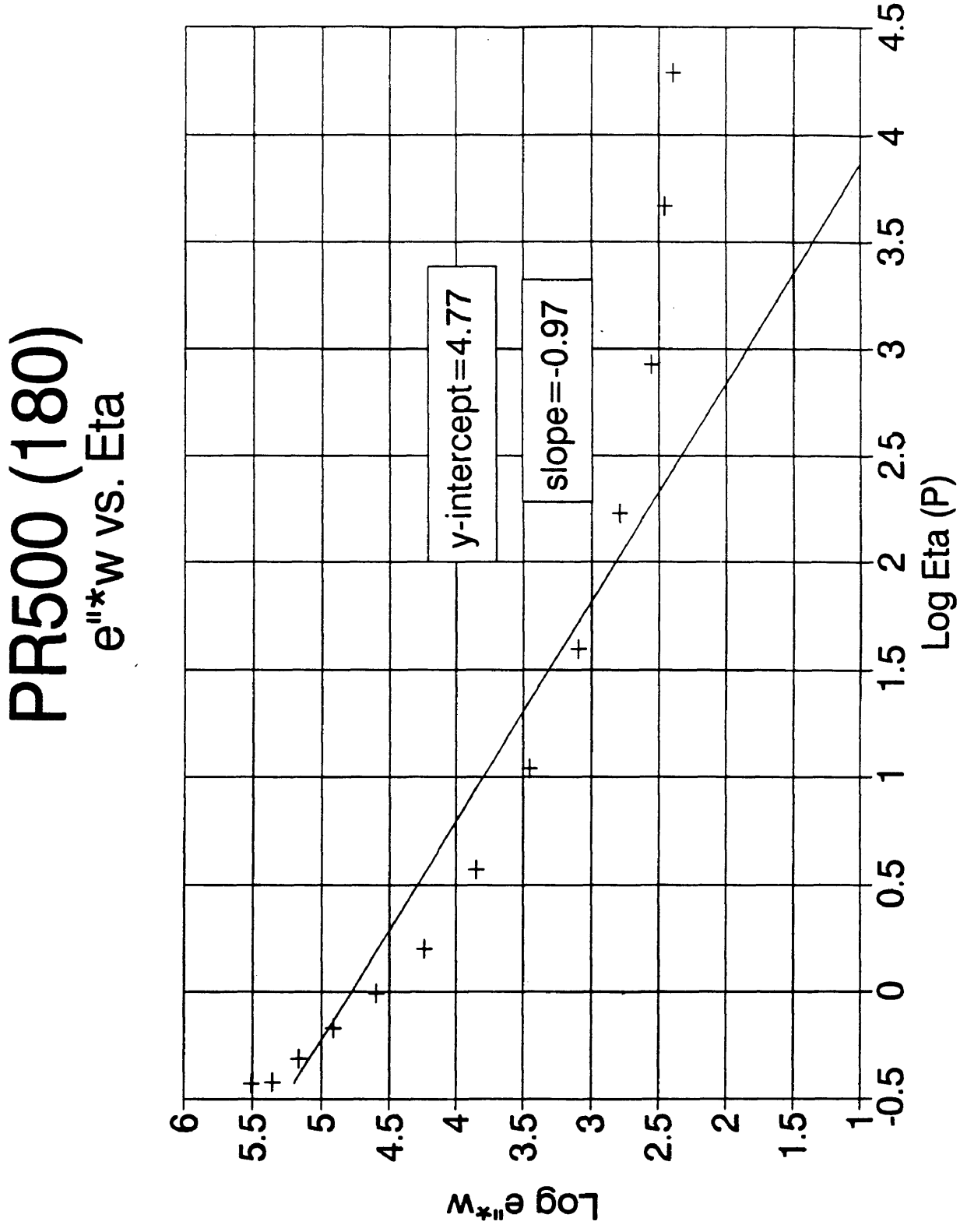
PR500 (180)
e"*w vs. Eta
y-intercept=4.77
slope=-0.97
Log e"*w
Log Eta (P)
6
5.5
5
4.5
4
3.5
3
2.5
2
1.5
1
-0.5
0
0.5
1
1.5
2
2.5
3
3.5
4
4.5

Figure 5.15

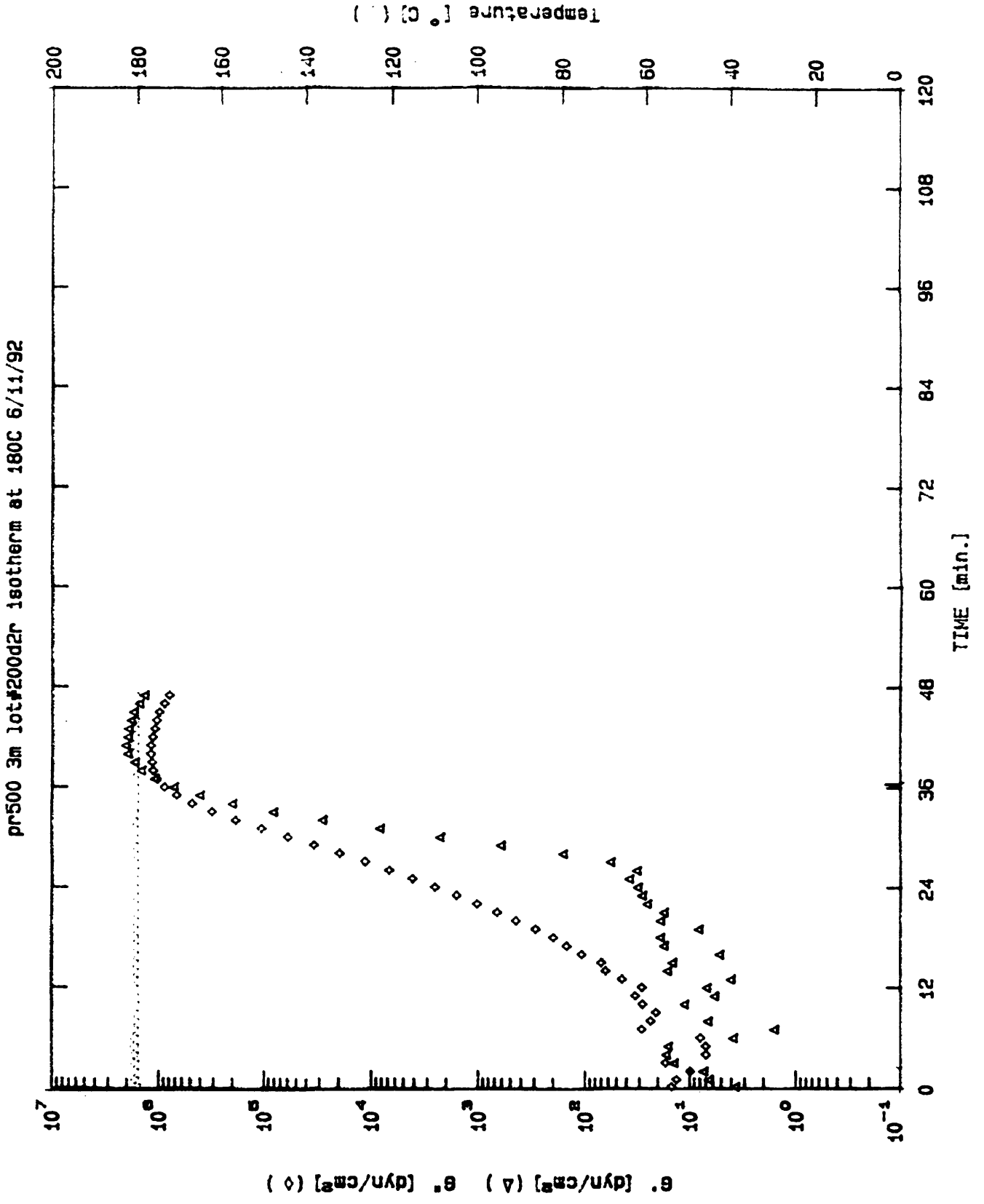
pr500 3m lot#200d2r isotherm at 180C 6/11/92
Temperature [° C] ( )
TIME [min.]
G' [dyn/cm²] (Δ) G" [dyn/cm²] (◇)

Figure 5.16

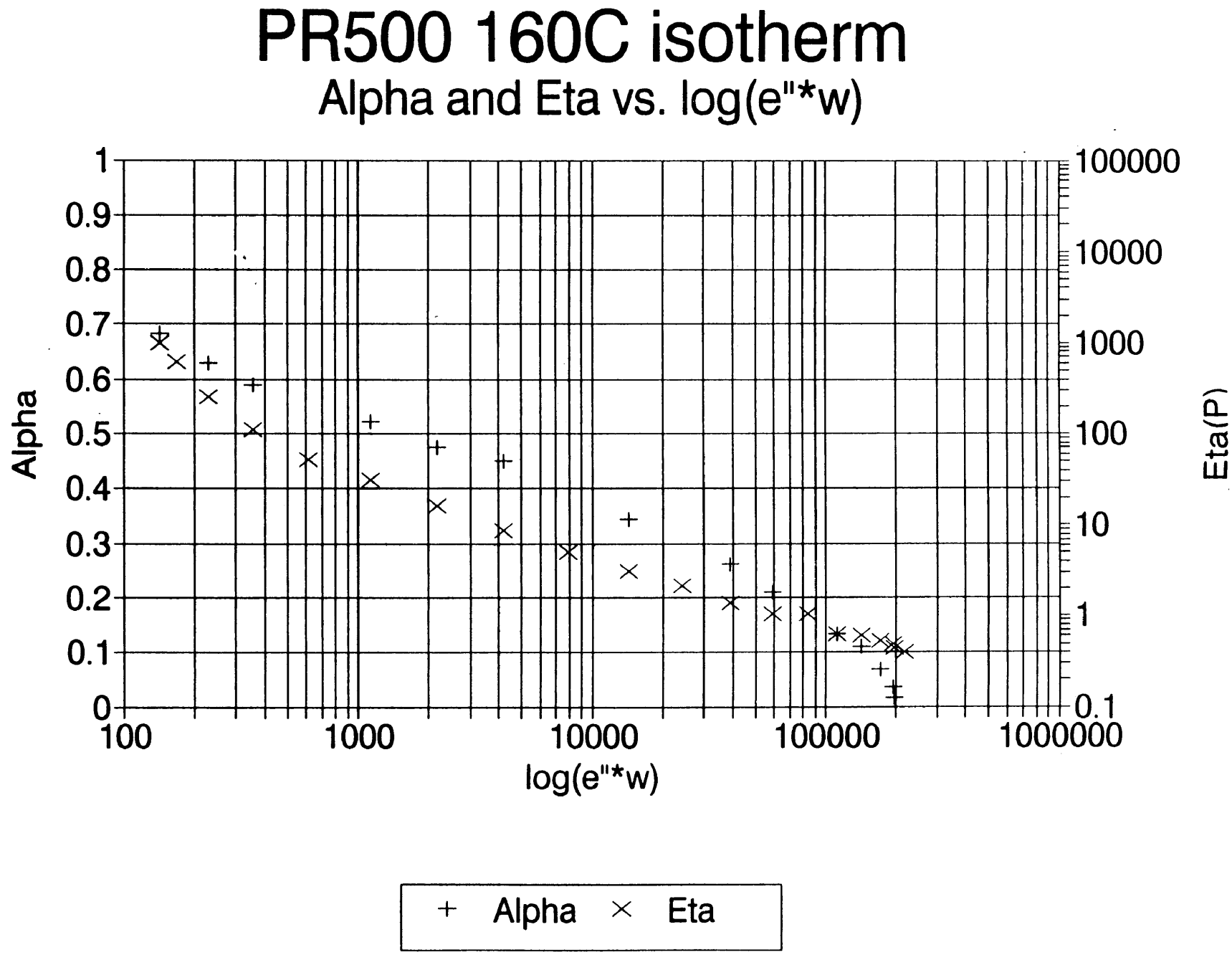
PR500 160C isotherm
Alpha and Eta vs. log(e"*w)
Alpha
Eta(P)
log(e"*w)
1
0.9
0.8
0.7
0.6
0.5
0.4
0.3
0.2
0.1
0
100000
10000
1000
100
10
1
0.1
100
1000
10000
100000
1000000
+ Alpha × Eta

Figure 5.17

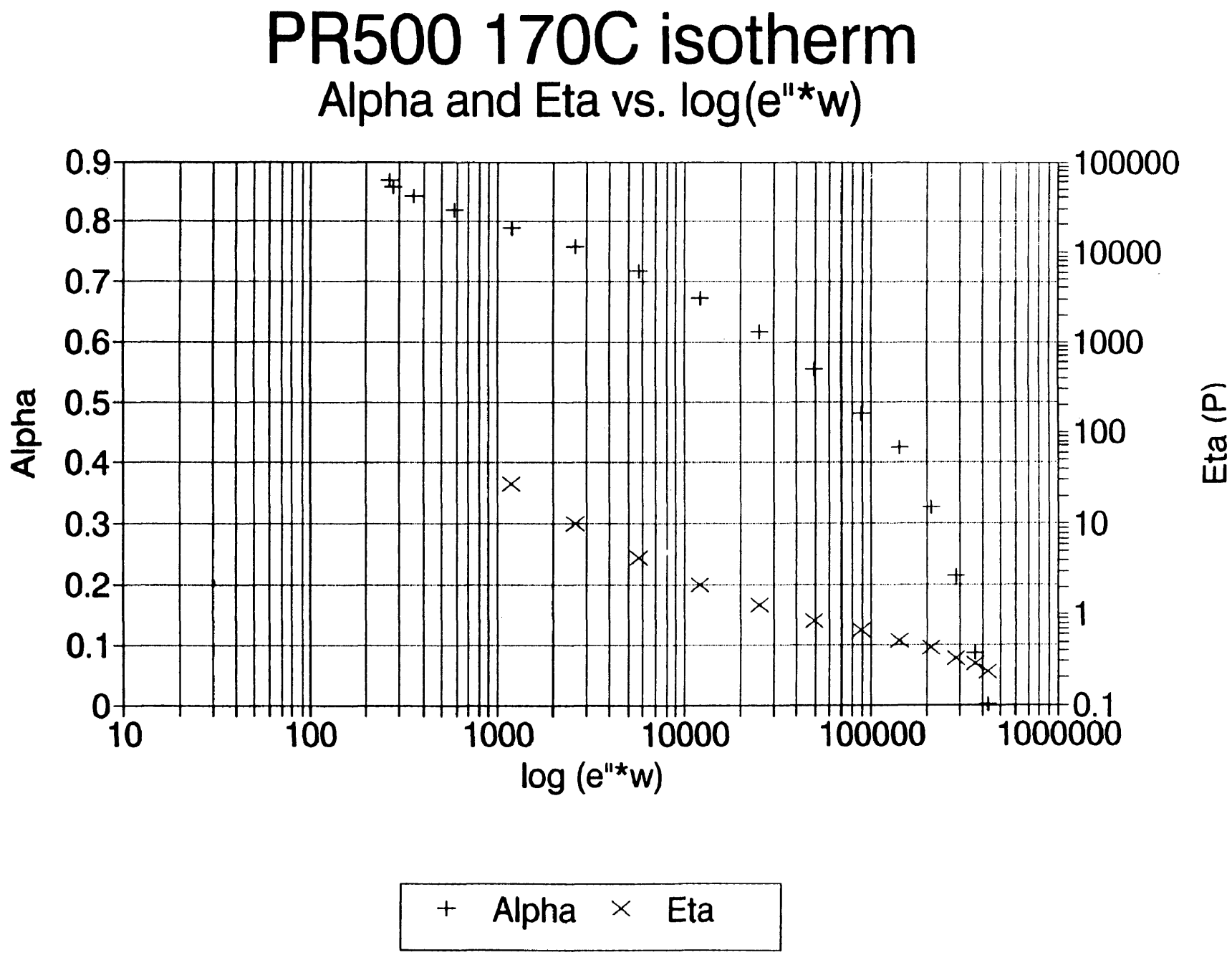
PR500 170C isotherm
Alpha and Eta vs. log(e"*w)
Alpha
Eta (P)
log (e"*w)
0.9
0.8
0.7
0.6
0.5
0.4
0.3
0.2
0.1
0
100000
10000
1000
100
10
1
0.1
10
100
1000
10000
100000
1000000
+ Alpha × Eta

Figure 5.18

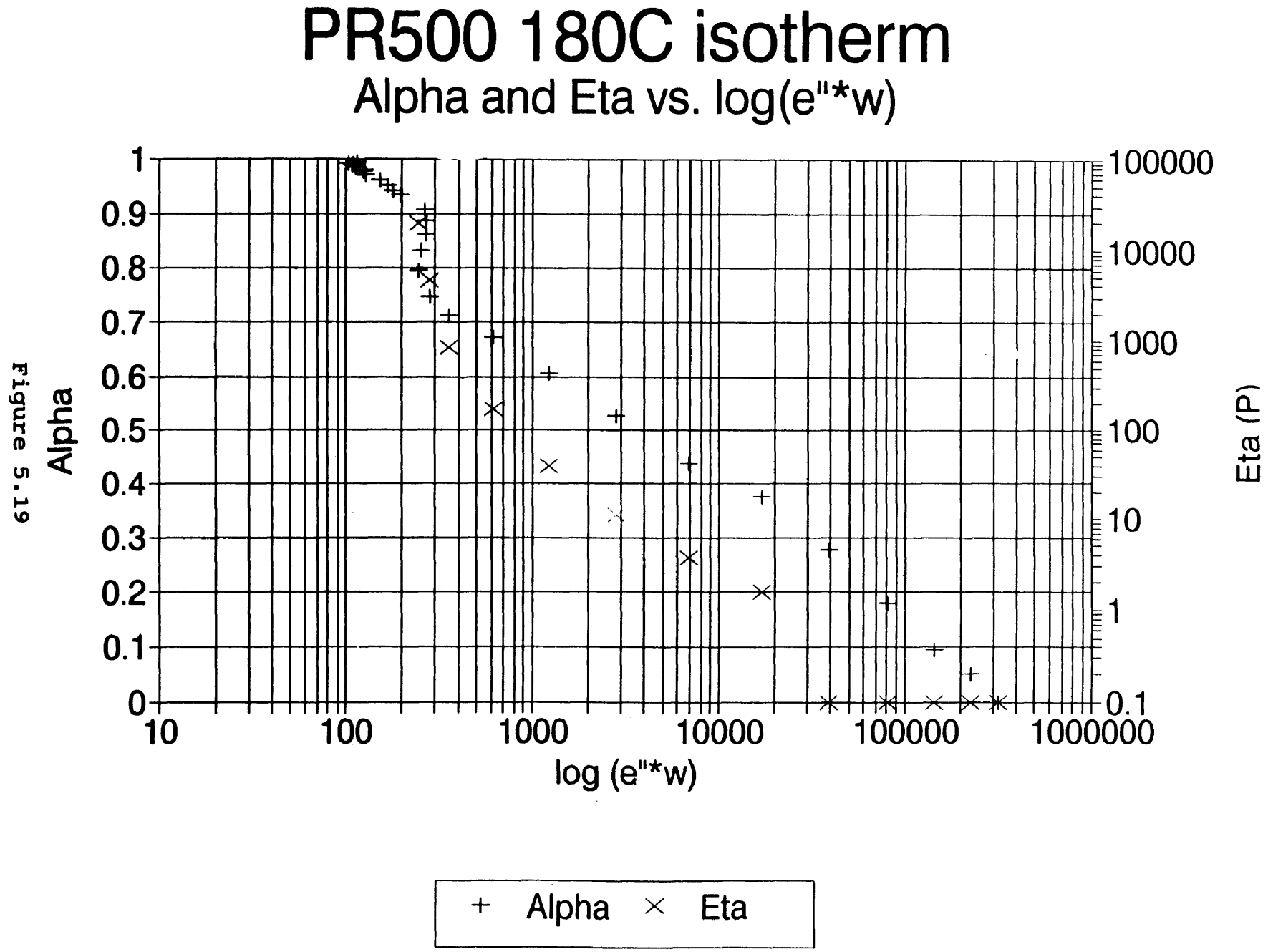
PR500 180C isotherm
Alpha and Eta vs. log(e"*w)
Alpha
Eta (P)
log (e"*w)
1
0.9
0.8
0.7
0.6
0.5
0.4
0.3
0.2
0.1
0
100000
10000
1000
100
10
1
0.1
10
100
1000
10000
100000
1000000
+ Alpha × Eta

Figure 5.19

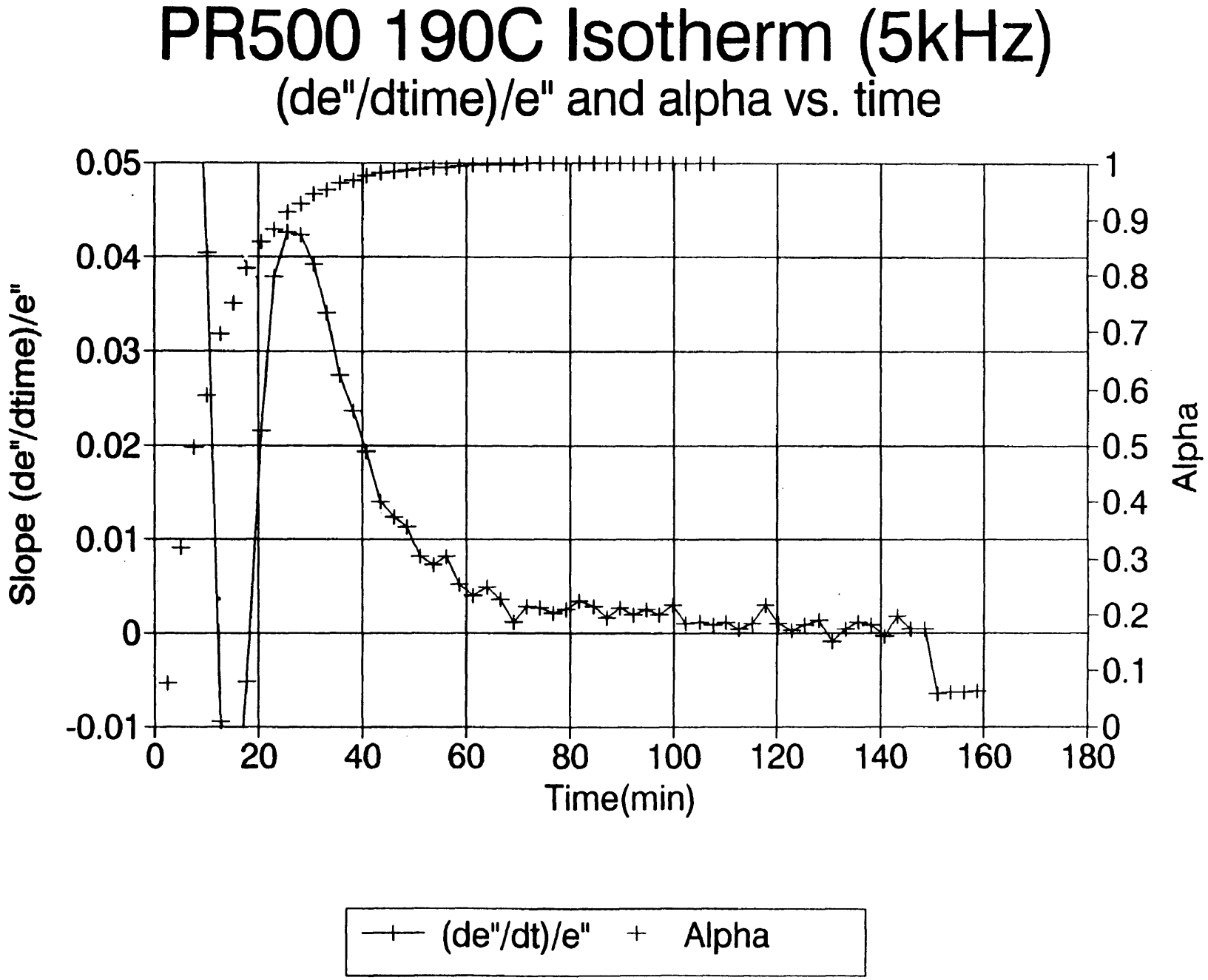
PR500 190C Isotherm (5kHz)
(de"/dtime)/e" and alpha vs. time
Slope (de"/dtime)/e"
Alpha
Time(min)
0.05
0.04
0.03
0.02
0.01
0
-0.01
1
0.9
0.8
0.7
0.6
0.5
0.4
0.3
0.2
0.1
0
0
20
40
60
80
100
120
140
160
180
(de"/dt)/e"
Alpha

Figure 5.20

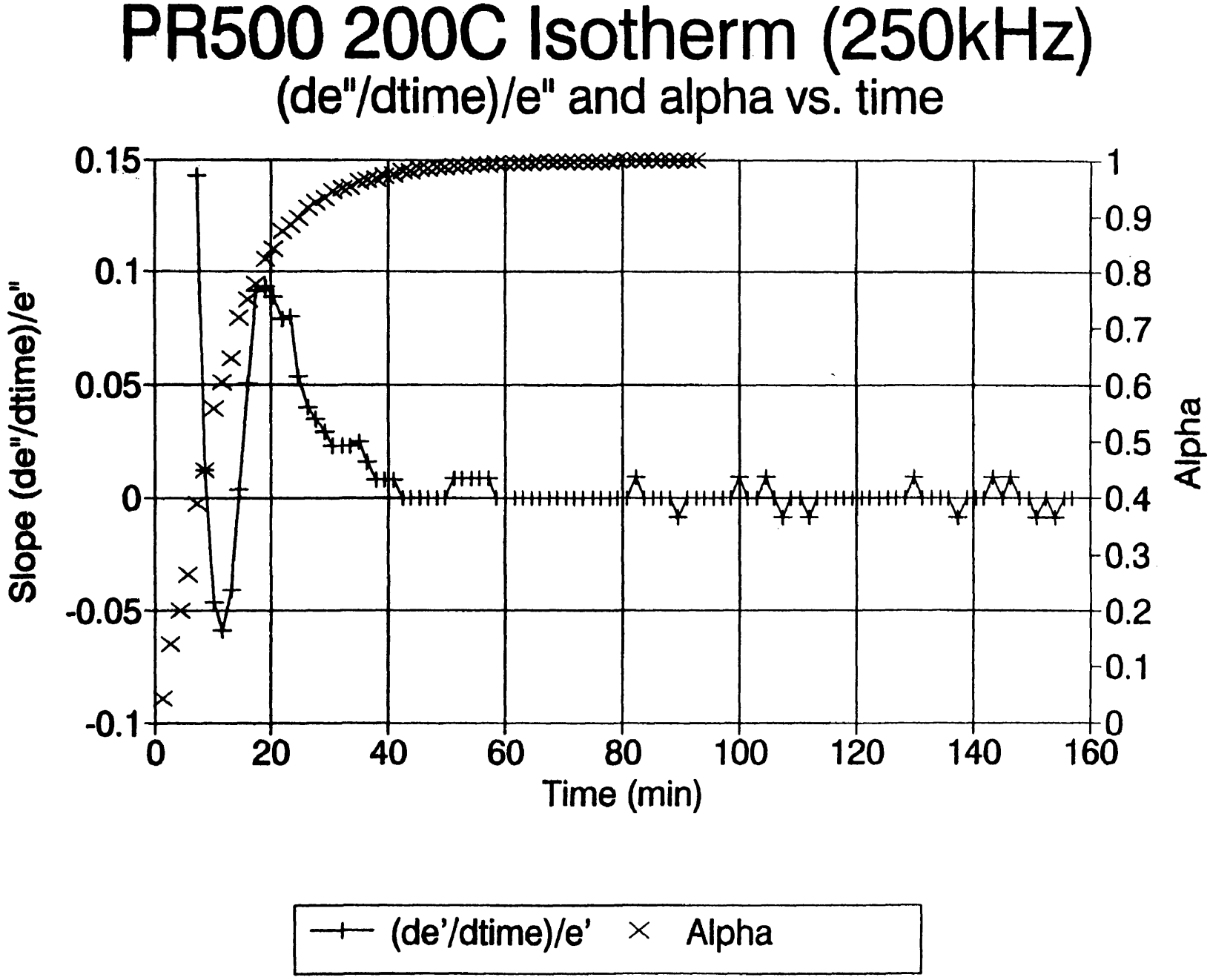
PR500 200C Isotherm (250kHz)
(de"/dtime)/e" and alpha vs. time
Slope (de"/dtime)/e"
Alpha
Time (min)
0.15
0.1
0.05
0
-0.05
-0.1
1
0.9
0.8
0.7
0.6
0.5
0.4
0.3
0.2
0.1
0
0
20
40
60
80
100
120
140
160
(de'/dtime)/e'
Alpha

Figure 5.21

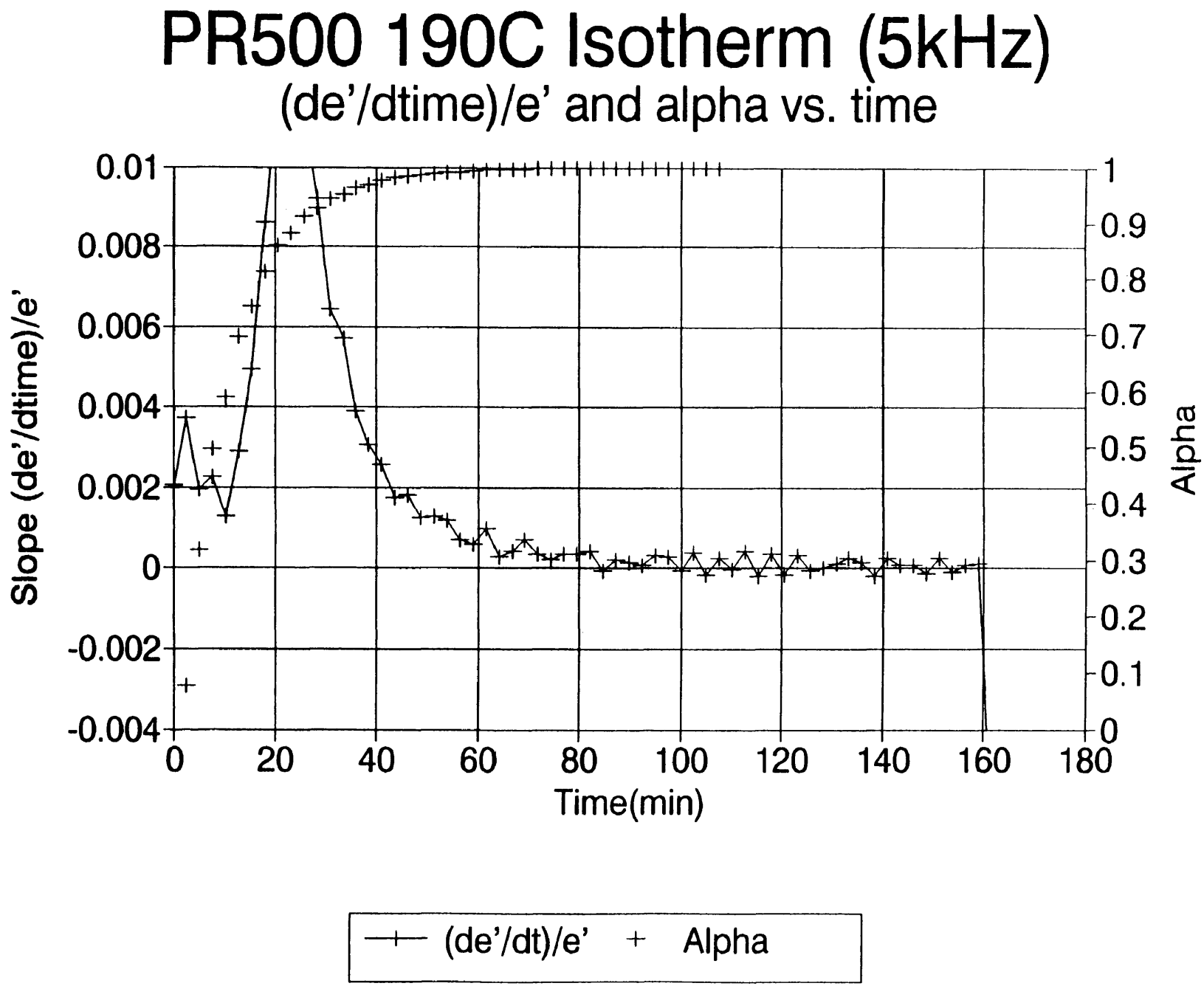
PR500 190C Isotherm (5kHz)
(de'/dtime)/e' and alpha vs. time
Slope (de'/dtime)/e'
Alpha
Time(min)
0.01
0.008
0.006
0.004
0.002
0
-0.002
-0.004
1
0.9
0.8
0.7
0.6
0.5
0.4
0.3
0.2
0.1
0
0
20
40
60
80
100
120
140
160
180
(de'/dt)/e'
Alpha

Figure 5.22

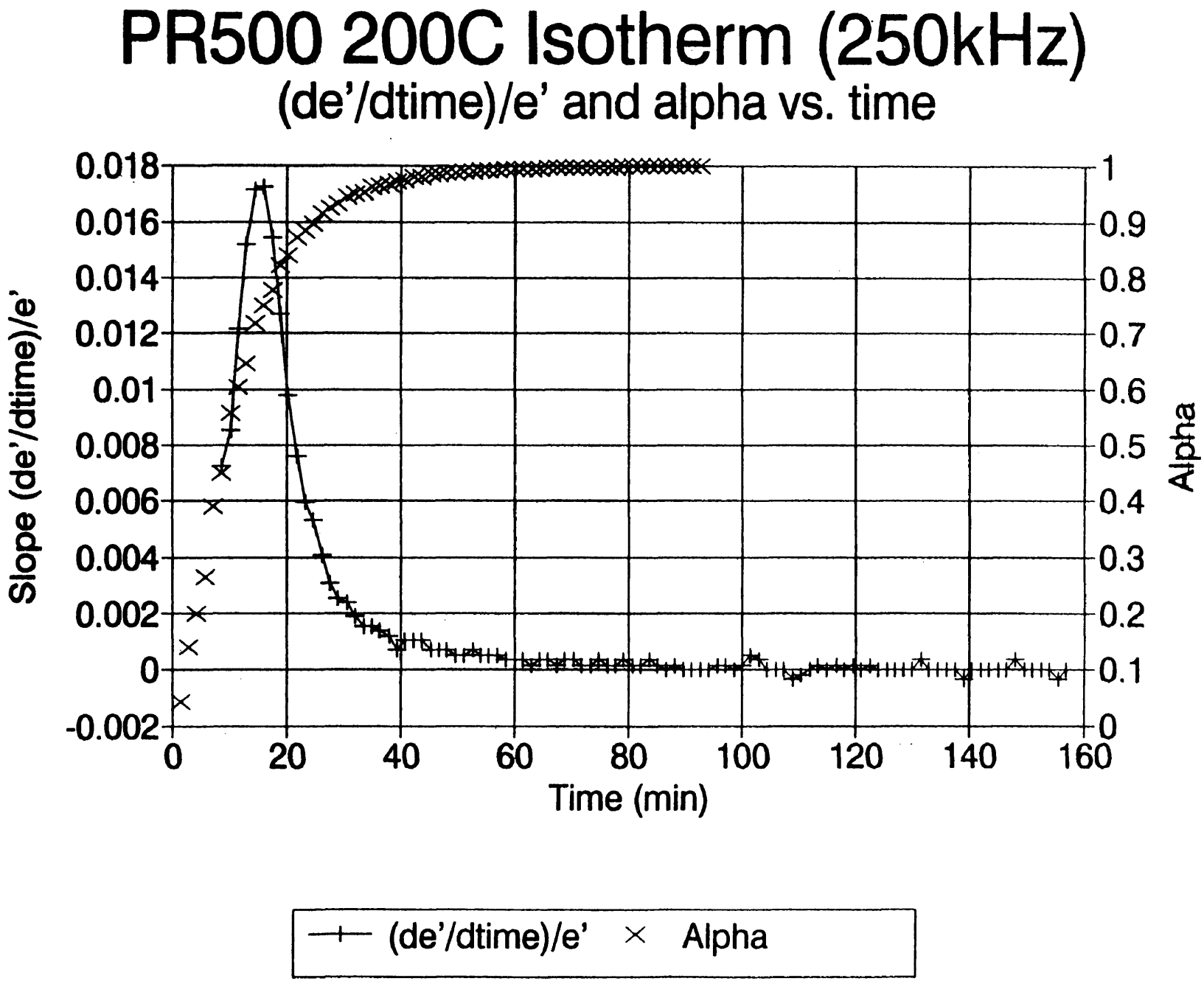
PR500 200C Isotherm (250kHz)
(de'/dtime)/e' and alpha vs. time
Slope (de'/dtime)/e'
Alpha
Time (min)
0.018
0.016
0.014
0.012
0.01
0.008
0.006
0.004
0.002
0
-0.002
1
0.9
0.8
0.7
0.6
0.5
0.4
0.3
0.2
0.1
0
0
20
40
60
80
100
120
140
160
(de'/dtime)/e'
Alpha

Figure 5.23

Chapter V References

1. Cole, K. C., "A New Approach to Modeling the Cure Kinetics of Epoxy Amine Thermosetting Resins. 1. Mathematical Development," *Macromolecules*, Vol. 24, 1991.

2. Ryan, M. E., Dutta, A., "Kinetics of Epoxy Cure: a Rapid Technique for Kinetic Parameter Estimation," *Polymer*, Vol. 20, 1979.

3. Winter, H. H., "Can the Gel Point of a Crosslinking Polymer be Detected by the G'-G" Crossover?", *Polymer Engineering and Science*, Vol. 27, No. 22, 1987.

Chapter VI

Characterization of E905L Resin

British Petroleum E905L triazine-epoxy-amine resin is another developmental resin currently being considered for use in aerospace composites. Unlike the resins previously examined, E905L resin exhibits a complex curing reaction. This analysis therefore involves the development of a more intricate kinetic model than has been previously discussed.

Reaction Kinetics

The complex curing behavior of E905L resin was first observed in a DSC ramp of uncured resin from 50° to 300°C at 5°C/min. The ramp revealed two distinct exothermic peaks, or valleys, separated by a peak at 175°C (Fig. 6.1). The two peaks suggested that the E905L resin system polymerized through two independent reactions. Since the peaks occurred at different temperatures, the reaction was separated into a low and a high temperature reaction. Therefore, the total heat of the reaction could be calculated as the sum of the two reaction heats.

In order to develop an accurate kinetic model, it was

necessary to produce separate models for the high and low temperature reactions. Chiou and Letton described an experimental technique to isolate the separate reactions for a complex-curing epoxy resin.[1] First, a temperature is determined where one of the reactions proceeds at a considerably faster rate than the other. The sample is then aged at the predetermined temperature to eliminate one of the reactions, leaving the other reaction. This approach was taken to isolate the high temperature reaction for E905L.

A 121°C isotherm for 3 hrs was determined to be the optimal aging criterion for the E905L samples. At 121°C the low temperature reaction was dominant and went to completion. Previous studies indicated that 3 hrs was the minimal amount of aging required to completely remove the low temperature reaction. Furthermore, aging the sample for longer than 3 hrs did not significantly affect the high temperature reaction[2].

High Temperature Reaction

Data for the high temperature model was obtained by performing DSC isotherms and ramps on the aged samples. Using a procedure similar to that described in Chapter IV, the isotherms and ramps were fit to the nth order rate equation.

[6-1] $$d\alpha/dt = k(1-\alpha)^n$$

Similarly, the values of the rate constant, k, and the rate order, n, were generated by the SYSTAT® fitting program. The value of n_H was taken as the average of the n values for the 180°, 190° and 215°C isothermal data. The average n_H was found to be 1.41.

The temperature dependence of k was previously determined using the Arrhenius equation. However, in analyzing the total reaction of E905L, it was found that the temperatures considered for the high temperature reaction provided too narrow a range to accurately predict the buildup of alpha. This is understandable since E905L reacts over a much larger range from 100° to 250°C. As a result, a temperature ramp of an aged sample was used to determine the activation energy for the high temperature reaction. In using ramp data, a new method was used combining the Arrhenius equation, $k = Ae^{-B/T}$, and the kinetic equation, $d\alpha/dt = k(1-\alpha)^{nH}$, such that

[6-2] $$\text{Ln } (d\alpha/dt(1-\alpha)^{nH}) = \text{Ln } A - B/T$$

Temperature ramps from 50° to 300°C at 2 and 5°C/min were analyzed. Values of alpha, $d\alpha/dt$ and heat were generated for each of the ramps. Plots of $\text{Ln}[d\alpha/dt/(1-\alpha)^{nH}]$ versus inverse temperature were then constructed for the two temperature ramps (Fig. 6.2 and Fig. 6.3). The slopes of the two curves produced values for the activation energy. The two slopes were then averaged to produce a final value

of B_H equal to 11,700 K. The value of the Arrhenius preexponential factor, A_H, was calculated from the average B_H and the 190°C isotherm value of k (0.49), determined in SYSTAT®. The final value for A_H was calculated to be 4.8×10^9.

The high temperature reaction model was thus resolved using the isothermal value of the reaction order and the combination of ramp and isothermal values for the rate constant, k. The high temperature model produced in this analysis was

[6-3] $$d\alpha/dt_{High} = (4.8 \times 10^9) e^{-11700/T} (1-\alpha)^{1.41}$$

where $d\alpha/dt_{High}$ represents the buildup in alpha for the high temperature reaction only. This method most accurately predicted the buildup of alpha for the high temperature reaction, in agreement with both ramp and isothermal data.

Low Temperature Reaction

The low temperature reaction was analyzed using DSC isothermal data taken at 110°, 120° and 130°C. In this temperature range, the low temperature reaction is dominant, and the high temperature reaction contributes a very small amount to $d\alpha/dt_{Total}$. Previous papers describe procedures to subtract out the high temperature contribution; however, in this investigation the high temperature contribution was so slight that it was neglected in the experimental data.[3]

Overall, the inclusion of the high temperature reaction did not affect the kinetic fitting of the total reaction.

Isothermal data were analyzed using the SYSTAT® fitting program. The nth order rate equation

[6-4] $$d\alpha/dt = k(1-\alpha)^n$$

was also selected for the low temperature reaction. The value of n_L was calculated as the average n for the low temperature isothermal data. A value of 0.66 was the average n_L. The temperature dependence of k was evaluated using the Arrhenius relation. The values of A_L and B_L were resolved as 3.41×10^8 min and 9386 K, respectively. This produced the following kinetic model for the low temperature reaction:

[6-5] $$d\alpha/dt_{Low} = (3.41 \times 10^8) e^{-9386/T} (1-\alpha)^{0.66}$$

While each of the reactions made a unique contribution to the total degree of cure, the fraction of α_{Total} donated by the low and high temperature components of alpha had to be determined. The contributions made by the two components were predicted using the heat of each of the reactions divided by the total heat of reaction. The low temperature contribution was calculated to be 0.41 of the total reaction. The high temperature contribution was the difference, 0.59. This produced the final rate equation for E905L resin system,

[6-6] $$d\alpha/dt_{Total} = 0.41\ d\alpha/dt_{Low} + 0.59\ d\alpha/dt_{High}$$

where $d\alpha/dt_{Low}$ and $d\alpha/dt_{High}$ represent the low and high

temperature contributions, respectively. The fit of the theoretical to the experimental $d\alpha/dt$ curve for each of the isotherms is pictured in Figures 6.4 through 6.9. The calculated buildup in the degree of cure provided excellent agreement with the experimental data. This model was then used to predict alpha in correlations and in monitoring the RTM process.

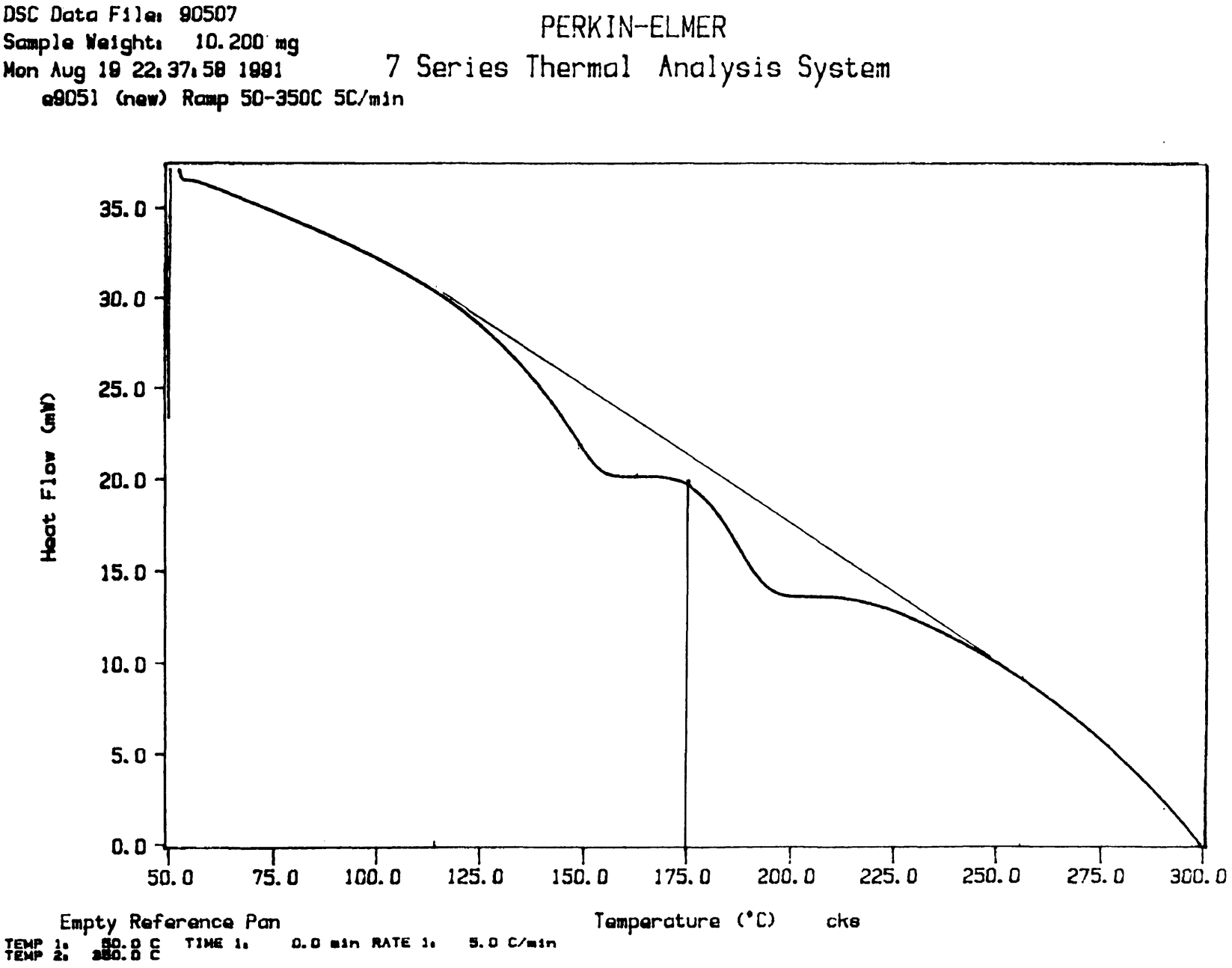
DSC Data File: 90507
Sample Weight: 10.200 mg
Mon Aug 19 22:37:58 1991
e9051 (new) Ramp 50-350C 5C/min
PERKIN-ELMER
7 Series Thermal Analysis System
35.0
30.0
25.0
20.0
15.0
10.0
5.0
0.0
Heat Flow (mW)
50.0
75.0
100.0
125.0
150.0
175.0
200.0
225.0
250.0
275.0
300.0
Temperature (°C)
Empty Reference Pan
TEMP 1: 50.0 C TIME 1: 0.0 min RATE 1: 5.0 C/min
TEMP 2: 350.0 C

Figure 6.1

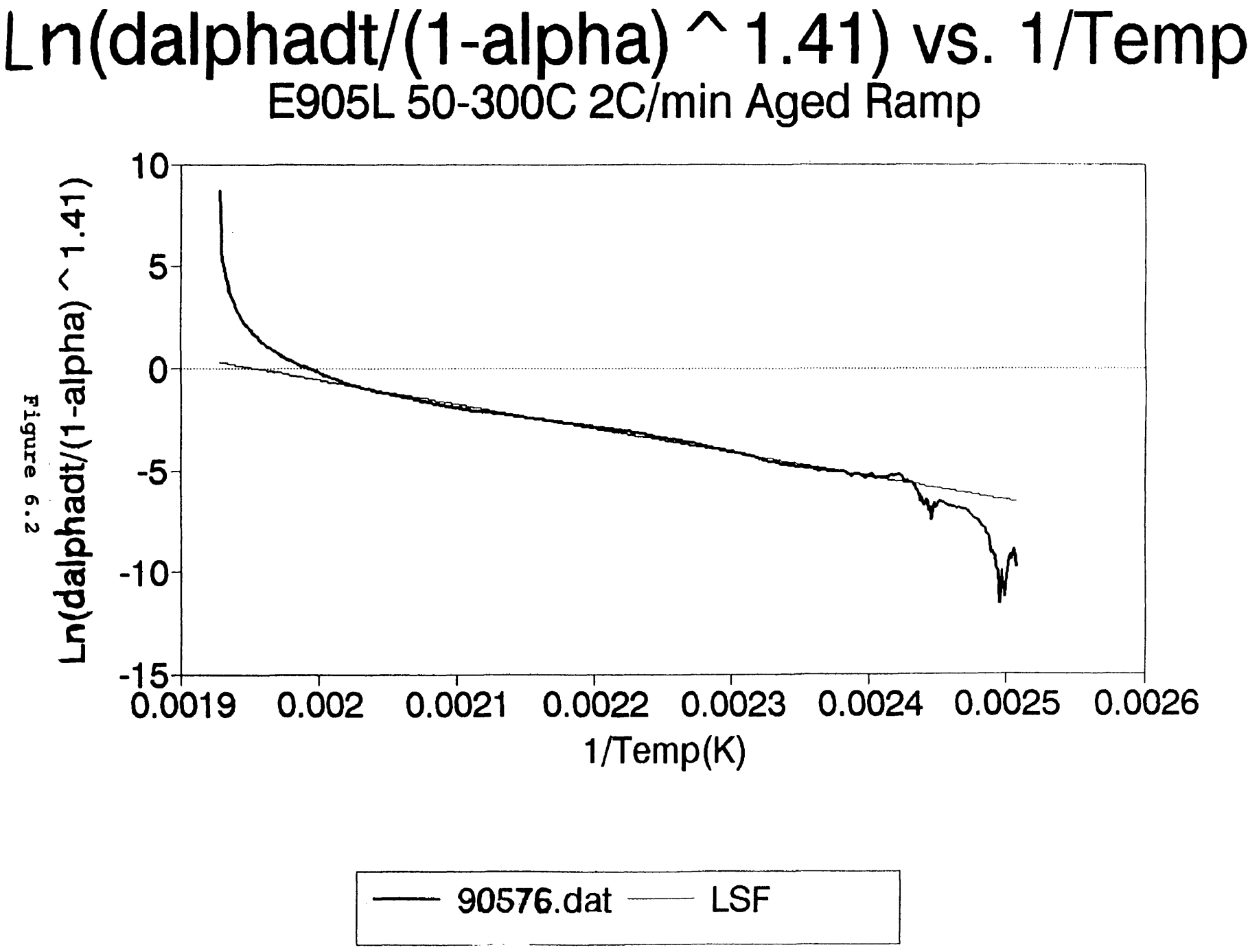
Ln(dalphadt/(1-alpha) ^ 1.41) vs. 1/Temp
E905L 50-300C 2C/min Aged Ramp
Ln(dalphadt/(1-alpha) ^ 1.41)
10
5
0
-5
-10
-15
0.0019
0.002
0.0021
0.0022
0.0023
0.0024
0.0025
0.0026
1/Temp(K)
90576.dat
LSF

Figure 6.2

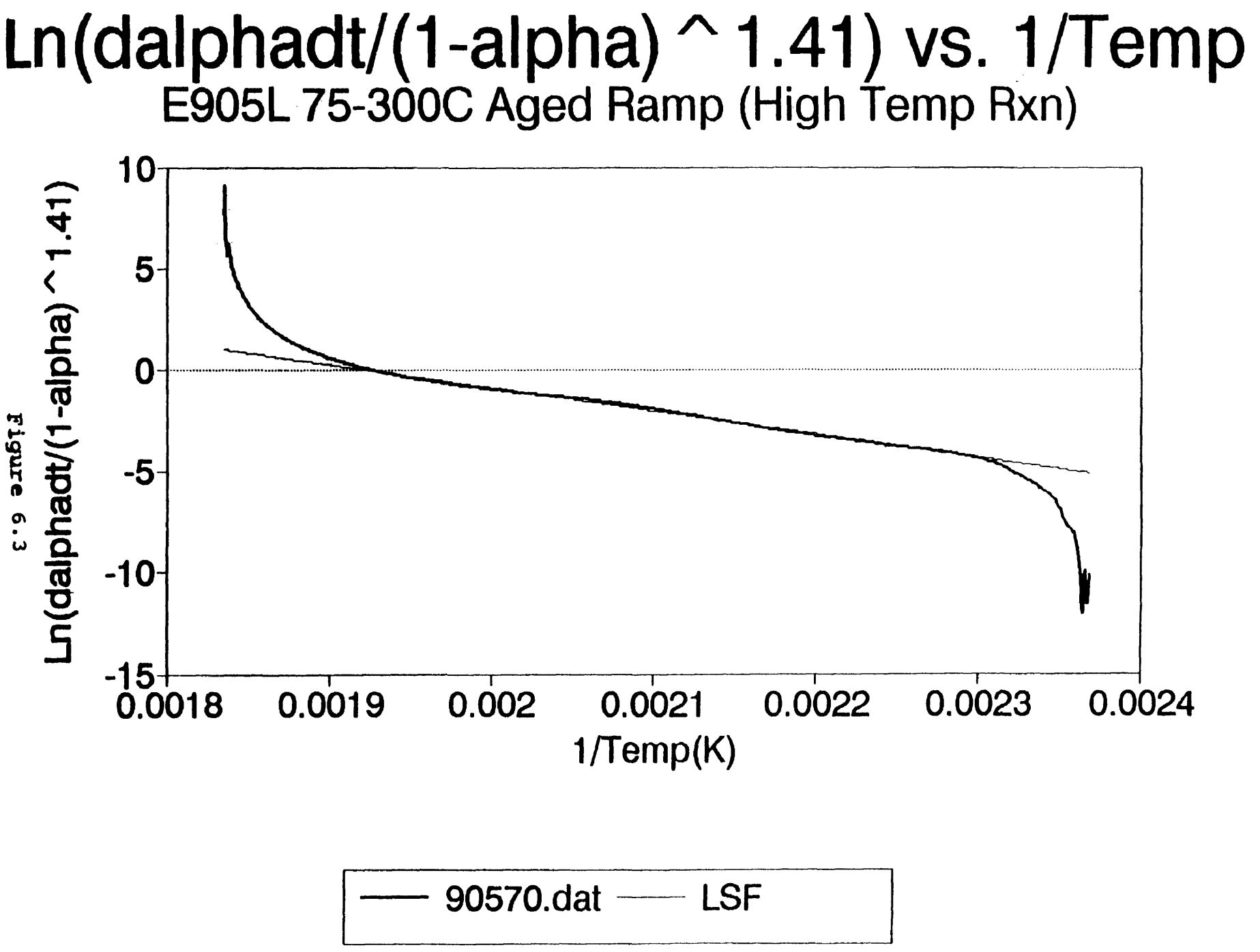
Ln(dalphadt/(1-alpha) ^ 1.41) vs. 1/Temp
E905L 75-300C Aged Ramp (High Temp Rxn)
Ln(dalphadt/(1-alpha) ^1.41)
10
5
0
-5
-10
-15
0.0018
0.0019
0.002
0.0021
0.0022
0.0023
0.0024
1/Temp(K)
90570.dat
LSF

Figure 6.3

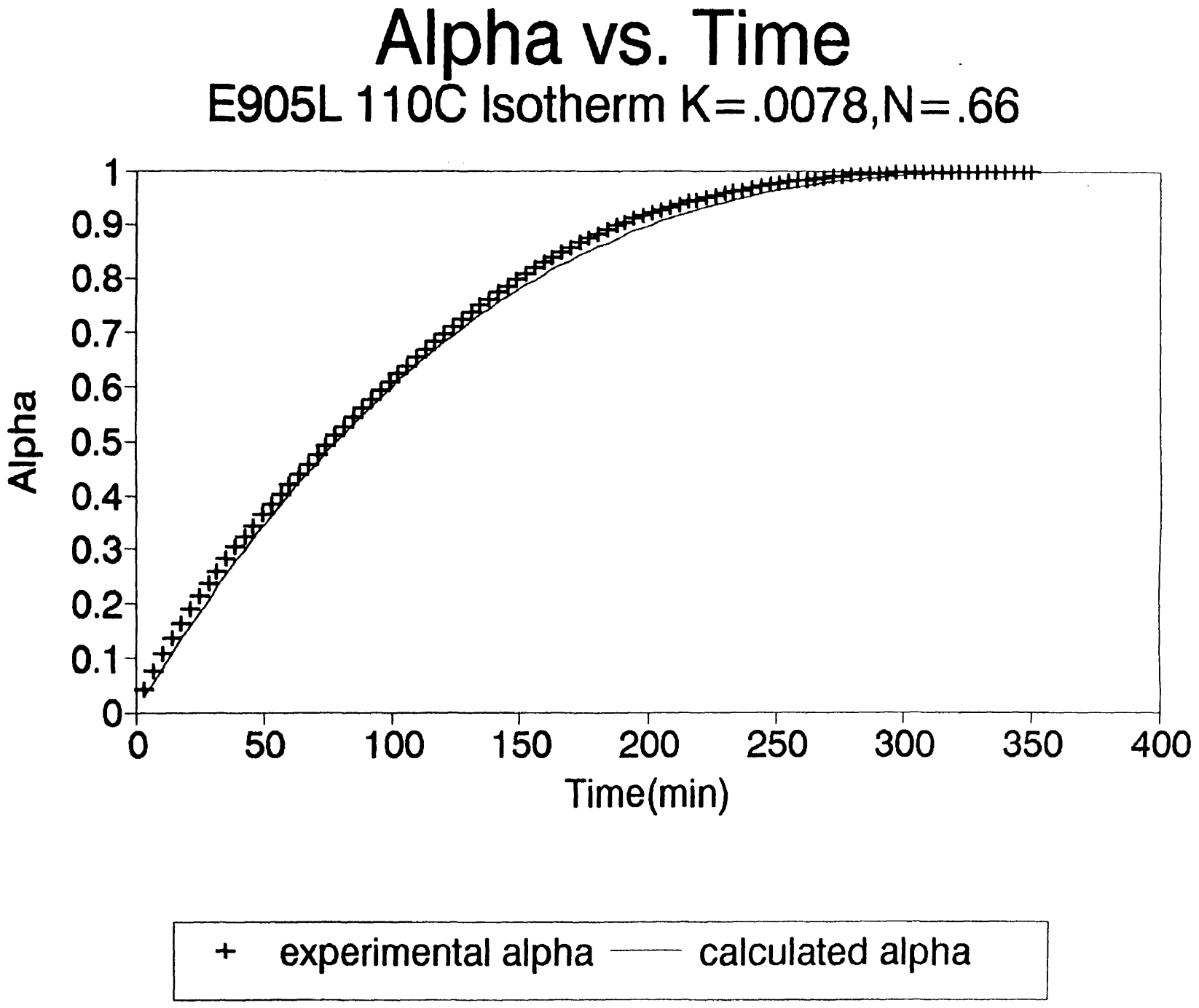
Alpha vs. Time
E905L 110C Isotherm K=.0078,N=.66
Alpha
1
0.9
0.8
0.7
0.6
0.5
0.4
0.3
0.2
0.1
0
0
50
100
150
200
250
300
350
400
Time(min)
+ experimental alpha
calculated alpha

Figure 6.4

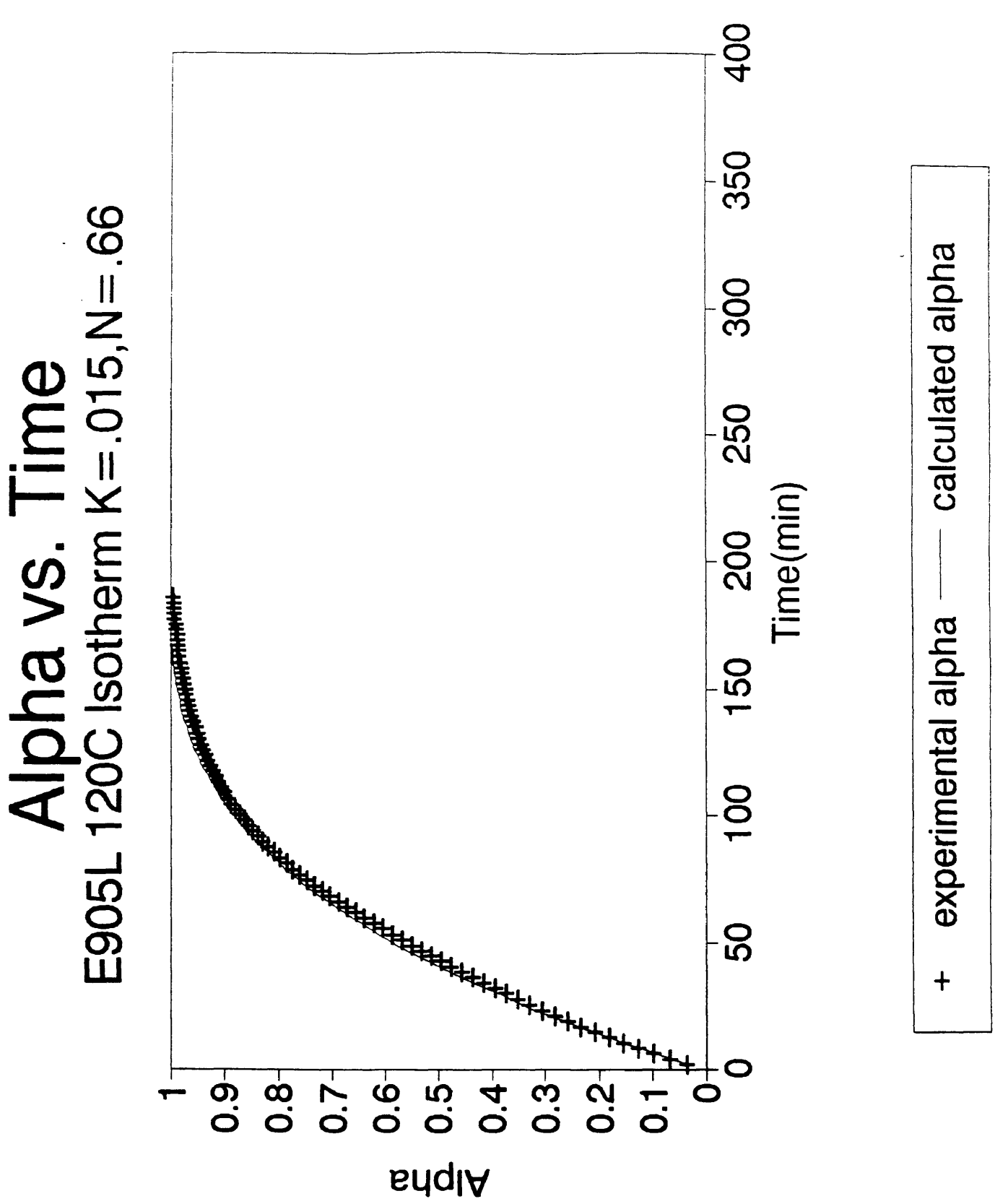
Alpha vs. Time
E905L 120C Isotherm K=.015,N=.66
Alpha
1
0.9
0.8
0.7
0.6
0.5
0.4
0.3
0.2
0.1
0
0
50
100
150
200
250
300
350
400
Time(min)
+ experimental alpha —— calculated alpha

Figure 6.5

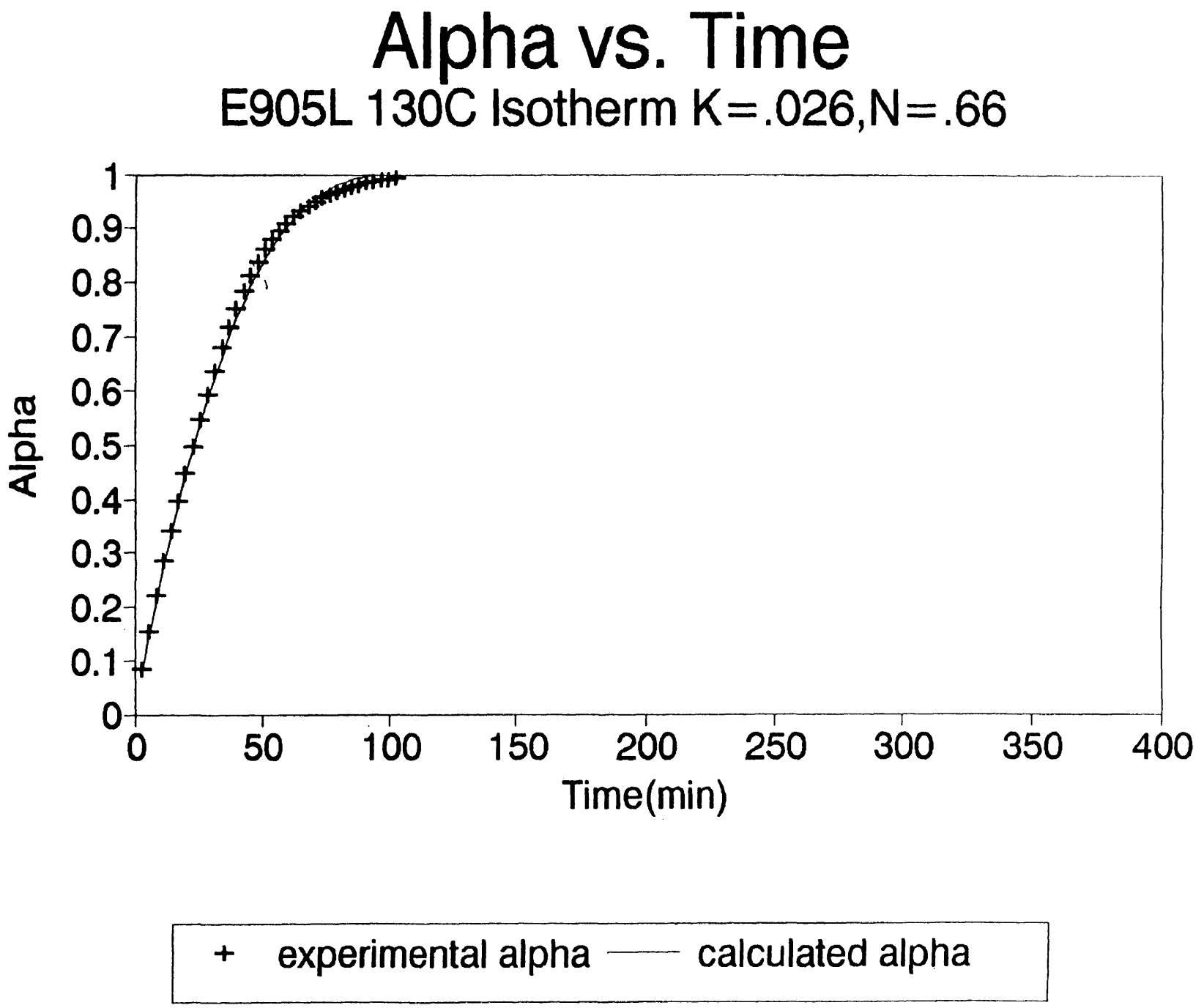
Alpha vs. Time
E905L 130C Isotherm K=.026,N=.66
Alpha
1
0.9
0.8
0.7
0.6
0.5
0.4
0.3
0.2
0.1
0
0
50
100
150
200
250
300
350
400
Time(min)
+ experimental alpha
calculated alpha

Figure 6.6

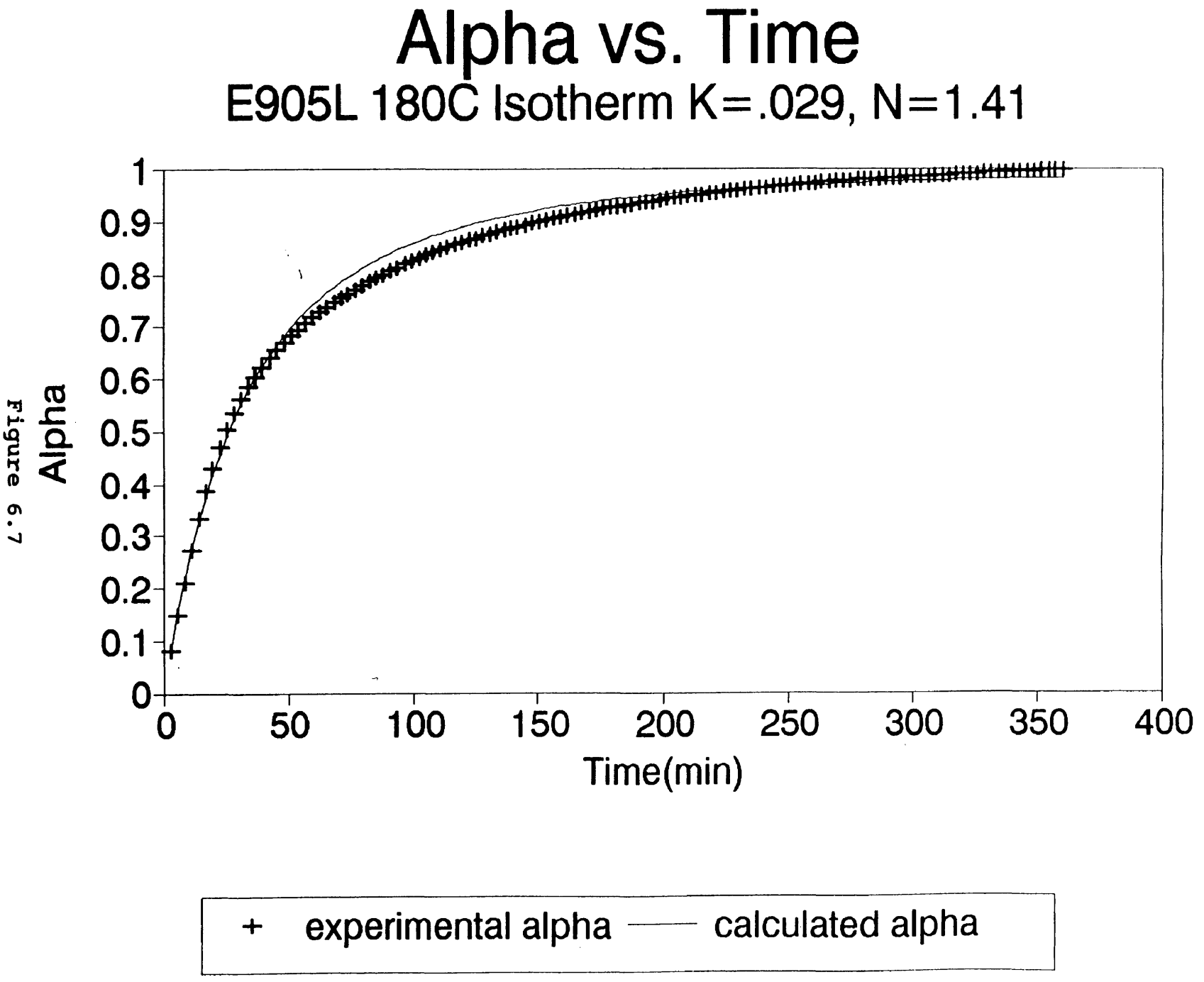
Alpha vs. Time
E905L 180C Isotherm K=.029, N=1.41
Alpha
1
0.9
0.8
0.7
0.6
0.5
0.4
0.3
0.2
0.1
0
0
50
100
150
200
250
300
350
400
Time(min)
+ experimental alpha
calculated alpha

Figure 6.7

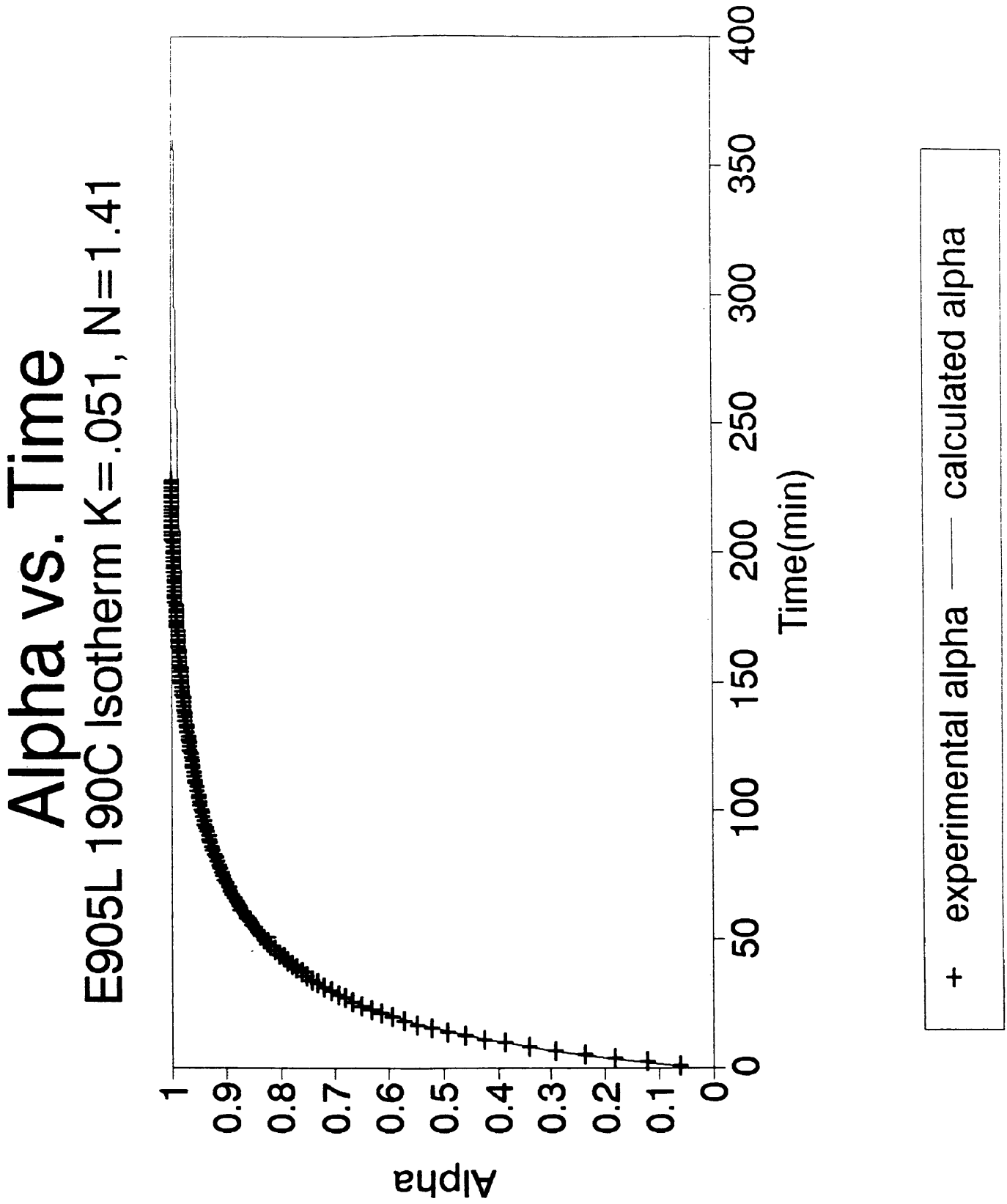
Alpha vs. Time
E905L 190C Isotherm K=.051, N=1.41
Alpha
1
0.9
0.8
0.7
0.6
0.5
0.4
0.3
0.2
0.1
0
0
50
100
150
200
250
300
350
400
Time(min)
+ experimental alpha
calculated alpha

Figure 6.8

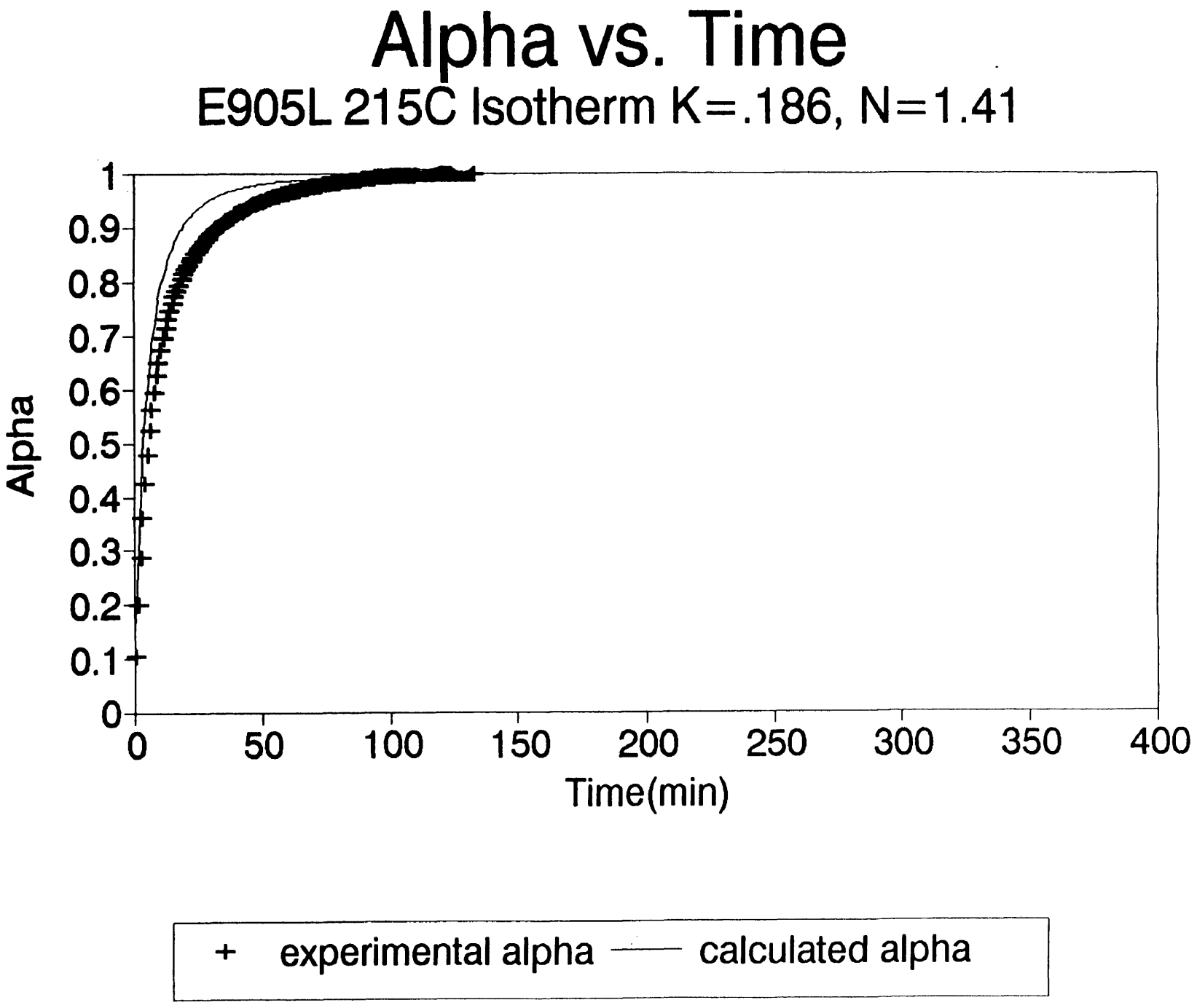
Alpha vs. Time
E905L 215C Isotherm K=.186, N=1.41
Alpha
1
0.9
0.8
0.7
0.6
0.5
0.4
0.3
0.2
0.1
0
0
50
100
150
200
250
300
350
400
Time(min)
+ experimental alpha
calculated alpha

Figure 6.9

Chapter VI References

1. Chiou, P., Letton, A., "Reaction Kinetics and Chemoviscosity of a Thermoset Exhibiting Complex Curing Behavior," Mechanical Engineering Department, Texas A&M University, College Station, Texas 1990.

2. Kranbuehl, D., Polis, D., Short, C., and Wang, Y. "Use of FDEMS Sensing for Insitu, On-line Monitoring of Degree of Cure during Polymerization of a 2-stage, High Performance RTM Composite Resin," *Society of Plastic Engineers*, Vol. 2, 1993.

3. Kingsley, P. J., Masters Thesis, "Dielectric Monitoring and Control of an Automated Resin Transfer Molding Process" College of William and Mary, 1991.

Chapter VII

Conclusions

In characterizing the three epoxy-amine curing reactions, the morphology of each of the resins was examined to provide a fundamental understanding of the cure process. Kinetic models of the individual resin systems, based on the epoxy-amine reaction, were then developed to predict the degree of cure under any time or temperature condition. The predicted degree of cure and measured viscosity were then correlated with the frequency dependent dielectric measurement $\epsilon''*\omega$. These calibrations related the dielectric properties of the resin systems to the cure processing properties, α and η. Through these correlations, the RTM process could then be intelligently controlled to optimize the end properties of the composite part.

VITA

Christina Kaye Short

The author was born in Logan, Utah on December 16, 1970. She graduated from Frank W. Cox High School in Virginia Beach, Virginia, in June, 1988. She continued her education at the College of William and Mary where she received a Bachelor of Science degree in Chemistry in May, 1992. She was a candidate for the degree of Master of Arts in Chemistry at the College of William and Mary from May, 1992, to August, 1993.